Final Report

on

SURFACE-TENSION INDUCED INSTABILITIES:

EFFECTS OF LATERAL BOUNDARIES

NASA-Lewis Research Center
Contract No. NAS3-22274

to

SHD Associates, Inc.
2735 Simpson St.
Evanston, IL 60201

June 1981

(NASA-CR-165530) SURFACE-TENSION INDUCED INSTABILITIES: EFFECTS OF LATERAL BOUNDARIES Final Report (SHD Associates, Inc.) 130 p HC A07/MF A01 CSCI 20D

N82-11390

Unclas
G3/34 01212

TABLE OF CONTENTS

SUMMARY

In this report we consider a liquid in a cylindrical container having either circular or rectangular cross-section. The bottom of the container is a rigid, perfect heat conductor while the upper surface is a free interface between the liquid and the bounding gas. The bottom of the container is uniformly heated and heat is lost to the gas at the top. The basic state consists of zero velocity (motionless liquid) having a linear, purely conductive temperature profile. If the vertical temperature gradient is large enough, this pure conduction state becomes unstable due to the joint effects of two mechanisms. The surface tension on the interface depends on temperature and Marangoni convection sets in. The non-dimensional measure of the surface-tension gradient is the Marangoni number M. The vertical gravity field sets up an adverse density gradient so that buoyancy effects lead to convection. The non-dimensional measure of the buoyancy is the Rayleigh number R.

We formulate the general problem of nonlinear convective instability driven by the joint effects of thermocapillarity and buoyancy. The upper free surface has a general heat transfer condition applied and the interface is allowed to deform. Sidewalls confine the layer. The problem solved involves a special case of the general problem. The surface tension on the interface is so large that surface deflections are neglected. The sidewalls are adiabatic and impenetrable but for mathematical simplicity are allowed to be "slippery".

In order to determine the effect of sidewalls on the critical Marangoni number in finite containers, it is first necessary to develop the basic equations and boundary conditions. The basic equations are the

Navier-Stokes, continuity and energy equations, and the boundary conditions express the conditions of no slip and constancy of temperature at the bottom surface of the layer, conservation of momentum and energy at the free interface, and the sidewall conditions alluded to above.

If we denote by a the ratio of the mean fluid depth to the radius of the cylinder, then we find the critical conditions $M > M_c = M_c(a)$ for the instability of the pure conduction state. At most values of the aspect ratio a, linear stability theory selects a single cell shape of steady Marangoni convection that replaces the pure condition when the conduction is unstable. The cell shape is characterized by an integer m since all solutions are proportional to $\exp(im\phi)$ where ϕ is the cylindrical azimuthal angle. Thus $m = 0$ corresponds to axisymmetric ring cells. Alternatively, $m = 1$ corresponds to convection patterns in which there is upflow in one half the container and downflow in the other half. Clearly, the modes for larger m correspond to more complicated cellular patterns. The linear theory shows that as the aspect ratio a is increased from zero that the preferred modes follow the sequence $m = 1$, $m = 2$, $m = 0$, $m = 3$, etc. We study convection near intersections between modes and away from such intersections.

The linear instability theory for the case of the rectangular container is even more complicated, as two aspect ratios are necessary to describe the container. We denote the dimensionless length and width of the rectangle as (a_1,a_2). Again, modes of convection are denoted by integers (m_1,m_2) corresponding to the number of cells in the horizontal directions (x,y). Thus (1,0) is a single roll cell with axis in the y direction. Parameter studies result in a map in the (a_1,a_2) plane which gives the modes which

are preferred according to linear theory. We shall be especially concerned with boxes which are of shallow depth relative to their length a_2; this means we shall focus for fixed a_2 on the progression of roll cells (m,0) as the length a_1 of the box increases. Again, we study convection near intersections between modes and away from these.

In all the above calculations, both for the circular and the rectangular geometries, results are obtained for various Rayleigh numbers (measuring buoyancy) and various Biot numbers (measuring heat transfer to the gas). However, for all the nonlinear results obtained both the Rayleigh and Biot numbers are set to zero. Subsequent work will cover cases involving non-zero values of these numbers.

In order to determine the mode of convection that is observable in an experiment, it is necessary to develop a nonlinear theory. Such a theory predicts the amplitude and direction of fluid motion, and for container sizes for where two different modes of convection compete, is capable of making predictions of the convection pattern as a result of such a nonlinear competition.

Consider a single mode, whose amplitude is denoted by A(t). Then according to linear theory, A satisfies an equation of the form,

$$\nu \frac{dA}{dt} = (M - M_c)A \tag{3.1}$$

where ν is a constant which depends upon the mode in question, the aspect ratio, and the Prandtl number. According to (3.1), A will grow in time when $M > M_c$, and decay when $M < M_c$: this is the result of linear theory. When $M > M_c$, (3.1) is no longer valid for all times, and a nonlinear theory is necessary to describe the convection. The nonlinear analog to eq. (3.1) may be derived using eigenfunction expansions. In the simplest case,

such a procedure results in the amplitude equation,

$$\nu \frac{dA}{dt} = (M - M_c)A - kA^3 \tag{3.2}$$

where k is a computable constant which depends upon the mode, the aspect ratio, and the Prandtl number. Conclusions regarding the form and amplitude of the convection may be made by examining the solutions to eq. (3.2) and their stability. For example, there are three solutions to eq. (3.2), $A = 0$, $A = \pm [k^{-1}(M - M_c)]^{\frac{1}{2}}$. It is easy to show that for $k > 0$, $M > M_c$, the null solution is unstable and the other solutions are stable. Conversely, if $k < 0$, real solutions exist for $M < M_c$ only, and these are all unstable. Thus for $k > 0$, the system evolves to a state of steady convection whose magnitude is given by $|A|$. The purpose of our nonlinear theory is to derive the amplitude equations analogous to eq. (3.2) for Marangoni convection in finite containers and to determine the steady solutions and their stability. For example, (subcritical) convection can in some cases exist for $M < M_c$, even though a linear theory would predict no convection.

When the container has aspect ratio close to those values for which two modes become unstable simultaneously, one must write a pair of equations for the amplitudes, $A_1(t)$ and $A_2(t)$, say. These will be of the form

$$\nu_1 \frac{dA_1}{dt} = (M - M_{c1})A_1 - f_1(A_1, A_2) \tag{3.3a}$$

$$\nu_2 \frac{dA_2}{dt} = (M - M_{c2})A_2 - f_2(A_1, A_2) \tag{3.3b}$$

where f_1, f_2 are nonlinear functions of their arguments, and $f_1(0,0) = f_2(0,0) = 0$. Clearly, near these aspect ratios, more steady solutions exist to eq. (3.3) then in the case of a simple mode, and the behavior is more complex.

We have derived the forms of eqs. (3.3) for finite amplitude Marangoni convection in cylinders and boxes, and have determined completely the steady solutions and their stability. We discuss in detail here the results for the cylindrical containers. Results for the rectangular box are similar in many ways.

A nonlinear theory of convection is developed so that at each aspect ratio a of the cylinder, we can compute the whole fluid and temperature field. As long as $m \neq 0$ so the convection is non-axisymmetric, we find that the instability is supercritical i.e. even when disturbances of conduction become larger, there is no sustained convection for $M < M_c(a)$. However, when $m = 0$ and the convection is axisymmetric, we find a range of subcritical convection at $M < M_c(a)$ as long as the disturbance level is large enough. The theory for $m = 0$ also distinguishes the flow direction at the cylinder center. It rises in the center when the Prandtl number Pr of the fluid satisfies $Pr \geq 1$ and descends in the center of Pr is small.

There is a special value a_A of the aspect ratio a where two distinct instability modes, $m = 1$ and $m = 2$, of linear theory are equally likely. In this case our nonlinear theory can be applied for, say, a near a_A, and predictions can be made for fixed a and for M increasing above M_c. We find very interesting phenomena. For $a > a_A$, the linearized prediction (at $M = M_c$) of convection is mode $m = 2$. Then, as M is raised, there can be a sudden transition to $m = 1$ convection and possibly time-periodic motion. Alternatively, the mode $m = 2$ can persist. On the other hand for $a < a_A$, the linearized prediction (at $M = M_c$) of convection is mode $m = 1$ and the nonlinear theory shows that mode $m = 1$ must be replaced by mode $m = 2$. We thus see a lack of symmetry in the behavior on the two sides of $a = a_A$.

There is a special value of a_B of the aspect ratio a where two distinct instability modes, m = 2 and m = 0, of linear theory are equally likely. For $a > a_B$, linearized theory gives axisymmetric convection as preferred. Our nonlinear theory shows that this convection is subcritical (i.e. occurs at $M < M_c$). As M is increased, there is a tendency to remain on the axisymmetric mode with no further transition though m = 2 convection can exist under certain conditions. On the other hand, when $a < a_B$, there is a very complicated sequence of transitions predicted. At the neutral curve ($M = M_c$) linearized theory states that mode m = 2 appears. However, nonlinear theory gives the following result. As M is increased above M_c, mode m = 2 convection begins. As M is increased further, this mode m = 2 becomes unstable and there is a sudden transition to the axisymmetric mode m = 0 which then persists for increasing M. However, if M now decreases below M_c there would be a sudden transition not to the mode m = 2 but to pure conduction. Hence, there can be dynamic hysteresis loops in this case. Notice again the lack of symmetry for $a > a_B$ and $a < a_B$. The behaviors are quite different.

These behaviors are predicted to occur for Marangoni convection, but not for buoyancy-driven convection. In all our nonlinear work we have neglected buoyancy by setting the Rayleigh number R = 0 and have examined pure Marangoni convection $M \neq 0$. Rosenblat, in an independent study, has examined the complementary problem of pure buoyancy driven convection, $R \neq 0$, M = 0, in a cylinder. He finds linear stability curves similar to those obtained here. He analyzes the nonlinear theory and finds the following behaviors. All modes of convection, including the mode m = 0, bifurcate supercritically. Near intersections, the transitions for R increasing are always symmetric in the sense that on either side, the mode predicted by linear theory (at $R = R_c$) suddenly become unstable (at $R > R_c$) to mixed

modes composed of the modes at the intersection point. Hence, there is no subcritical instability, no lack of symmetry near intersections and no dynamical hysteresis.

Comparison of the above two sets of predictions is crucial for evaluation of possible space experiments since under micro-gravity conditions the first behaviors should occur,while for thick layers on Earth, buoyancy dominates and the second behaviors should occur.

The structure of this report is as follows. Chapter I gives the full analysis for convection in circular cylinders. This includes discussion of previous work, formulation of the governing equations and boundary conditions, linear and nonlinear stability theory, and finally discussion of the physical implications of the theory. Chapter II gives the parallel development for convection in rectangular cylinders. Certain mathematical details are postponed to Appendices. Thus, all Tasks required by the contract are fulfilled though in a different order than specified. The structure was chosen in order to emphasize the physical understanding of the phenomena. All aspects of the circular geometry are completed first. Then all aspects of the rectangular geometry are examined.

CHAPTER I. CONVECTION IN CIRCULAR CYLINDERS

1. INTRODUCTION

Consider a uniform layer of liquid having infinite horizontal extent, bounded on the bottom by a solid plate and having a free surface on the top. When the plate is heated with respect to the gas at the free surface, a purely conductive static state may exist, in which β is the (constant) magnitude of the temperature gradient. If the free surface possesses surface tension σ, the variations $\sigma(T)$ of surface tension with temperature T can induce Marangoni instability. This thermocapillary instability was identified and explained by Pearson (1958) who showed, using a linear stability theory, that a critical value of Marangoni number M must be exceeded before the conductive state becomes unstable. Here,

$$M = \frac{\left|\frac{d\sigma}{dT}\right|_0 \beta d^2}{\kappa_0 \mu_0} \tag{1.1}$$

where $\frac{d\sigma}{dT}$ is the (negative) rate of change of surface tension with temperature, the subscript zero denoting a constant value at a given reference temperature T_0, d is the thickness of the undisturbed layer; κ_0 and μ_0 are the thermal diffusivity and dynamic viscosity of the liquid, respectively.

The critical value M_c of M depends on other parameters: the surface Biot number h, which is the non-dimensional version of the heat transfer coefficient at the free surface, and a capillary number C, which is a non-dimensional version of the mean surface tension $\sigma_0 \equiv \sigma(T_0)$. Here

$$C = \mu_0 \kappa_0 / \sigma_0 d \quad . \tag{1.2}$$

Pearson (1958) limited his analysis to $C \to 0$, which means that the free surface does not deform as a result of disturbances. He finds, for $h = 0$ and a perfectly conducting lower boundary, $M_c \approx 79.6$ in the absence of gravity.

When a vertical gravity field is present, so that the layer is heated from below, Nield (1964) shows, using Pearson's model, that buoyancy-induced instabilities and thermocapillary instabilities reinforce on another.

Since the work of Pearson and Nield, linear stability theory on the Marangoni convection problem has been extended in several directions to include two dynamical phases, $C \neq 0$, and further effects of an imposed vertical gravity field; Scriven and Sternling (1964), Smith (1966), Zeren and Reynolds (1972). A recent survey, Sørensen (1978), discusses these as well as many other extensions. Palmer and Berg (1971) find that the theory of Nield (1964) predicts well the experimental conditions for the onset of convection in shallow layers.

As in the case of Rayleigh-Bénard convection due to buoyancy effects, the horizontal planform of the convective state and the amplitude of the motion (and heat transfer) are undetermined by linear stability theory. In addition as in Rayleigh-Bénard convection, the critical point M_c, corresponding to the critical horizontal wave number, is infinitely degenerate; there are an infinite number of planforms allowable by linear theory. Nonlinear effects presumably select from this set those that appear in experiments. The first nonlinear analysis of Marangoni instability is due to Scanlon and Segel (1967). They consider an infinite-Prandtl-number fluid, an infinity-deep layer and only <u>two</u> planform functions from the infinite set. Their prediction is that hexagonal-cells is the only planform that exists and is stable when the conductive state becomes unstable. Hexagons exist and are stable for an interval of $M < M_c$ so that subcritical convection is predicted. They do not attempt to enlarge the set of planform functions beyond the chosen two. However, their prediction is in qualitative accord with experimental observations. Koschmieder (1967)

always finds very regular hexagons in shallow layers, the regularity stemming from the precise thermal controls used. These pictures should be compared with those of Bénard (1900) who finds irregular, polygonal cells in convection dominated by thermocapillarity.

The only other nonlinear analysis of Marangoni instability is due to Kraska and Sani (1979). They consider six planform functions (including those of Scanlon and Segel) and also complete a nonlinear analysis. However, they encounter difficulties in analyzing the stability of their nonlinear states and find a lack of closure in adding any seventh state to the original six. These difficulties may be related to the adjoint operator they define, which seems not to be appropriate to the problem.

All of the above work is stimulated by the recognition that Marangoni instability is the prototype instability associated with the transport of heat and/or mass across interfaces. The presence of such instabilities can augment the transport rates by orders of magnitude compared to that of pure conduction. Particular aspects of these transport processes have motivated many of the generalizations mentioned above.

In recent years there has been a new interest in flows driven by thermocapillary forces. With the advent of Spacelab research, there is the possibility of performing fluid mechanics experiments in space. The micro-gravity environment allows interfacial forces to dominate gravity so that one may be able to design experiments that focus on effects submerged on Earth by gravitational effects. The present work is motivated by such considerations.

There are special difficulties in microgravity environments. These are illustrated in Figure 1.

Figure 1

Here, a mass of liquid is placed in a wide dish. On Earth, as shown in Fig. 1a, the liquid fills the dish nearly uniformly except for small menisci near the edges. A meniscus has a width W that scales as $B^{-\frac{1}{2}}d$ where B is the Bond number,

$$B = \rho_0 g d^2/\sigma_0 \quad , \tag{1.3}$$

ρ_0 is the liquid density and g is the gravitational potential. Thus on Earth W is usually a fraction of d, whereas for gravity at 10^{-6}g, the meniscus "fills the whole dish", as shown in Fig. 1b. Alternatively, depending upon the liquid volume, the contact angle and the wetting properties of the solid, the liquid mass might form in to a sessile drop or sphere or be detached entirely from the container as shown in Figures 1c and 1d. Thus, any Marangoni instability study to be applied to microgravity conditions must allow for the experimental necessity of near-by, confining sidewalls. Figure 2a shows a possible configuration of the free surface when the aspect ratio is near unity. The sidewalls help to both confine the liquid and limit the degree of curvature of the free surface.

Figure 2

In the present studies we address the problem of Marangoni instabilities in a cylinder. Our particular interest is to explore the nonlinear interactions near $M = M_c$ and in particular transitions from one convective state to another that may occur at supercritical conditions. Given the difficulty of such a study, we make several simplifying assumptions. (i) We let the capillary number $C \to 0$. Hence, the top free surface is non-deformable. In addition, we take the contact angle at the sidewalls to be compatible with a flat free surface. Thus, in the basic, conductive state there are no menisci and in the convective state the free surface remains flat (Figure 2b). (ii) In order to allow the linear stability theory to be solved using normal modes (separation of variables), we idealize the sidewall boundary conditions in the following way. The sidewalls consist of a circular cylinder through which there is zero heat flux and zero mass flow. However, we allow the walls to be "slippery" so that rather than the no-slip condition, we apply the conditions of zero tangential vorticity. Clearly, such an idealization modifies the predictions of a theory. We shall discuss in detail some implications of this idealization and suggest how results of such a theory should be applied.

In the language of bifurcation theory, we study the perfect problem. Imperfections due to horizontal temperature gradients or free-surface deflections will not be treated here. Note that the change from "slippery" to no-slip sidewalls is <u>not</u> an imperfection .

Given the model described, we shall find the nonlinear Marangoni convective-states and determine their stability. Clearly, the presence of the sidewall makes the spectrum at $M = M_c$ discrete so that the complete behavior can be examined. Of course, hexagonal cells for small containers will never appear, since the allowable cell shapes are dominated by the sidewall constraints.

We obtain its behavior, its amplitude and hence can find all transport quantities of the convection. At certain aspect ratios two linearized modes are equally likely at critical conditions. We analyze such double eigenvalues and find certain strong behaviors. The transitions as M is increased for aspect ratios on one side of the double eigenvalues, differ substantially from those on the other side of the double eigenvalue. Such a demarcation of behaviors should be characteristic of the nonlinearities and hence should be observable in an experiment.

The technique of nonlinear stability theory we use is due to Rosenblat (1979), who makes an eigenfunction expansion of the nonlinear problem. This "infinite-matrix" form is systematically simplified by defining a new small parameter related to the separation of the eigenvalues of the matrix. The results coincide with the usual waekly nonlinear bifurcation theory very near M_c, but gives a wider range of validity. It is the wider range that allows us to predict the successive transitions.

2. FORMULATION

Consider a viscous liquid, which partially fills a cylindrical container of circular cross-section. The mean depth of the liquid is d, and the radius of the cylinder is taken to be ad, so that the mean aspect ratio (ratio of radius to mean depth) is a. The axis of the cylinder is anti-parallel to the direction of gravity, and the upper surface of the liquid is open to an ambient gas.

The liquid is assumed to be Newtonian, to have constant viscosity μ_0 and to be heat conducting with constant thermal diffusivity κ_0. The density ρ^* of the liquid is taken to vary with the temperature T^* according to the equation of state

$$\rho^* = \rho_0[1 - \alpha(T^* - T_0)] \tag{2.1}$$

where ρ_0, T_0 are constant reference density and temperature respectively, and where α is the coefficient of volumetric expansion. The liquid-gas interface has a surface tension σ^* which varies with temperature according to the formula

$$\sigma^* = \sigma_0 - \sigma_1(T_s^* - T_0) \tag{2.2}$$

where σ_0, σ_1 are constants and T_s^* is the temperature at the interface.

The Boussinesq approximation is assumed; the governing equations in the bulk of the liquid are the Navier-Stokes, continuity and energy-balance equations:

$$\rho_0\left[\frac{\partial \underline{v}^*}{\partial t^*} + (\underline{v}^*\cdot\nabla^*)\underline{v}^*\right] = \nabla^*\cdot\underline{\tau}^* - \rho^* g\hat{z} \tag{2.3}$$

$$\nabla^*\cdot\underline{v}^* = 0 \tag{2.4}$$

$$\frac{\partial T^*}{\partial t^*} + (\underline{v}^*\cdot\nabla^*)T^* = \kappa_0\nabla^{*2}T^* \tag{2.5}$$

where $\underline{v}^*$ is the velocity vector, g is the acceleration due to gravity, $\underline{\tau}^*$ is the stress tensor, $\hat{z}$ is a unit vector in the upward vertical direction, and t^*, ∇^* refer to dimensional time and space derivatives respectively. For a Newtonian liquid the stress tensor has the form

$$\underline{\tau}^* = -p^*\underline{I} + \mu_0[\nabla^*\underline{v}^* + (\nabla^*\underline{v}^*)^T] \tag{2.6}$$

where p^* is the pressure and $\underline{I}$ is the identity tensor.

We shall work in a cylindrical polar coordinate system, with the origin at the center of the lower circular boundary. The mean height of the liquid is located at $z^* = d$, and the lateral boundary at $r^* = ad$.

The lower boundary is at $z^* = 0$ and is assumed to be a rigid, perfectly conducting plane. Thus, we have

$$T^* = T_0 + \beta d \quad \text{on} \quad z^* = 0 \tag{2.7a}$$

and

$$\underline{v}^* = \underline{0} \quad \text{on} \quad z^* = 0 \tag{2.7b}$$

where we shall take $\beta > 0$.

The upper boundary is a free surface, denoted S, which is cooled by heat transfer to the gas. We take the heat transfer relationship to have the form

$$-\underline{n}\cdot\nabla^*T^* = h^*(T^* - T_0) + \beta \quad \text{on} \quad S \tag{2.8a}$$

where $\underline{n}$ is unit normal to S directed into the gas, and h^* is the heat transfer coefficient. We write

$$S: \; z^* = d^* + \eta^*(\underline{r}_1^*, t^*), \tag{2.9}$$

where $\underline{r}_1^*$ denotes position vector in the horizontal plane, so that the kinematic boundary condition takes the form

$$-\frac{\partial \eta^*}{\partial t^*} + \underline{v}^*\cdot\nabla^*(z^* - d^* - \eta^*) = 0 \quad \text{on} \quad S. \tag{2.8b}$$

Finally, we have the dynamic (stress) boundary conditions, which are

$$\underline{\underline{\tau}}^*\cdot\underline{n} = 2H^*\sigma^*\underline{n} - \underline{n}\times(\underline{n}\times\nabla^*\sigma^*) \quad \text{on} \quad S \tag{2.8c}$$

where H^* is the mean curvature of the surface. Equation (2.8c) expresses the fact that the stress tensor experiences a jump in the normal direction due to

surface tension and a jump in the tangential direction due to (thermally-induced) variations in surface tension.

The lateral boundary S_L is assumed to be adiabatic. This give the condition

$$\nabla^* T^* \cdot \underline{n}_L = 0 \quad \text{on} \quad S_L \tag{2.10a}$$

where $\underline{n}_L$ is unit normal vector in the outward direction. If the boundary were rigid we would have $\underline{v}^* = \underline{0}$ there. However, as explained in the Introduction, we take instead the idealized, mathematically simpler condition that the sidewall is a nondeformable surface on which the tangential vorticity is zero. Nondeformability implies that S_L coincides with $r^* = ad$, $0 < z^* < d + \eta^*$, and we have the conditions

$$\underline{v}^* \cdot \underline{n}_L = 0 \quad \text{on} \quad S_L \tag{2.10b}$$

and

$$\underline{n}_L \times (\underline{n}_L \times \nabla^* \times \underline{v}^*) = \underline{0} \quad \text{on} \quad S_L. \tag{2.10c}$$

To close the system we require a condition at the contact line where the free surface meets the sidewall. In this paper we shall assume the contact angle to be fixed at the value $\pi/2$, so that we have the condition

$$\nabla^* \eta^* \cdot \underline{n}_L = 0. \tag{2.11}$$

An equilibrium solution of the system (2.1)-(2.11) is the following:

$$\underline{v}^* = \underline{0}, \quad T^* = \bar{T} = T_0 + \beta(d - z^*) \quad ,$$

$$\rho^* = \bar{\rho} = \rho_0 \{1 - \alpha\beta(d - z^*)\} \quad , \quad \sigma^* = \sigma_0, \quad \eta^* = 0, \quad (2.12)$$

$$\underline{\underline{T}}^* = \bar{\underline{\underline{T}}} = \rho_0 g d \{(z^*/d - 1) + \tfrac{1}{2}\alpha\beta d(z^*/d - 1)^2\}\underline{\underline{I}}.$$

This is the conduction solution, whose stability we propose to examine. The gas pressure has here been set equal to zero. Note that the liquid-gas interface is flat, and that the temperature at the upper boundary is T_0, which implies that β is the vertical temperature gradient.

We now perturb the basic state (2.12), and at the same time introduce appropriate dimensionless forms of the equations and boundary conditions. We scale lengths on the depth d, and write

$$r = r^*/d \quad , \quad z = z^*/d \quad , \quad \eta = \eta^*/d \qquad (2.13)$$

with $\underline{r} = (r, \phi, z)$ in cylindrical polar coordinates. Unit vectors in the corresponding directions will be denoted $(\hat{\underline{r}}, \hat{\underline{\phi}}, \hat{\underline{z}})$. The liquid occupies the region $0 \leq r < a$, $0 < z < 1 + \eta$ in this dimensionless coordinate system; the equation of the free surface S is

$$z = 1 + \eta(\underline{r}_1, t) \qquad (2.14)$$

where $\underline{r}_1$ is dimensionless position vector in the horizontal plane and t is dimensionless time, defined below; the lateral boundary S_L is $r = a$, $0 < z < 1 + \eta$.

Since our interest is focussed on motions driven by surface-tension gradients, it is appropriate to base velocities on the Marangoni velocity scale V_M, defined by

$$V_M = \sigma_1 \beta d/\mu_0. \tag{2.15}$$

The time-scale will then be d/V_M, so that we write

$$t = t^* V_M/d. \tag{2.16}$$

We now introduce the following representations:

$$\underline{v}^* = V_M \underline{v} = V_M(u, v, w)$$

$$T^* = \bar{T} + \beta d\theta \quad = T_0 + \beta d(1 - z + \theta)$$

$$p^* = \bar{p} - \alpha\rho_0 \beta d\theta \quad = p_0 - \alpha\rho_0 \beta d(1 - z + \theta) \tag{2.17}$$

$$\sigma^* = \sigma_0 + \sigma_1 \beta d(\eta - \theta)$$

$$\underline{\tau}^* = \bar{\underline{\tau}} + (\mu_0 V_M/d)\underline{\tau} = \rho_0 g d \left\{(z - 1) + \frac{1}{2}\alpha\beta d(z - 1)^2\right\}\underline{I} + (\mu_0 V_M/d)\underline{\tau},$$

where the perturbation field quantitites θ, $\underline{v}$ and $\underline{\tau}$ are functions of $\underline{r}$ and t, and where the forms of p^* and σ^* derive directly from (2.1) and (2.2) respectively. The stress tensor $\underline{\tau}$ can be written in the form

$$\underline{\tau} = -p\underline{I} + [\nabla\underline{v} + (\nabla\underline{v})^T] \tag{2.18}$$

where p is the pressure.

We substitute (2.13)-(2.18) into the governing equations and boundary conditions (2.1)-(2.11). The equations in the bulk of the liquid for the perturbation field quantities are found to be

$$Pr^{-1}M\left\{\frac{\partial \underline{v}}{\partial t} + (\underline{v}\cdot\nabla)\underline{v}\right\} = -\nabla p + \nabla^2\underline{v} + M^{-1}R\theta\hat{\underline{z}} \tag{2.19}$$

$$\nabla\cdot\underline{v} = 0 \tag{2.20}$$

$$M\left\{\frac{\partial\theta}{\partial t} - w + (\underline{v}\cdot\nabla)\theta\right\} = \nabla^2\theta \tag{2.21}$$

where the parameters appearing here are

Marangoni number
$$M = \frac{V_M d}{\kappa_0} = \frac{\sigma_1 \beta d^2}{\mu_0 \kappa_0} \tag{2.22a}$$

Rayleigh number
$$R = \frac{\alpha\beta g d^4 \rho_0}{\mu_0 \kappa_0} \tag{2.22b}$$

Prandtl number
$$Pr = \frac{\mu_0}{\rho_0 \kappa_0} . \tag{2.22c}$$

The boundary conditions are as follows. On the lower horizontal boundary, equations (2.7) reduce to

$$\theta = 0 \quad \text{on} \quad z = 0, \qquad 0 \le r \le a, \tag{2.23a}$$

$$\underline{v} = \underline{0} \quad \text{on} \quad z = 0, \qquad 0 \le r \le a. \tag{2.23b}$$

On the upper surface S, given now by (2.14), the heat loss condition (2.8a) becomes

$$\underline{n}\cdot\nabla\theta = \underline{n}\cdot\hat{\underline{z}} - 1 - h(\theta - \eta) \quad \text{on} \quad S \tag{2.24a}$$

where

$$h = h^{*}d \tag{2.22d}$$

is the surface Biot number. The kinematic condition (2.8b) becomes

$$\frac{\partial \eta}{\partial t} + u\frac{\partial \eta}{\partial r} + \frac{v}{r}\frac{\partial \eta}{\partial \phi} - w = 0 \quad \text{on} \quad S. \tag{2.24b}$$

It is convenient to decompose the stress condition (2.8c) into an equation normal to the surface and an equation tangential to the surface. If we write normal and tangential components as

$$(\underline{\underline{\tau}}\cdot\underline{n})_n \equiv (\underline{\underline{\tau}}\cdot\underline{n})\cdot\underline{n}, \qquad (\underline{\underline{\tau}}\cdot\underline{n})_{ta} \equiv (\underline{\underline{\tau}}\cdot\underline{n}) - [(\underline{\underline{\tau}}\cdot\underline{n})\cdot\underline{n}]\underline{n},$$

we obtain the dynamic surface conditions

$$G(\eta + \tfrac{1}{2}\alpha\delta T\eta^2) + MC(\underline{\underline{\tau}}\cdot\underline{n})_n - 2H\{1 + MC(\eta - \theta)\} = 0 \quad \text{on} \quad S \tag{2.24c}$$

and

$$(\underline{\underline{\tau}}\cdot\underline{n})_{ta} + \underline{n}\times\{\underline{n}\times\nabla(\eta - \vartheta)\} = 0 \quad \text{on} \quad S \tag{2.24d}$$

where $H = H^{*}d$ is dimensionless mean curvature, and where the two new parameters appearing here are

$$\underline{\text{Bond number}} \qquad G = \frac{\rho_0 g d^2}{\sigma_0} \tag{2.22c}$$

capillary number $$C = \frac{\mu_0 \kappa_0}{\sigma_0 d}. \tag{2.22f}$$

On the lateral boundary S_L we have that $\underline{n}_L = \hat{\underline{r}}$. Hence the boundary conditions (2.10) become

$$\frac{\partial \theta}{\partial r} = 0 \quad \text{on} \quad S_L \tag{2.25a}$$

$$u = 0 \quad \text{on} \quad S_L \tag{2.25b}$$

$$\frac{\partial}{\partial r}(rv) = \frac{\partial w}{\partial r} = 0 \quad \text{on} \quad S_L. \tag{2.25c}$$

The contact-angle condition (2.11) becomes

$$\frac{\partial \eta}{\partial r} = 0 \quad \text{on} \quad r = a. \tag{2.26}$$

Finally, we recall the stipulation that the mean depth of the liquid is d. This is effectively a condition of volume conservation and can be expressed as

$$\int_0^a \int_0^{2\pi} r\eta(r, \varphi, t)\, d\varphi\, dr = 0. \tag{2.27}$$

The problem to be studied comprises the system of equations (2.19)-(2.21), together with the conditions (2.23)-(2.27). There are six parameters M, R, Pr, G, h and C, defined by equations (2.22); the aspect ratio a is a parameter of the problem.

For our purposes the principal parameter is the Marangoni number M,

which measures the effect of surface-tension gradients. We shall determine M_c, the critical value of M at which the conduction solution becomes unstable, as a function of the other parameters, that is,

$$M_c = M_c(R, Pr, G, C, h, a). \tag{2.28}$$

We shall then investigate the properties of the convection as M increases above M_c for various values of the other parameters.

3. ZERO CAPILLARY NUMBER LIMIT

In this paper we shall confine our analysis to the case where the capillary number C is zero. The capillary number is associated with deflection of the free surface; the limit $C \to 0$ corresponds to a flat surface, Davis and Homsy (1980), a restriction which enables onset of convection to be analyzed relatively simply. In this limit equation (2.24c) reduces to

$$G(\eta + \tfrac{1}{2}\alpha\beta d\eta^2) - 2H = 0 \tag{3.1}$$

where the standard definition of the mean curvature H is given by

$$2H = \nabla_1 \cdot \left[\frac{\nabla_1 \eta}{[1+(\nabla_1 \eta)^2]^{1/2}}\right] \tag{3.2}$$

(∇_1 being the gradient in the horizontal plane). Equation (3.1) is thus a differential equation for the surface deflection $\eta = \eta(r, \varphi, t)$, which is required to satisfy the conditions (2.26) and (2.27). A solution is clearly

$$\eta \equiv 0, \tag{3.3}$$

representing an undeformed free surface. The fact that there can be no other solution in the class of functions η with $|\eta|$ sufficiently small is easily established with the aid of the implicit function theorem. We confine our attention to these weakly-nonlinear interactions that apply when M is close to M_c and when convective motions are of small amplitude.

On the basis of this reasoning we infer that the upper free surface remains flat and undeformed. The equation of S is now $z = 1$, $0 < r < a$, and the outward unit normal to it is $\underline{n} = \hat{\underline{z}}$. The lateral boundary S_L is $r = a$, $0 < z < 1$. The problem to be solved in the limit $C \to 0$ therefore comprises the equations (2.19)-(2.21) in the bulk of the liquid, together with boundary conditions as follows. On the lower boundary the conditions are (2.23) or, equivalently,

$$\theta = u = v = w = 0 \quad \text{on } z = 0, \qquad 0 < r < a. \tag{3.4}$$

On the upper free surface (2.24a) reduces to

$$\frac{\partial \theta}{\partial z} + h\theta = 0 \quad \text{on} \quad z = 1, \qquad 0 < r < a \tag{3.5a}$$

while (2.24b) becomes simply

$$w = 0 \quad \text{on} \quad z = 1, \qquad 0 < r < a. \tag{3.5b}$$

In view of (3.3) the condition (2.24c) is redundant. We simplify (2.24d) by noting that

$$(\underline{\underline{\tau}} \cdot \underline{n})_{tg} = \left[\frac{\partial u}{\partial z} + \frac{\partial w}{\partial r}\right]\hat{\underline{r}} + \left[\frac{\partial v}{\partial z} + \frac{1}{r}\frac{\partial}{\partial \phi}(rw)\right]\hat{\underline{\phi}}$$

and that

$$\underline{n} \times (\underline{n} \times \nabla\vartheta) = -\frac{\partial\theta}{\partial r}\,\hat{\underline{r}} - \frac{1}{r}\frac{\partial\theta}{\partial\phi}\,\hat{\underline{\phi}}.$$

Hence (2.24d) can be decomposed into the two conditions

$$\frac{\partial u}{\partial z} + \frac{\partial\theta}{\partial r} = 0 \quad \text{on} \quad z = 1, \qquad 0 < r < a \tag{3.5c}$$

and

$$\frac{\partial v}{\partial z} + \frac{1}{r}\frac{\partial\theta}{\partial\phi} = 0 \quad \text{on} \quad z = 1, \qquad 0 < r < a. \tag{3.5d}$$

The lateral boundary conditions (2.25) are

$$\frac{\partial\theta}{\partial r} = u = \frac{\partial}{\partial r}(rv) = \frac{\partial w}{\partial r} = 0 \quad \text{on} \quad r = a, \qquad 0 < z < 1. \tag{3.6}$$

In summary, therefore, we are required to solve the equations (2.19)-(2.21) subject to the boundary conditions (3.4)-(3.6). With $C = 0$ and the Bond number G no longer appears, Davis and Homsy (1980), so we have in place of (2.28) the dependence

$$M_c = M_c(K, Pr, h, a) \tag{3.7}$$

for the critical Marangoni number.

4. LINEAR STABILITY PROBLEM

The critical Marangoni number at which the conduction solution loses stability is determined from linearization of the system (2.19)-(2.21) together with the (linear) boundary conditions (3.4)-(3.6). Although this linear problem is not self-adjoint, we assume the validity of the principle of exchange of stabilities, namely that the growth rate of the most dangerous disturbance changes from real and negative to real and positive as M increases through its critical value. Vidal and Acrivos (1966) show for the linear problem on the infinite layer that this is true and so we apply the same result to our case.

When the principle of exchange of stabilities holds, the governing equations for the linear stability problem at criticality are

$$\nabla^2 \underline{v} - \nabla p + M^{-1} R \theta \hat{\underline{z}} = 0 \tag{4.1}$$

$$\nabla \cdot \underline{v} = 0 \tag{4.2}$$

$$\nabla^2 \theta + Mw = 0 \tag{4.3}$$

subject to the boundary conditions (3.4)-(3.6). We apply the operator curl curl to equation (4.1) and then take the z-component of the resultant equation, we obtain

$$\nabla^4 w + M^{-1} R \nabla_1^2 \theta = 0 \tag{4.4}$$

where ∇_1^2 is the planform Laplacian. Thus (4.3) and (4.4) constitute a pair of equations for the unknown functions w and θ. The appropriate boundary

conditions are determined by simplifying (3.4)-(3.6); they are found to be

$$\theta = w = \frac{\partial w}{\partial z} = 0 \quad \text{on} \quad z = 0, \qquad 0 < r < a, \tag{4.5}$$

$$\frac{\partial \theta}{\partial z} + h\theta = w = \frac{\partial^2 w}{\partial z^2} - \nabla_1^2 \theta = 0 \quad \text{on} \quad z = 1, \qquad 0 < r < a, \tag{4.6}$$

$$\frac{\partial \theta}{\partial r} = \frac{\partial w}{\partial r} = 0 \quad \text{on} \quad r = a, \qquad 0 < z < 1. \tag{4.7}$$

The system (4.3)-(4.4) reduces to a pair of ordinary differential equations through separation of variables. It was in order to effect this reduction that we introduced the artificial condition on the vorticity at the lateral boundary. We put

$$\begin{aligned} w(r, \phi, z) &= \cos m\phi \, J_m(\lambda r) Y(z) \\ \theta(r, \phi, z) &= \cos m\phi \, J_m(\lambda r) X(z) \end{aligned} \tag{4.8}$$

where $m = 0, 1, 2, \ldots$ is the azimuthal wave number, J_m is the Bessel function of order m, and $\lambda > 0$ is determined by the equation

$$J_m'(\lambda a) = 0. \tag{4.9}$$

The condition (4.9) ensures that the lateral boundary conditions (4.7) are both satisfied. Substituting (4.8) into (4.3)-(4.6) we obtain the equations

$$(D^2 - \lambda^2)X + MY = 0, \qquad (D^2 - \lambda^2)^2 Y - M^{-1} R \lambda^2 X = 0 \tag{4.10}$$

where D denotes differentiation with respect to z, with boundary conditions

$$X = Y = DY = 0 \quad \text{on} \quad z = 0 \tag{4.11}$$

and

$$DX + hX = Y = D^2Y + \lambda^2 X = 0 \quad \text{on} \quad z = 1. \tag{4.12}$$

Apart from notation, the boundary-value problem (4.10)-(4.12) is identical with that solved by Nield (1964) in his determination of the critical Marangoni number for a layer of unbounded horizontal extent. The difference between Nield's problem and the one presently under consideration lies in the significance of the parameter λ: for the unbounded layer λ is wave number in the horizontal plane and can assume all real values, whereas for the finite cylinder λ is restricted to the set of values defined by (4.9).

Nield (1964) solved (4.10)-(4.12) by expanding in Fourier sine series on the interval (0, 1); complete details of the calculations can be found in the cited paper and are accordingly omitted here. It suffices to observe that the system (4.10)-(4.12) contains the four parameters M, R, λ and h, so that nontrivial solutions exist if and only if a functional relationship of the form

$$\Phi(M, R, \lambda, h) = 0 \tag{4.13}$$

holds among these parameters. Nield (1964) obtained an explicit representation of (4.13), namely

$$M = M(R, \lambda, h) = W/U \tag{4.14}$$

where W, U are given by

$$W = (1 + h + 2\lambda^2 \sum_{n=1}^{\infty} \frac{d_n^2 - R}{\Delta_n}) \sum_{n=1}^{\infty} \frac{(n\pi)^2 d_n}{\Delta_n} + 2R\lambda^2 \left(\sum_{n=1}^{\infty} \frac{(n\pi)^2 \cos n\pi}{\Delta_n} \right)^2, \tag{4.15}$$

$$U = 2\lambda^2 \sum_{n=1}^{\infty} \frac{(n\pi)^2}{\Delta_n} \cdot \sum_{n=1}^{\infty} \frac{(n\pi)^2 d_n}{\Delta_n} - 2\lambda^2 \sum_{n=1}^{\infty} \frac{(n\pi)^2 \cos n\pi}{\Delta_n} \cdot \sum_{n=1}^{\infty} \frac{(n\pi)^2 d_n \cos n\pi}{\Delta_n}, \tag{4.16}$$

with

$$d_n \equiv (n\pi)^2 + \lambda^2 \tag{4.17}$$

and

$$\Delta_n \equiv d_n^2 - R\lambda^2. \tag{4.18}$$

It is convenient to write (4.9) in the form

$$J_m'(s_{mi}) = 0, \qquad \lambda_{mi} = s_{mi}/a \tag{4.19}$$

where s_{mi} denotes the i-th positive zero of J_m'. Thus the integer $i = 1, 2, 3, \ldots$ can be regarded as effectively a <u>radial wave number</u>, and the functional form of (4.14) is

$$M = M(R, h, a, m, i). \tag{4.20}$$

The critical Marangoni number for fixed R, h and a is then defined to be

$$M_c = M_c(R, h, a) = \min_{m,i} M(R, h, a, m, i). \qquad (4.21)$$

Computations of the Marangoni number as a function of the other parameters have been performed using the formulae (4.14)-(4.16), the Fourier series, of course, being suitably truncated. In general it was found that 4-digit accuracy could be achieved with 10 terms. Figure 3 shows the variation of M with aspect ratio a for fixed values R = 0, h = 0, and for the six wave-number pairs m = 0, 1, 2, 3, 4, i = 1 and m = 1, i = 2. These six were chosen because for moderate aspect ratios, $0 < a < 2.5$ approximately, the critical Marangoni number occurs for one or other of them. We see from Figure 3 that m = 1, i = 1 is the critical wave-number pair for small aspect ratios, $a < 1.15$. On the interval $1.15 < a < 1.65$ (approximately) the critical mode has m = 2, i = 1, and with further increase in aspect ratio this is replaced by the axisymmetric mode m = 0, i = 1 on $1.65 < a < 1.9$. Next, the mode m = 3, i = 1 is critical in $1.9 < a < 2.3$, while for $2.3 < a < 2.5$ the modes m = 4, i = 1 and m = 1, i = 2 give nearly the same numerical value of the Marangoni number.

Figure 3

The ordering of critical modes just described is retained for other values of R and h. In fact, this ordering is a direct consequence of the ordering of the numbers s_{mi} defined by (4.19), which is in turn a consequence of the sidewall boundary conditions; it is not surprising, therefore, that it should be invariant with respect to other physical parameters.

Figure 4 illustrates the variation of critical Marangoni number M_c with aspect ratio a for different value of Rayleigh number R, and at a fixed value h = 0. These curves show that M_c decreases as R increases for each value of a. Although not illustrated, computations show that the same behavior (M_c decreasing with increasing R) occurs when $h \neq 0$.

Figure 4

Figure 5 depicts the variation of M_c with a for various values of surface Biot number h, and at the fixed value R = 0. We see that M_c increases with h at each value of a. Computations show the same tendency at non-zero value of Rayleigh number

Figure 5

The general pattern of behavior described here is consistent with that obtained by Nield (1964) for an unbounded layer.

5. EIGENFUNCTION EXPANSIONS

We propose to study the nonlinear stability problem by means of a modified Galerkin procedure. We represent the field quantities by series of functions of the spatial variables, with time-dependent coefficients. Following a suggestion of Eckhaus (1965), we shall take as the basis functions the eigenfunctions of the linear stability problem. The time-dependent coefficients will then effectively be the amplitudes of the appropriate convective modes, determined from nonlinear ordinary differential equations to which the governing partial differential equations reduce. The series are truncated in a rational way, according to criteria discussed by Rosenblat (1979).

Galerkin methods require that the function basis of the expansion should consititute a complete set in an appropriate sense. In this regard it can be shown, Appendix A, that the Marangoni number cannot be used as the eigenvalue parameter on which to construct a complete set of eigenfunctions of the linear stability problem. This is because the expression (4.14) gives M as a single-valued funtion of R, other parameters being held fixed, and corresponding to this there will be only a single eigenfunction. On the other hand, if (4.14) is solved for R, the resulting expression has the form

$$R = R(M, h, a, m, i) \tag{5.1}$$

and is not single-valued; in fact there is a countably infinite number of solutions of the form (5.1) to the equation (4.14). In other words, there are infinitely many values of R for each value of M, and correspondingly

infinitely many eigenfunctions.

Although the critical Marangoni number is given correctly by the results of the previous Section, the implication of the foregoing paragraph is that the Rayleigh number is the "true" eigenvalue parameter of the linear stability problem. We need to take this into account in setting up the Galerkin procedure, even though much of the subsequent analysis will become redundant through truncation and approximation.

Let $\hat{M}$ be a fixed value of the Marangoni number and consider the linear eigenvalue problem

$$\nabla^2 \underline{v} - \nabla p + \hat{M}^{-1} R\theta \hat{z} = \underline{0} \tag{5.2}$$

$$\nabla \cdot \underline{v} = 0 \tag{5.3}$$

$$\nabla^2 \theta + \hat{M} w = 0 \tag{5.4}$$

with boundary conditions (3.4)-(3.6), and with the Rayleigh number R regarded as the eigenvalue parameter. Nontrivial solutions of this boundary-value problem exist for certain values of R, denoted R_{mij}, where m is the azimuthal wave number, i is the radial wave number, and $j = 1, 2, 3, \ldots$ is the particular value implied by (5.1). Thus

$$R_{mij} = R_j(\hat{M}, h, a, m, i) \tag{5.5}$$

and we assume the ordering $R_{mi1} < R_{mi2} < \ldots$ for other parameters fixed. Graphs of the functions (5.5) can be found in the paper by Rosenblat, Homsy and

Davis (1981). The integer j is in effect a vertical wave number.

Corresponding to each eigenvalue R_{mij} there is an eigenvector $(\underset{\sim}{v}_{mij}, \theta_{mij})$ of the linear boundary-value problem. The forms of w_{mij} and θ_{mij} are given by (4.8), while the other two velocity components can be calculated from (5.2) and (5.3). The components, which are required in the subsequent computations, are found to be

$$\begin{aligned} u_{mij} &= (1/\lambda_{mi})\cos m\phi\, J_m'(\lambda_{mi} r) DY_{mij}(z) \\ v_{mij} &= (-m/\lambda_{mi}^2 r)\sin m\phi\, J_m(\lambda_{mi} r) DY_{mij}(z) \\ w_{mij} &= \cos m\phi\, J_m(\lambda_{mi} r) Y_{mij}(z) \\ \theta_{mij} &= \cos m\phi\, J_m(\lambda_{mi} r) X_{mij}(z) \end{aligned} \tag{5.6}$$

where X_{mij}, Y_{mij} are the eigensolutions of the boundary-value problem (4.10)-(4.12) with $R = R_{mij}$, $M = \hat{M}$ and $\lambda = \lambda_{mi}$.

The explicit forms of the functions X and Y, and their various derivatives, are obtained from the Fourier series representations of Nield (1964). We omit all details of the calculations but, for the sake of completeness, we list in Appendix B the forms of the functions.

In the modified Galerkin-Eckhaus method to be used below we require also the adjoint eigenfunctions. The system adjoint to (5.2)-(5.4) is easily shown to be

$$\nabla^2 \underset{\sim}{v}^* - \nabla p^* + \hat{M}\theta^* \underset{\sim}{z} = 0 \tag{5.7}$$

$$\nabla \cdot \underline{v}^* = 0 \tag{5.8}$$

$$\nabla^2 \theta^* + \hat{M}^{-1} R w^* = 0 \tag{5.9}$$

with the adjoint boundary conditions

$$\theta^* = u^* = v^* = w^* = 0 \quad \text{on} \quad z = 0, \qquad 0 \leq r < a, \tag{5.10}$$

$$\frac{\partial \theta^*}{\partial z} + h\theta^* + \frac{\partial w^*}{\partial z} = w^* = \frac{\partial u^*}{\partial z} = \frac{\partial v^*}{\partial z} = 0 \quad \text{on} \quad z = 1, \qquad 0 \leq r < a, \tag{5.11}$$

$$u^* = \frac{\partial}{\partial r}(rv^*) = \frac{\partial w^*}{\partial r} = \frac{\partial \theta^*}{\partial r} = 0 \quad \text{on} \quad r = a, \qquad 0 < z < 1. \tag{5.12}$$

These forms are consistent with those of Davis (1969) and Davis and Homsy (1980).

The adjoint problem (5.7)-(5.12) can be solved by the same Fourier series method as the direct problem, and, naturally, the eigenvalues R_{mij} are the same and have the representation (5.5). The adjoint eigenvectors are denoted $(\underline{v}^*_{mij}, \theta^*_{mij})$; a relatively simple calculation gives the following explicit representations:

$$\begin{aligned}
u^*_{mij} &= \lambda_{mi} \cos m\phi \, J'_m(\lambda_{mi} r) DY^*_{mij}(z) \\
v^*_{mij} &= -(m/r) \sin m\phi \, J_m(\lambda_{mi} r) DY^*_{mij}(z) \\
w^*_{mij} &= \lambda^2_{mi} \cos m\phi \, J_m(\lambda_{mi} r) Y^*_{mij}(z) \\
\theta^*_{mij} &= \cos m\phi \, J_m(\lambda_{mi} r) X^*_{mij}(z)
\end{aligned} \tag{5.13}$$

where X^*_{mij}, Y^*_{mij} are eigensolutions of the boundary-value problem

$$(D^2 - \lambda^2)X^* + \hat{M}^{-1}R\lambda^2 v^* = 0, \qquad (D^2 - \lambda^2)^2 Y^* - \hat{M}X^* = 0 \tag{5.14}$$

with boundary conditions

$$X^*(0) = Y^*(0) = DY^*(0) = 0 \tag{5.15}$$

and

$$DX^*(1) + hX^*(1) + \lambda^2 DY^*(1) = Y^*(1) = D^2 Y^*(1) = 0 \tag{5.16}$$

for $R = R_{mij}$. The forms of the funtions X^*, Y^* are given in the Appendix B.

Our purpose is to study the nonlinear evolution of disturbances as the Marangoni number increases through its critical value, and at a fixed Rayleigh number. To simplify the discussion we take henceforth

$$R = 0 \tag{5.17}$$

so that pure Marangoni convection will be examined. As a further simplification, and again without essential loss of generality, we take the surface Biot number $h = 0$. The nonlinear system (2.19)-(2.21) can now conveniently be written in the form

$$\nabla^2 \underline{v} - \nabla p = MPr^{-1}\left[\frac{\partial \underline{v}}{\partial t} + (\underline{v}\cdot\nabla)\underline{v}\right] \tag{5.18}$$

$$\nabla\cdot\underline{v} = 0 \tag{5.19}$$

$$\nabla^2\theta + Mw = M\left\{\frac{\partial\theta}{\partial t} + (\underline{v}\cdot\nabla)\theta\right\} \tag{5.20}$$

and the boundary conditions are (3.4)-(3.6) with h = 0.

We shall solve this problem for values of M close to critical by expanding the field quantities in series of the eigenvectors $(\underline{v}_{mij}, \theta_{mij})$ with time-dependent coefficients. First, however, we let $(\underline{v}^*_{mij}, \theta^*_{mij})$ denote an eigensolution of the adjoint problem (with h = 0) in the case that $\hat{M} = M_c$, the critical value at a fixed aspect ratio and with R = 0; the corresponding eigenvalue is R_{mij}. Because of the ordering of Rayleigh numbers stipulated immediately following equation (5.5), this means that $R_{mil} = 0$ for some m and some i. Let $(\underline{v}, \theta)$ be a vector with div $\underline{v} = 0$ satisfying the boundary conditions (3.4)-(3.6), and consider the expression

$$Q \equiv \langle \underline{v}^*_{mij}\cdot(\nabla^2\underline{v} - \nabla p) + \theta^*_{mij}(\nabla^2\theta + Mw)\rangle, \tag{5.21}$$

M arbitrary, where $\langle\cdot\rangle$ denotes integration over the volume $0 < r < a$, $0 \le \phi < 2\pi$, $0 < z < 1$ occupied by the fluid. Integrating by parts and noting again that $(\underline{v}^*_{mij}, \theta^*_{mij})$ solves the adjoint linear problem with $\hat{M} = M_c$ and $R = R_{mij}$, we easily find that

$$Q = (M - M_c)\langle\theta^*_{mij}w\rangle - M_c^{-1}R_{mij}\langle w^*_{mij}\theta\rangle. \tag{5.22}$$

Observe that Q = 0 when $M = M_c$ and $R_{mij} = 0$, which is consistent with the definition of the linear stability problem and its adjoint at criticality.

Next, let $(\underline{v}, \theta)$ denote a solution of the nonlinear system (5.18)-

(5.20) with boundary conditions (3.4)-(3.6), for some given value of M. Take the scalar product of (5.18) with $\underline{v}^*_{mij}$, the product of (5.20) with θ^*_{mij}, add, and integate over the fluid volume. Using (5.22) we then obtain the equation

$$(M - M_c)\langle\theta^*_{mij} w\rangle - M_c^{-1} R_{mij}\langle w^*_{mij}\theta\rangle = M\langle\theta^*_{mij}\frac{\partial\theta}{\partial t} + Pr^{-1}\underline{v}^*_{mij}\cdot\frac{\partial\underline{v}}{\partial t}\rangle \tag{5.23}$$

$$+ M\langle\theta^*_{mij}(\underline{v}\cdot\nabla)\theta + Pr^{-1}\underline{v}^*_{mij}\cdot(\underline{v}\cdot\nabla)\underline{v}\rangle.$$

Now choose a finite set $\mathcal{S}$ of eigensolutions $(\underline{v}_{mij}, \theta_{mij})$ of the linear stability problem. Let $N > 1$ be the number of elements in $\mathcal{S}$, and for convenience write

$$\mathcal{S} = \{mij\} \tag{5.24}$$

which means that an element of the set has azimuthal wave number m, radial wave number i and vertical wave number j. We can thus refer to $mij = p$, say, as the vector wave number of an element of $\mathcal{S}$.

We assume that the solution vector $(\underline{v}, \theta)$ can be represented, to a good approximation, by a linear combination of elements of the set $\mathcal{S}$, with time-dependent coefficients. Thus we set

$$(\underline{v}, \theta) = \sum_{\mathcal{S}} A_{mij}(t)(\underline{v}_{mij}, \theta_{mij}); \tag{5.25}$$

substitution of (5.25 into (5.23) reduces the latter to a system of N ordinary nonlinear differential equations for the amplitude functions A_{mij}.

The details of this reduction are considerably simplified on account

of the following orthogonality relations. First of all we have the bi-orthogonality condition

$$\langle w^*\theta \rangle_{p\,q} = 0 \quad \text{when } p \neq q \tag{5.26}$$

for any two fields with vector wave numbers p, q. Next, since the azimuthal dependence has the form of trigonometrical functions, we deduce from the latter's orthogonality properties that

$$\langle \theta^*_{mij} w_{nk\ell} \rangle = \langle \underset{\sim}{v}^*_{mij} \cdot \underset{\sim}{v}_{nk\ell} \rangle = \langle \theta^*_{mij} \theta_{nk\ell} \rangle = 0 \quad \text{when} \quad m \neq n \tag{5.27}$$

for any values of i, j, k, ℓ. Similarly, since the radial dependence has the form of Bessel functions, we have that

$$\langle \theta^*_{mij} w_{nk\ell} \rangle = \langle \underset{\sim}{v}^*_{mij} \cdot \underset{\sim}{v}_{nk\ell} \rangle = \langle \theta^*_{mij} \theta_{nk\ell} \rangle = 0 \quad \text{when} \quad i \neq k \tag{5.28}$$

for any values of m, j, n, ℓ.

There remains the question of the choice of the set $\mathcal{S}$. For ease of computation it is desirable that $\mathcal{S}$ should comprise as few elements as reasonably possible. Next, since we are concerned with the weakly nonlinear interactions that cause the onset of convection, we must certainly include in $\mathcal{S}$ the critical mode (or modes); as pointed out in the previous Section the nature of the critical mode depends on the aspect ratio. Finally, $\mathcal{S}$ must include a minimal number of other modes needed to generate nonlinear evolution into convection of the critical mode. By "minimal" we mean the non-critical modes with the smallest damping rates. As can be seen from (5.23), when M is close to M_c the damping rate of a non-critical mode is determined

approximately by the magnitude of S_{mij}, so that we retain only those modes with the smallest values of R_{mij} and neglect all others. A discussion of the procedure and its validity can be found in Rosenblat (1979).

6. EVOLUTION AT SIMPLE POINTS

We study in this Section weakly nonlinear evolution into convection at three specific values of the aspect ratio, namely a = 0.90, a = 1.50 and a = 1.80. As can be seen from Figure 1, the loss of stability of the basic conduction state at each of these values is simple in the sense that only one mode loses stability as the Marangoni number increases through its critical value. In each case we reduce the problem to a single ordinary nonlinear differential equation of Landau type, and examine its solutions and their stability.

A. The case a = 0.90.

Figure 3 shows that the critical mode at this aspect ratio is the mode 111, that is, azimuthal, radial and vertical wave numbers all equal to unity. We find that

$$M_c = 79.5 \tag{6.1}$$

and, by hypothesis, $R_{111} = 0$. Now the quadratic self-interaction of the mode 111 generates the modes 0ij, 2ij with i, j = 1, 2, ... Computations show, however, that

$$R_{011} = \min_{i,j} R_{01j}, \qquad R_{211} = \min_{i,j} R_{21j}, \tag{6.2}$$

and, moreover, that these Rayleigh numbers are widely separated. For this reason we take $\mathcal{A}$ to comprise three modes:

$$\mathcal{S} = \{111, 011, 211\}, \tag{6.3}$$

and substitute into (5.23) the form

$$(\underline{v}, \theta) = A_{111}(\underline{v}_{111}, \theta_{111}) + A_{011}(\underline{v}_{011}, \theta_{011}) + A_{211}(\underline{v}_{211}, \theta_{211}), \tag{6.4}$$

where the A_{ijk} are functions of time.

Using the orthogonality relations (5.26)-(5.28) to eliminate several of the terms, we obtain the following set of equations:

$$\nu_{111}\dot{A}_{111} = (M - M_c)A_{111} - Z_{111} \tag{6.5}$$

$$\nu_{011}\dot{A}_{011} = (M - M_c - M_c^{-1}R_{011}f_{011})A_{011} - Z_{011} \tag{6.6}$$

$$\nu_{211}\dot{A}_{211} = (M - M_c - M_c^{-1}R_{211}f_{211})A_{211} - Z_{211} \tag{6.7}$$

where the prime denotes differentiation with respect to t, where

$$\nu_{mij} = \frac{M\langle\theta^*_{mij}\theta_{mij}\rangle + Pr^{-1}\langle\underline{v}^*_{mij}\cdot\underline{v}_{mij}\rangle}{\langle\theta^*_{mij}w_{mij}\rangle}, \tag{6.8}$$

$$f_{mij} = \frac{\langle w^*_{mij}\theta_{mij}\rangle}{\langle\theta^*_{mij}w_{mij}\rangle} \tag{6.9}$$

and where the Z_{ijk} are homogeneous quadratic functions of A_{111}, A_{011} and A_{211}. The general form of the Z_{ijk} is given by

$$\langle \theta^*_p w_p \rangle Z_p = M\langle \theta^*_p (\sum_{\mathcal{S}} A_q \underline{v}_q \cdot \nabla) \sum_{\mathcal{S}} A_r \theta_r + Pr^{-1} \underline{v}^*_p \cdot (\sum_{\mathcal{S}} A_q \underline{v}_q \cdot \nabla) \sum_{\mathcal{S}} A_r \underline{v}_r \rangle \qquad (6.10)$$

where p, q, r refer to vector wave numbers.

Each of the two terms on the right of (6.10) contains N^2 integrals when $\mathcal{S}$ has N elements. However, several of these integrals are identically zero by virtue of the orthogonality relations (5.22)-(5.24). In the present case we find that, for the mode 111, only 4 of the 9 integrals are non-zero, and we obtain for the associated quadratic nonlinearity an expression of the form

$$d_{111} Z_{111} = M A_{111} (\alpha_0 A_{011} + \alpha_2 A_{211}) \qquad (6.11)$$

where

$$d_{mlj} = \langle \theta^*_{mlj} w_{mlj} \rangle \qquad (6.12)$$

and where

$$\alpha_m = \langle \theta^*_{111} (\underline{v}_{111} \cdot \nabla \theta_{mll} + \underline{v}_{mll} \cdot \nabla \theta_{111}) + Pr^{-1} \underline{v}^*_{111} \cdot (\underline{v}_{111} \cdot \nabla \underline{v}_{mll} + \underline{v}_{mll} \cdot \nabla \underline{v}_{111}) \rangle \qquad (6.13)$$

for m = 0 and m = 2. Using similar considerations we obtain

$$d_{011} Z_{011} = M(\alpha_{01} A^2_{111} + \alpha_{00} A^2_{011} + \alpha_{02} A^2_{211}) \qquad (6.14)$$

and

$$d_{211}z_{211} = M(\alpha_{21}A_{111}^2 + \alpha_{202}A_{011}A_{211}) \qquad (6.15)$$

where

$$\alpha_{mk} = \langle \vartheta^*_{m11}\underline{v}_{k11}\cdot\nabla\theta_{k11} + Pr^{-1}\underline{v}^*_{m11}\cdot(\underline{v}_{k11}\cdot\nabla)\underline{v}_{k11}\rangle \qquad (6.16)$$

for $m = 0$, $k = 0, 1, 2$ and $m = 2$, $k = 1$, and

$$\alpha_{202} = \langle \theta^*_{211}(\underline{v}_{011}\cdot\nabla\vartheta_{211} + \underline{v}_{211}\cdot\nabla\vartheta_{011}) + Pr^{-1}\underline{v}^*_{211}\cdot(\underline{v}_{011}\cdot\nabla\underline{v}_{211} + \underline{v}_{211}\cdot\nabla\underline{v}_{011})\rangle. \qquad (6.17)$$

Equations (6.5)-(6.7) are the evolution equation for the mode 111 at the aspect ratio $a = 0.9$. The null solution, $A_{111} = A_{011} = A_{211} = 0$, corresponds to the conduction state, and at fixed Rayleigh number, $R = R_{111} = 0$, is stable for $M < M_c$ and unstable for $M > M_c$.

To study bifurcation from the critical point and the evolution of convection in the neighborhood of $M = M_c$, we can simplify the system (6.5)-(6.7) in the following way. The modes A_{011} and A_{211} are relatively strongly damped at $M = M_c$, and are present only due to the quadratic self-interaction of the critical mode A_{111}. Hence, we can neglect the time-derivative terms in (6.6) and (6.7) and replace M by M_c in these equations. Moreover, when M is close to M_c the magnitudes of A_{011} and A_{211} are small compared with A_{111}; hence in the right-hand sides of (6.14) and (6.15) we can neglect the quadratic terms involving A_{011} and A_{211} by comparison with the terms involving A_{111}^2. Taking these approximations together, and substituting (6.14) and (6.15) into (6.6), (6.7) respectively, we obtain

$$A_{011} = \frac{-M_c^2\alpha_{101}A_{111}^2}{R_{011}f_{011}d_{011}}, \qquad A_{211} = \frac{M_c^2\alpha_{202}A_{111}^2}{R_{211}f_{211}d_{211}}. \qquad (6.18)$$

We now substitute (6.18) into (6.11), and then substitute the latter, with M replaced by M_c, into (6.5). This gives the single equation

$$\nu_{111}\dot{A}_{111} = (M - M_c)A_{111} - \omega_{111}A_{111}^3 \tag{6.19}$$

where

$$\omega_{111} = -\frac{M_c^3}{d_{111}}\left(\frac{a_0 a_{01}}{R_{011} f_{011} d_{011}} + \frac{a_2 a_{21}}{R_{211} f_{211} d_{211}} \cdots\right). \tag{6.20}$$

Equation (6.19) is the Landau equation for the evolution of the critical mode 111. The coefficients ν_{111}, ω_{111} are determined by numerical integration of the appropriate products of eigenfunctions. The computations have been performed at various values of Prandtl number and some results are shown in Table 1. We infer from the calculations that

$$\nu_{111} > 0, \qquad \omega_{111} > 0 \tag{6.21}$$

for all Prandtl numbers.

Pr	$\nu_{111} \times 10^{-4}$	$\omega_{111} \times 10^{-3}$
0.1	0.37	1.2
1.0	0.13	0.16
10.0	0.10	0.11
∞	0.10	0.10

Table 1

From (6.19) and (6.21) we infer that a solution bifuractes from the critical value M_c having the representation

$$A_{111} = \pm \sqrt{\{(M - M_c)/\omega_{111}\}}. \qquad (6.22)$$

The solution exists only for $M > M_c$ (supercritically) and is known from elementary bifurcation theory to be stable. Because of the representation (6.4), we conclude that at aspect ratio $a = 0.9$ the onset of convection is supercritical and, for small $M - M_c$, has to leading order the form of a non-axisymmetric mode with azimuthal wave number 1.

3. The case a = 1.50.

From Figure 3 we see that at this aspect ratio the critical mode is 211: the azimuthal wave number is 2, and the radial and vertical wave numbers are both unity. The critical Marangoni number is

$$M_c = 79.5 \qquad (6.23)$$

with $S_{211} = 0$. The quadratic interaction of the mode 211 with itself generates the modes 0ij, 4ij, with i, j = 1, 2, 3, ..., but because of the ordering of the associated Rayleigh numbers we approximate by neglecting all except the modes 011 and 411. Thus,

$$\mathcal{S} = \{211, 011, 411\} \tag{6.24}$$

and

$$(\underline{v}, \theta) = A_{211}(\underline{v}_{211}, \theta_{211}) + A_{011}(\underline{v}_{011}, \theta_{011}) + A_{411}(\underline{v}_{411}, \theta_{411}). \tag{6.25}$$

We substitute (6.25) into (5.23) to obtain a system of three ordinary differential equations for the amplitudes, namely

$$\nu_{211}\dot{A}_{211} = (M - M_c)A_{211} - Z_{211} \tag{6.26}$$

$$\nu_{011}\dot{A}_{011} = (M - M_c - M_c^{-1}R_{011}f_{011})A_{011} - Z_{011} \tag{6.27}$$

$$\nu_{411}\dot{A}_{411} = (M - M_c - M_c^{-1}R_{411}f_{411})A_{411} - Z_{411} \tag{6.28}$$

where the coefficients have the forms (6.8)-(6.10). Proceeding as in the previous case we find that

$$d_{211}Z_{211} = MA_{211}(\beta_0 A_{011} + \beta_4 A_{411}) \tag{6.29}$$

where

$$\beta_m = \langle \theta^*_{211}(\underline{v}_{211}\cdot\nabla\theta_{m11} + \underline{v}_{m11}\cdot\nabla\theta_{211}) + Pr^{-1}\underline{v}^*_{211}\cdot(\underline{v}_{211}\cdot\nabla\underline{v}_{m11} + \underline{v}_{m11}\cdot\nabla\underline{v}_{211})\rangle \tag{6.30}$$

for $m = 0$ and $m = 4$; also,

$$d_{011}Z_{011} = M(\beta_{02}A_{211}^2 + \beta_{00}A_{011}^2 + \beta_{04}A_{411}^2) \tag{6.31}$$

and

$$d_{411}Z_{411} = M(\beta_{42}A_{211}^2 + \beta_{404}A_{011}A_{411}) \tag{6.32}$$

where

$$\beta_{mk} = \langle \theta^*_{m11}\underline{v}_{k11}\cdot\nabla\theta_{k11} + Pr^{-1}\underline{v}^*_{m11}\cdot(\underline{v}_{k11}\cdot\nabla)\underline{v}_{k11}\rangle \tag{6.33}$$

for $m = 0$, $k = 0$, 2, 4 and $m = 4$, $k = 2$, and

$$\beta_{404} = \langle \theta^*_{411}(\underline{v}_{011}\cdot\nabla\theta_{411} + \underline{v}_{411}\cdot\nabla\theta_{011}) + Pr^{-1}\underline{v}^*_{411}\cdot(\underline{v}_{011}\cdot\nabla\underline{v}_{411} + \underline{v}_{411}\cdot\nabla\underline{v}_{011})\rangle. \tag{6.34}$$

Using the same reasoning as before, we can solve (6.27) and (6.28) approximately to find A_{011} and A_{411} in terms of A_{211}^2. We obtain

$$A_{011} = \frac{-M_c^2\beta_{02}A_{211}^2}{R_{011}f_{011}d_{011}}, \qquad A_{411} = \frac{-M_c^2\beta_{42}A_{211}^2}{R_{411}f_{411}d_{411}}. \tag{6.35}$$

Substituting (6.35) and (6.29) into (6.26), we find that the latter reduces to the simple Landau equation

$$\nu_{211}\dot{A}_{211} = (M - M_c)A_{211} - \sigma_{211}A_{211}^3 \tag{6.36}$$

where

$$\sigma_{211} = -\frac{M_c^3}{f_{211}}\left(\frac{\beta_0\beta_{02}}{R_{011}f_{011}d_{011}} + \frac{\beta_4\beta_{42}}{R_{411}f_{411}d_{411}}\right). \tag{6.37}$$

Computed values of the coefficients ν_{211}, ω_{211} for various Prandtl numbers are given in Table 2, from which it can be seen that both coefficients are always positive. We infer that

$$A_{211} = \pm\sqrt{|(M - M_c)/\omega_{211}|} \tag{6.38}$$

represents a stable supercritical conduction solution for $M - M_c$ small, and corresponds to a non-axisymmetric mode with azimuthal wave number 2.

Pr	$\nu_{211} \times 10^{-4}$	$\omega_{211} \times 10^{-2}$
0.1	0.37	6.2
1.0	0.13	0.98
10.0	0.10	0.50
∞	0.10	0.45

Table 2

C. The case a = 1.80.

Figure 3 shows that the critical mode at this aspect ratio is the axisymmetric mode 011. We find that

$$M_c = 79.7 \tag{6.39}$$

with $R_{011} = 0$. The quadratic self-interaction of this mode generates all the modes 0ij with i j = 1, 2, ..., but by virtue of the ordering of the Rayleigh numbers R_{0ij} we retain only the mode 021. Thus

$$\mathcal{S} = \{011, 021\} \tag{6.40}$$

and we substitute

$$\underline{V} = A_{011}(\underline{v}_{011}, \theta_{011}) + A_{021}(\underline{v}_{021}, \theta_{021}) \tag{6.41}$$

into (5.23) to obtain a pair of amplitude equations:

$$\nu_{011}\dot{A}_{011} = (M - M_c)A_{011} - Z_{011} \tag{6.42}$$

$$\nu_{021}\dot{A}_{021} = (M - M_c - M_c^{-1}R_{021}f_{021})A_{021} - Z_{021}. \tag{6.43}$$

Using the formula (6.10) we find that

$$d_{011}Z_{011} = M(\gamma_{11}A_{011}^2 + \gamma_{112}A_{011}A_{021} + \gamma_{12}A_{021}^2). \tag{6.44}$$

$$d_{021}Z_{021} = M(\gamma_{21}A_{011}^2 + \gamma_{212}A_{011}A_{021} + \gamma_{22}A_{021}^2) \tag{6.45}$$

where

$$\gamma_{ik} = \langle v_{011}^{\star}(\underline{v}_{02k}\cdot\nabla)\theta_{02i} + Pr^{-1}\underline{v}_{011}^{\star}\cdot(\underline{v}_{02i}\cdot\nabla)\underline{v}_{02k}\rangle \tag{6.46}$$

for i, k = 1, 2, and

$$\gamma_{112} = \langle \theta^*_{011}(\underline{v}_{011}\cdot\nabla\theta_{021} + \underline{v}_{021}\cdot\nabla\theta_{011}) + Pr^{-1}\underline{v}^*_{011}\cdot(\underline{v}_{011}\cdot\nabla\underline{v}_{021} + \underline{v}_{021}\cdot\nabla\underline{v}_{011})\rangle. \tag{6.47}$$

We approximate as before for M close to M_c and on the assumption that the magnitude of A_{021} is much smaller than that of A_{011}. We then solve (6.43) and (6.45) to obtain

$$A_{021} = \frac{-M_c^2\gamma_{21}A_{011}^2}{R_{021}f_{021}d_{021}}. \tag{6.48}$$

We substitute this and (6.44) into (6.42), with M replaced by M_c in the nonlinear terms and with the term containing A_{021}^2 omitted on the grounds that it is smaller than those retained. This leads to a single equaitons for the critical-mode amplitude, namely

$$\nu_{011}\dot{A}_{011} = (M - M_c)A_{011} - \gamma_0 A_{011}^2 - \omega_{011}A_{011}^3 \tag{6.49}$$

where

$$\gamma_0 = \frac{M_c\gamma_{11}}{d_{011}} \tag{6.50}$$

and

$$\omega_{011} = \frac{-M_c^3\gamma_{21}\gamma_{112}}{R_{021}d_{011}d_{021}\omega_{011}}. \tag{6.51}$$

Computed values of the coefficients are given in Table 3.

Pr	$\nu_{011} \times 10^{-4}$	$\gamma_0 \times 10^{-2}$	$\omega_{011} \times 10^{-3}$
0.1	0.36	0.32	1.8
1.0	0.12	-0.19	0.23
10.0	0.10	-0.24	0.15
∞	0.98	-0.25	0.14

Table 3

Observe that ν_{011}, ω_{011} are both positive, but that γ_0 is positive for low Prandtl numbers and negative for moderate and large Prandtl numbers.

One solution of (6.49) is $A_{011} = 0$, which corresponds to the conduction state. This solution is stable for $M < M_c$ and unstable for $M > M_c$. Other solutions are determined from roots of the equation

$$\omega_{011} A_{011}^2 + \gamma_0 \nu_{011} - (1 - M_c) = 0. \qquad (6.52)$$

All the solutions are illustrated in Figure 6a for the case $\gamma_0 > 0$, and in Figure 6b for the case $\gamma_0 < 0$. A conduction solution exists for both $M < M_c$ and $M > M_c$ (across critical bifurcation), but the subcritical branch turns around at a value M_0 of M and continues into the half-plane $M > M_c$.

Figure 6

We determine the stability of the solutions in the following way. Let $\tilde{T}$ denote any time-dependent solution of (6.49). We set

$$A_{011} = \bar{A} + a_0 \tag{6.53}$$

in equation (6.49) and linearize, to obtain the stability equation

$$\dot{a}_0 = (M - M_c - 2\gamma_0\bar{A} - 3\omega_{011}\bar{A}^2)a_0. \tag{6.54}$$

A simple calculation shows that the subcritical branch OP in Figure 6 is unstable, and that the branches OR, PQ are stable. This is the standard result for transcritical bifurcation.

These calculations settle in principle the question of the direction of the flow at the center of the container because the asymmetry of the bifurcation diagram implies a preferred branch. As M increases towards M_c, a disturbance, however small, to the conduction solution will result in loss of stability of the latter before M reaches the critical value M_c, and a consequent snap-through to the branch PQ. (See, for example, Rosenblat 1979, for a fuller discussion of this process.) As M increases still futher the system stays on the branch PQ which is thus "preferred" to the branch OR. Of course, when $M > M_c$ one could find a disturbance of large enough size that would cause the system to jump from this branch to the other. The fact that both supercritical branches are stable is similar to the result of Liang, Vidal and Acrivos (1969) for axisymmetric buoyancy driven convection in a cylinder.

From (5.6) we see that the vertical velocity component for the mode 011 is

$$w_{011} = A_{011} Y_{011}(z) \tag{6.55}$$

at the center of the container. Numerical calculations show that $Y_{011}(z) > 0$ on $0 < z < 1$; here the sign of A_{011} determines the direction of the flow, giving upflow when $A_{011} > 0$ and downflow when $A_{011} < 0$. The preferred branch PQ has $A_{011} < 0$ for very small Prandtl numbers and $A_{011} > 0$ for moderate and large Prandtl numbers. We infer that there will be downflow at the center when $Pr \ll 1$, which is the case for liquid metals, and upflow when $Pr > 1$, which applies for common liquids.

7. EVOLUTION AT DOUBLE POINTS.

It is evident from Figures 3 - 5 that there are certain values of the aspect ratio at which two modes lose stability simultaneously. In this Section we shall investigate the onset of convection in the neighborhoods of such double points and the secondary bifurcations that can result.

A. Intersection of modes 111, 211.

At the point marked A in Figure 3 the curves of M as a function of aspect ratio for the modes 111 and 211 intersect. The value of a at which this intersection takes place is denoted a_A (≈ 1.20). The common value of M_{111}, M_{211} at this point will be denoted M_c; computations give

$$M_c = M_{111} = M_{211} = 85.2 \quad . \tag{7.1}$$

By hypothesis we have that $R_{111} = R_{211} = 0$.

We are interested in studying the onset of convection at values of a slightly less and slightly greater than a_A. As noted in the previous Section, the self-interaction of the mode 111 generates modes with azimuthal wave numbers 0 and 2, while the self-interaction of the mode 211 generates modes with m = 0 and m = 4. In addition, the interaction of modes 111 and 211 generates a mode with m = 3. For reasons indicated earlier, we approximate by retaining only the leading (in the sense of Rayleigh-number ordering) member of each of these generated sets. This leads us to select a 5-element set of expansion functions, namely

$$\mathcal{S} = \{111,211,011,311,411\} \tag{7.2}$$

Substituting the appropriate eigenfunction expansion into (5.23), we obtain a system of five ordinary differential equations for the amplitudes. These equations are conveniently written as follows:

$$\nu_{m11}\dot{A}_{m11} = (M - M_{m11})A_{m11} - Z_{m11} \quad , \quad m = 1 \text{ and } m = 2 \tag{7.3}$$

and

$$\nu_{m11}\dot{A}_{m11} = (M - M_c^{-1}R_{m11}f_{m11})A_{m11} - Z_{m11} \quad , \quad m = 0,3 \text{ and } 4 \, . \tag{7.4}$$

Note that in (7.3) we have retained M_{m11} in place of M_c; the reason for this will soon become apparent.

We reduce the system (7.3)-(7.4) as in the previous Section. We use (6.10) to calculate the quadratic nonlinearities in (7.4) and find

$$d_{011}Z_{011} = M(\alpha_{01}A_{111}^2 + \alpha_{02}A_{211}^2 + \alpha_{00}A_{011}^2 + \alpha_{03}A_{311}^2 + \alpha_{04}A_{411}^2) \tag{7.5a}$$

$$d_{311}Z_{311} = M\alpha_{312}A_{111}A_{211} \tag{7.5b}$$

and

$$d_{411}Z_{411} = M(\alpha_{42}A_{211}^2 + \beta_{404}A_{011}A_{411} + \alpha_{413}A_{111}A_{311}) \quad , \tag{7.5c}$$

where the α_{mk} are given by (6.16), β_{404} is given by (6.34), and where

$$\alpha_{mjk} = \langle \theta^*_{m11}(\underline{v}_{j11}\cdot\nabla\theta_{k11} + \underline{v}_{k11}\cdot\nabla\theta_{j11}) + Pr^{-1}\underline{v}^*_{m11}\cdot(\underline{v}_{j11}\cdot\nabla\underline{v}_{k11} + \underline{v}_{k11}\cdot\nabla\underline{v}_{j11})\rangle \quad . \tag{7.6}$$

We now solve (7.4) approximately by neglecting the time-derivative terms, replacing M by M_c, and neglecting as relatively small the quadratic terms involving A_{011}, A_{311} and A_{411} on the right-hand sides of equations (7.5). This process gives the approximations

$$A_{011} = \frac{-M_c^2}{R_{011} f_{011} d_{011}} (\alpha_{01} A_{111}^2 + \alpha_{02} A_{211}^2)$$

$$A_{411} = \frac{-M_c^2 \alpha_{42} A_{211}^2}{R_{411} f_{411} d_{411}} , \quad A_{311} = \frac{M_c^2 \alpha_{312} A_{111} A_{211}}{R_{311} f_{311} d_{311}} . \tag{7.7}$$

These formulae can be compared with (6.18) and (6.35), it being noted in particular that $\alpha_{02} = \beta_{02}$ and $\alpha_{42} = \beta_{42}$.

The quadratic nonlinearities in (7.3) are found to be given by

$$d_{111} Z_{111} = M A_{111} (\alpha_0 A_{011} + \alpha_2 A_{211}) + M \alpha_{123} A_{211} A_{311} \tag{7.8}$$

and

$$d_{211} Z_{211} = M(\alpha_{21} A_{111}^2 + \beta_0 A_{211} A_{011} + \beta_4 A_{211} A_{411} + \alpha_{213} A_{111} A_{311}) \tag{7.9}$$

where α_0, α_2 are defined by (6.13), α_{21} by (6.16), β_0, β_4 by (6.30), α_{213}, α_{123} by (7.6). We now substitute (7.7)-(7.9) into (7.3) to obtain the following pair of equations:

$$\nu_{111} \dot{A}_{111} = (M - M_{111}) A_{111} - c_1 A_{111} A_{211} - \omega_1 A_{111}^3 - \sigma_1 A_{111} A_{211}^2 \tag{7.10}$$

$$\nu_{211} \dot{A}_{211} = (M - M_{211}) A_{211} - c_2 A_{111}^2 - \sigma_2 A_{111}^2 A_{211} - \omega_2 A_{211}^3 \tag{7.11}$$

where the coefficients are defined by the following formulas.

$$c_1 = M_c \alpha_2 / d_{111} \quad , \quad c_2 = M_c \alpha_{21} / d_{211} \quad ,$$

$$\sigma_1 = \frac{-M_c^3}{d_{111}} \left\{ \frac{\alpha_0 \alpha_{02}}{R_{011} f_{011} d_{011}} + \frac{\alpha_{123} \alpha_{312}}{R_{311} f_{311} d_{311}} \right\}$$

$$\sigma_2 = \frac{-M_c^3}{d_{211}} \left\{ \frac{\beta_0 \alpha_{01}}{R_{011} f_{011} d_{011}} + \frac{\alpha_{213} \alpha_{312}}{R_{311} f_{311} d_{311}} \right\} \tag{7.12}$$

$$\omega_1 = \frac{-M_c^3 \alpha_0 \alpha_{01}}{R_{011} f_{011} d_{011} d_{111}} \quad , \quad \omega_2 = \omega_{211}$$

where ω_{211} is defined by (6.37). Computed values of the coefficients are given in Table 4.

Pr	$\nu_{111} \times 10^{-4}$	$c_1 \times 10^{-2}$	$\omega_1 \times 10^{-2}$	$\sigma_1 \times 10^{-3}$	$\nu_{211} \times 10^{-3}$	$c_2 \times 10^{-3}$	$\sigma_2 \times 10^{-3}$	$\omega_2 \times 10^{-2}$
0.1	0.49	-1.2	14.0	2.0	3.7	1.3	1.6	4.2
1.0	0.19	-0.74	1.5	0.27	1.2	0.36	0.28	0.62
10.0	0.16	-0.69	0.93	0.18	0.91	0.26	0.20	0.31
∞	0.16	-0.69	0.88	0.7	0.89	0.25	0.19	0.28

Table 4

We propose to study the nature and stability of solutions of (7.10)-(7.11) in the neighborhood of the double point A, and for values of M reasonably close to M_c.

We consider first the case of aspect ratios slightly less than a_A, $a \lesssim a_A$. We then have that

$$M_{111} < M_{211} \tag{7.13}$$

and we define

$$\eta = M - M_{111}, \qquad \Delta = M_{211} - M_{111}. \tag{7.14}$$

Equations (7.10)-(7.11) can now be written in the form

$$\begin{aligned} \nu_1 \dot{A}_1 &= \eta A_1 - c_1 A_1 A_2 - \omega_1 A_1^3 - \sigma_1 A_1 A_2^2 \\ \nu_2 \dot{A}_2 &= (\eta - \Delta) A_2 - c_2 A_2^2 - \sigma_2 A_1^2 A_2 - \omega_2 A_2^3 \end{aligned} \tag{7.15}$$

where for the sake of brevity the notation has been simplified in an obvious way.

Because of the approximations used in their derivation, equations (7.15) can be regarded as valid only for small values of Δ and small values of η. A reasonable measure of smallness is the ratio of these quantities to the critical value of M, which is about 85. In the computations to be described presently we have taken values of Δ in the range $0 \leq \Delta \leq 5.0$ and of η in the range $0 \leq \eta \leq 2\Delta$. Results for significantly larger values are not easily substantiated on the basis of our approximation scheme.

Before proceeding further we formulate the stability problem associated with the system (7.15). Let $(\bar{A}_1, \bar{A}_2)$ denote a solution of (7.15) and set

$$A_1 = \bar{A}_1 + a_1, \qquad A_2 = \bar{A}_2 + a_2. \tag{7.16}$$

Linearization of the equations with respect to the disturbances leads to the linear system

$$\begin{aligned} \nu_1 \dot{a}_1 &= (\eta - c_1\bar{A}_2 - 3\omega_1\bar{A}_1^2 - \sigma_1\bar{A}_2^2)a_1 - (c_1 + 2\sigma_1\bar{A}_2)\bar{A}_1 a_2 \\ \nu_2 \dot{a}_2 &= -2(c_2 + \sigma_2\bar{A}_2)\bar{A}_1 a_1 + (\eta - \Delta - \sigma_2\bar{A}_1^2 - 3\omega_2\bar{A}_2^2)a_2. \end{aligned} \tag{7.17}$$

The exponents of this system determine the stability of the solution $(\bar{A}_1, \bar{A}_2)$.

We examine now the solutions of (7.15) and their stability. Observe

first that (7.15) has the trivial solution $A_1 = A_2 = 0$, which corresponds to the conduction state, and which is stable for $\eta < 0$ and unstable for $\eta > 0$. Moreover, for this solution one stability exponent changes sign at $\eta = 0$ and the other at $\eta = \Delta$, so that each of these values locates a bifurcation point for the appearance of a new (convection) solution.

The trivial solution is unique for $\eta < 0$. As η increases through zero, a pair of nontrivial solutions emerges, determined by the pair of equations

$$A_1^2 = (\eta - c_1 A_2 - \sigma_1 A_2^2)/\omega_1$$

$$\omega_2 A_2^3 + \sigma_2 A_1^2 A_2 + c_2 A_1^2 - (\eta - \Delta) A_2 = 0. \tag{7.18}$$

If Δ were large, these equations would reduce to $A_2 = 0$ and A_1 (equivalent to A_{111}) given by (6.22), and would correspond to a "pure" convection state with azimuthal wave number $m = 1$ at leading order. When Δ is small, however, the mode $m = 2$ has an effect, as expressed by the coupled equations (7.18), in two ways: the solution has $A_2 \neq 0$ and the parabolas (6.22) are distorted as η approaches Δ.

Numerical calculations show that solutions of (7.18) exist only on an interval $0 < \eta < \eta_T$, where $\eta_T > \Delta$. The value of η_T depends on Prandtl number, but computations reveal that $1 < \eta_T/\Delta < 1.2$ for the entire Prandtl number range. On $0 < \eta < \eta_T$ there is precisely one root $\bar{A}_2$ of the cubic in (7.18), and a corresponding pair of roots $+\bar{A}_1$, $-\bar{A}_1$. These solutions are illustrated in Figure 7: one pair of solutions is represented by the curves O_1UT_1, O_2T_2 and the other by the curves O_1LT_1, O_2T_2.

Figure 7

Calculations utilizing equations (7.17) show that these solutions are stable.

The remaining solutions of (7.15) are given by

$$A_1 \equiv 0, \qquad \eta - \Delta = \omega_2 \bar{A}_2^2. \tag{7.19}$$

These exist for $\eta > \Delta$ and are the "pure" $m = 2$ mode solutions considered in B. of Section 6. Their stability is determined by substituting (7.19) into (7.17), which gives

$$\nu_1 \dot{a}_1 = (\eta - c_1 \bar{A}_2 - \sigma_1 \bar{A}_2^2) a_1, \qquad \nu_2 a_1' = -2(\eta - \Delta) a_2. \tag{7.20}$$

Evidently it is the first of these equations that decides stability. Calculations show that the branch corresponding to positive $\bar{A}_2$, the upper branch ΔR in Figure 7, is unstable, while the lower branch, ΔS, is unstable initially but regains stability at precisely the value $\eta = \eta_T$ defined above.

The situation depicted in Figure 7 has been established numerically. In summary, the behavior of the system is as follows. For $\eta < 0$ ($M < M_{111}$) the conduction solution is stable, and is replaced on $0 < \eta < \eta_T$ ($M_{111} < M < M_T$, say) by a pair of mixed-mode solutions given by (7.18). For $\eta > \eta_T$, however, these give way to a single solution which at leading order is a pure convective state with $m = 2$. This behavior is qualitatively independent of Prandtl number.

For aspect ratios slightly greater than a_A, $a > a_A$, we have

$$M_{211} < M_{111}. \tag{7.21}$$

We then set

$$\eta = M - M_{211}, \qquad \Delta = M_{111} - M_{211} \tag{7.22}$$

to obtain the system

$$\begin{aligned} \nu_1 \dot{A}_1 &= (\eta - \Delta)A_1 - c_1 A_1 A_2 - \omega_1 A_1^3 - \sigma_1 A_1 A_2^2 \\ \nu_2 \dot{A}_2 &= \eta A_2 - c_2 A_1^2 - \sigma_2 A_1^2 A_2 - \omega_2 A_2^3. \end{aligned} \tag{7.23}$$

The stability equations for a solution $(\bar{A}_1, \bar{A}_2)$ of this system are similar to (7.17), except that the terms η and $\eta - \Delta$ are interchanged.

Figure 8

The results of numerical calculations for (7.23), illustrated in Figure 8, are as follows. The conduction solution $A_1 = A_2 = 0$ exists for all η, and is stable for $\eta < 0$ and unstable for $\eta > 0$. The solutions defined by

$$A_1 = 0, \qquad A_2^2 = \bar{A}_2^2 = \eta/\omega_2 \tag{7.24}$$

exist for $\eta > 0$. The lower branch O_2S is always stable, while the upper branch is stable for $0 < \eta < \eta_T$, where $\eta_T \in (0, \Delta)$ and has a value dependent

on Prandtl number. The solutions determined by

$$A_1^2 = (\eta - \Delta - c_1 A_2 - \sigma_1 A_2^2)/\omega_1$$

$$\omega_2 A_2^3 + \sigma_2 A_1^2 A_2 + c_2 A_1^2 - \eta A_2 = 0 \qquad (7.25)$$

exist on the interval $\eta_T < \eta < \Delta$. There are two such solutions, comprising a single root A_2 and corresponding $\pm A_1$. These solutions are found to be stable.

We see from Figure 8 that the conduction solution is replaced by the pair of solutions (7.24) on $0 < \eta < \eta_T$. Next, there is a region, $\eta_T < \eta < \Delta$, in which there are three stable solutions: the lower branch of (7.24) and the mixed-mode solutions of (7.25). However, for $\eta > \Delta$ there is only one (stable) solution, which is a pure nonaxisymmetric mode with $m = 2$. These results apply at all Prandtl numbers.

We see from Figures 7 and 8, and from the preceding discussions, that on either side of the aspect ratio a_A the system eventually attains the same state: a single convection solution with $m = 2$. In one way or another the mode with $m = 1$ is suppressed by the interaction when Δ is small. This interaction can therefore be regarded as being a mechanism for wave-number selection in the sense just described.

B. Intersection of modes 211, 011.

The point B in Figure 3 is the intersection of the curves for the modes 211 and 011. We denote the corresponding value of a by a_B (≈ 1.70). The common value of M_{211}, M_{011} at this point will be denoted by M_c; computations give

$$M_c = M_{211} = M_{011} = 80.6 \ . \tag{7.26}$$

By hypothesis we have that $R_{211} = R_{011} = 0$. Using the same reasoning as in the previous case, we take

$$\mathcal{S} = \{211, 011, 411, 021\} \tag{7.27}$$

as the set of eigenfunctions for the evolution of the modes 211 and 011 near the double point.

Substituting the associated eigenfunction expansion into (5.23) we obtain, by analogy with (7.3) and (7.4), the following ordinary differential equations.

$$\nu_{m11}\dot{A}_{m11} = (M - M_{m11})A_{m11} - Z_{m11}, \qquad m = 2 \text{ and } m = 0, \tag{7.28}$$

and

$$\nu_{m11}\dot{A}_{m11} = (M - M_c - M_c^{-1}R_{m11}f_{m11})A_{m11} - Z_{m11} \tag{7.29}$$

for $m = 4$, $i = 1$ and $m = 0$, $i = 2$. For the quadratic nonlinearities in (7.29) we use (6.10) to find that

$$d_{411}Z_{411} = M(\beta_{42}A_{211}^2 + \beta_{404}A_{011}A_{411} + \bar{\beta}_{404}A_{021}A_{411}) \tag{7.30}$$

where β_{42} is given by (6.33), β_{404} by (6.34) and $\bar{\beta}_{404}$ by (6.34) with the mode 011 replaced by the mode 021, and

$$d_{021}Z_{021} = M(\delta_{22}A_{211}^2 + \gamma_{21}A_{011}^2 + \gamma_{21}A_{011}^2 + \gamma_{212}A_{011}A_{211} + \gamma_{22}A_{021}^2 + \delta_{24}A_{411}^2), \tag{7.31}$$

where the γ_{ij} are given by (6.46)-(6.47), and where we define

$$\delta_{km} = \langle \theta^*_{0k1}(\underline{v}_{m11}\cdot\nabla)\theta_{m11} + Pr^{-1}\underline{v}^*_{0k1}\cdot(\underline{v}_{m11}\cdot\nabla)\underline{v}_{m11}\rangle \tag{7.32}$$

for k = 1, 2 and m = 2, 4. We now solve (7.29), making the same approximations as before, to obtain

$$A_{021} = \frac{-M_c^2}{R_{021}f_{021}d_{021}}(\delta_{22}A_{211}^2 + \gamma_{21}A_{011}^2), \qquad A_{411} = \frac{-M_c^2\beta_{42}A_{211}^2}{R_{411}f_{411}d_{411}}. \tag{7.33}$$

The quadratic nonlinearities in (7.27) are found to be given by

$$d_{211}Z_{211} = MA_{211}(\beta_0 A_{011} + \bar{\beta}_0 A_{021} + \beta_4 A_{411}), \tag{7.34}$$

where β_0, β_4 are given by (6.30), and $\bar{\beta}_0$ is also defined by (6.30) with 011 replaced by 021, and

$$d_{011}Z_{011} = M(\gamma_{11}A_{011}^2 + \gamma_{112}A_{011}A_{021} + \gamma_{12}A_{021}^2 + \delta_{12}A_{211}^2 + \delta_{14}A_{411}^2) \tag{7.35}$$

where the γ's are given by (6.46)-(6.47) and the δ's by (7.31).

We now substitute (7.33)-(7.35) into (7.28) to obtain the following pair of equations:

$$\nu_{211}\dot{A}_{211} = (M - M_{211})A_{211} - c_2A_{211}A_{011} - \sigma_2A_{211}A_{011}^2 - \omega_2A_{211}^3$$

$$\nu_{011}\dot{A}_{011} = (M - M_{011})A_{011} - \gamma_0A_{011}^2 - c_0A_{211}^2 - \sigma_0A_{011}A_{211}^2 - \omega_0A_{011}^3 \tag{7.36}$$

where

$$c_2 = M_c\beta_0/d_{211}, \qquad c_0 = M_c\delta_{12}/d_{011},$$

$$\sigma_2 = \frac{-M_c^3\bar{\beta}_0\gamma_{21}}{R_{021}d_{021}f_{021}d_{211}}, \qquad \sigma_0 = \frac{-M_c^3\delta_{22}\gamma_{112}}{R_{021}d_{021}f_{021}d_{011}} \tag{7.37}$$

$$\omega_2 = -\frac{M_c^3}{d_{211}}\left(\frac{\bar{\beta}_0\delta_{22}}{R_{021}d_{021}f_{021}} + \frac{\beta_4\beta_{42}}{R_{411}d_{411}f_{411}}\right),$$

where $\omega_0 = \omega_{011}$ defined by (6.51) and where γ_0 is given by (6.50). Computed values of the coefficients are given in Table 5.

Pr	$\nu_{211}\times10^{-4}$	$c_2\times10^{-1}$	$\sigma_2\times10^{-2}$	$\omega_2\times10^{-2}$	$\nu_{011}\times10^{-3}$	$\gamma_0\times10^{-2}$	c_0	$\sigma_0\times10^{-2}$	$\omega_0\times10$
0.1	0.40	0.22	6.9	11.0	3.6	0.36	-19.0	1.6	1.7
1.0	0.15	4.3	0.55	1.5	1.2	-0.21	- 1.4	0.22	0.21
10.0	0.12	4.7	0.30	0.98	0.96	-0.26	0.40	0.15	0.14
∞	0.12	4.8	0.28	0.94	0.94	-0.27	0.57	0.14	0.13

Table 5

We proceed with the analysis as in the previous case. For aspect ratios slightly less than a_B, $a < a_B$, we define

$$\eta = M - M_{211}, \qquad \Delta = M_{011} - M_{211} > 0, \tag{7.38}$$

whereup equations (7.36) become

$$\nu_2 \dot{A}_2 = \eta A_2 - c_2 A_2 A_0 - \sigma_2 A_2 A_0^2 - \omega_2 A_2^3$$

$$\nu_0 \dot{A}_0 = (\eta - \Delta) A_0 - \gamma_0 A_0^2 - c_0 A_2^2 - \sigma_0 A_0 A_2^2 - \omega_0 A_0^3 , \tag{7.39}$$

with an obvious abbreviated notation. The stability problem for a solution $(\bar{A}_2, \bar{A}_0)$ of (7.39) is determined from the equations

$$\nu_2 \dot{a}_2 = (\eta - c_2 \bar{A}_0 - \sigma_2 \bar{A}_0^2 - 3\omega_2 \bar{A}_2^2) a_2 - (c_2 \bar{A}_2 + 2\sigma_2 \bar{A}_2 \bar{A}_0) a_0$$

$$\nu_0 \dot{a}_0 = -(2c_0 \bar{A}_2 + 2\sigma_0 \bar{A}_0 \bar{A}_2) a_2 + (\eta - \Delta - 2\gamma_0 \bar{A}_0 - 3\omega_0 \bar{A}_0^2) a_0 . \tag{7.40}$$

Because of the proximity and flatness of the curves of Figure 3 in the neighborhood of the point B, we estimate that the range $0 \leq \Delta \leq 1.0$ is reasonable for Δ, with η not larger than 2Δ.

Figure 9

The solutions of (7.39) and their stability behavior are illustrated in Figure 9 for Pr = 1.0, 10.0 and ∞; for the case Pr = 0.1 the graphs of A_0 against η have to be reflected with respected to the η-axis. The conduction solution $A_2 = A_0 = 0$ loses stability at $\eta = 0$, and the solution which bifurcates from this point is primarily an m = 2 mode, modified by the presence of a small m = 0 component. The latter is due to the fact that (7.39) have no nontrivial solutions with $A_0 = 0$, owing to the presence of the term $c_0 A_2^2$. However, the modification is small because c_0 is a small quantity. This solution is represented by the curves OM, ON, in Figure 9, and derives from the equations

$$A_2^2 = (\eta - c_2 A_0 - \sigma_2 A_0^2)/\omega_2$$

$$0 = (\eta - \Delta)A_0 - \gamma_0 A_0^2 - c_0 A_2^2 - \sigma_0 A_0 A_2^2 - \omega_0 A_0^3. \tag{7.41}$$

A stability calculation shows that this solution is initially stable, but becomes unstable at a value $\eta = \eta_T > \Delta$.

The solution bifurcating at the point $\eta = \Delta$ is given by

$$A_2 = 0, \qquad \eta - \Delta - \gamma_0 A_0 - \omega_0 A_0^2 = 0. \tag{7.42}$$

This is identical with the transcritical solution described in C. of Section 6, and is represented by the asymmetric parabola QPR. However, the stability system shows that the branch PQ is stable (as in Figure 6), but that the whole branch PR is now unstable.

In particular we find that there is a value η_s of η, wit. $0 < \eta_s < \Delta$, at which one of the stability exponents for the branch PR changes sign. From the corresponding point S on PR there is secondary bifurcation of a solution joining S to the point T. This is a mixed-mode solution, and is actually a distinct solution of equations (7.40). We find that this solution is unstable.

Reviewing the situation as shown in Figure 9, we see that before η reaches 0, the system may stay on the null solution or snap-through to the axisymmetric branch PQ; on $0 < \eta < \eta_T$ the system may choose PQ or the predominantly $m = 2$ solution OM, ON, OL; but that for $\eta > \eta_T$ the only stable solution is the axisymmetric mode represented by the branch PQ. Thus, even

though the m = 2 mode appears first according to linear theory, it soon loses out to the axisymmetric mode as a result of the interactions.

We consider next the case where a is slightly greater than a_B, $a > a_B$, with

$$\eta = M - M_{011}, \quad \Delta = M_{211} - M_{011} > 0. \tag{7.43}$$

The governing equations are (7.39) with η and $\eta - \Delta$ interchanged, and the stability equations are (7.40) with η and $\eta - \Delta$ interchanged. The results are shown in Figure 10 for large and moderate Prandtl numbers; for very small Prandtl numbers the picture is generally the same apart from reflection in the η-axis.

Figure 10

The solution bifurcating from $\eta = 0$ is the transcritical axisymmetric solution given by

$$A_2 = 0, \qquad \eta = \gamma_0 A_0 - \omega_0 A_0^2 = 0, \tag{7.44}$$

represented by the curves PQ, PR in Figure 10. Calculations based on (7.40) show that the branch PQ is stable and PO is unstable, as in the non-interactive case depicted in Figure 6, but that OR, initially stable, loses stability at $\eta = \eta_s$, where $0 < \eta_s < \Delta$. This re-emphasizes the preference for the upper branch discussed in Section 8.

The solution bifurcating from $\eta = \Delta$ is a solution of the equation

$$A_2^2 = (\eta - \Delta - c_2 A_0 - \sigma_2 A_0^2)/\omega_2$$

$$0 = \eta A_0 - \gamma_0 A_0^2 - c_0 A_2^2 - \sigma_0 A_0 A_2^2 - \omega_0 A^3{}_0. \tag{7.45}$$

It is found to exist for $\eta > \Delta$ and to be a slight modification of the pure m = 2 solution described in B. of Section 6. This soluion is represented by the curves ΔL, ΔM and ΔN in Figure 10. Calculations show it to be unstable.

Finally, there is another solution of (7.45) which is a mixed mode and which bifurcates from the axisymmetric solution (7.44) at the point S. This solution is represented by the curves SU, SV, ST in Figure 10,and is found to be stable.

We see, therefore, that there are two stable solutions: The pure axisymmetric mode PQ, and the mixed mode emanating from S. The latter represents a distortion of the lower branch due to the modal interaction. Nevertheless the upper branch PQ is preferred as in the non-interactive situation.

8. DISCUSSION AND CONCLUSIONS

We have considered Marangoni instability in a circular cylinder under the simplifying assumptions that the upper free surface is non-deformable, i.e. $C \to 0$, and the sidewalls are adiabatic and impenetrable but "slippery".

The linear stability curves vary with surface Biot number h and Rayleigh number R as expected from the analyses of the unbounded layer. (The boundary-value problems are identical.) M_c decreases with R and increases with h and these features are shown in Figures 3-5. Here, the envelope of each set of curves gives M_c for each aspect ratio. Had we used the more realistic rigid-side-wall boundary conditions, this envelope would have been modified. We would still expect to have interlacing of the modes though the modes might interlace in a different sequence. Only the direct calculation of these neutral stability curves could determine this. We shall discuss below the implications of the use of slippery sidewall conditions.

Given the qualitative similarities of cases for various values of h and R, we investigate the nonlinear behavior only for the single set $h = 0$, $R = 0$. We have selected five aspect ratios and performed the bifurcation analyses for these.

Cases A, B and C of Section 6 relate to aspect ratios corresponding to simple eigenvalues M_c for which $m = 1,2,0$ respectively. We see that for $m \neq 0$ that we have supercritical bifurcation only. However, when $m = 0$, the axi-symmetric convection is subcritical and snap-through convection can be expected. It is only in this axi-symmetric case that flor direction is distinguished. For low Prandtl number Pr, there is downflow in the center while for all $Pr \geq 1$, there is upflow in the center. As is well-known, subcritical instabilities have associated transport values with hysteresis behavior. (This

will be discussed further for Case B of Section 7.) It is easy to calculate the degree of subcriticality possible in the axi-symmetric mode i.e. the $\Delta M/M_c$ at the nose of the curve. This varies from 0.18% at Pr = 0.1 to 1.4% at Pr = ∞. The only comparison available is to the results of Scanlon and Segel (1967) who examine an "infintely deep" layer having no sidewalls. In their analysis they have Pr = ∞ and find $\Delta M/M_c$ = 2.3%. The two analyses are in reasonable agreement. This gives further substance to our feeling that our results reflect the inherent nonlinear behavior of the system.

Case A of Section 7 examines a neighborhood of $a = a_A$ of Figure 3 where M_c is a double eigenvalue of modes m = 1 and m = 2. The nonlinear theory gives a coupled pair of nonlinear amplitude equations, (7.15). The analysis shows (Figure 8) that for a slightly larger than a_A the first mode to appear (at $M = M_c$) is the pure mode m = 2 as predicted by linear theory. As M is increased above M_c, the system remains in this mode and possibly no further transition is predicted. Alternatively, the system may progress through there the sequence: pure m = 2, mixed (1,2) mixed time-periodic and perhaps pure m = 2 as discussed in Section 7. On the other hand if a is slightly smaller than a_A the transition sequence (Figure 7) is completely different. Here, at $M = M_c$, a mixed (1,2) mode occurs and this mode becomes unstable for an $M > M_c$. Hence, there must be a transition to the pure mode m = 2. We find then that the mode m = 2 may persist and be stable for M large enough on either side of $a = a_A$ <u>independent of the prediction of linear theory</u>. This result depends on the stability of the time-periodic mode which has not been examined here but will be investigated further in later work.

Case B of Section 7 examines a neighborhood of $a = a_B$ of Figure 3 where M_c is a double eigenvalue of modes m = 2 and m = 0. The nonlinear theory gives a coupled pair of nonlinear amplitude equations (7.36). The analysis shows (Figure 8) that for a slightly larger than a_B the first mode to appear

(at $M = M_c$) is the pure axi-symmetric one. There is a snap-through at some $M < M_c$ (the snap-through is accompanied by a dynamical hysteresis behavior). With sufficiently small disturbances the system resides in this $m = 0$ mode for all M covered by the theory. Yet, for M large enough there can be a transition to the mixed (2,0) mode if the disturbances are large enough. On the other hand if a is slightly smaller than a_B (Figure 9) very small disturbances evolve as a mixed (2,0) mode until this mode becomes unstable at supercritical conditions. At this point there is a snap-through transition to the pure $m = 0$ mode. If M is then decreased, a dynamical hysteresis loop would be revealed since the jump back to the mixed mode would usually occur at much lower values of M; conceivably in fact the jump could be to the state of pure conduction. This interesting hysteresis loop could consist of <u>three</u> distinct states: mixed (2,0), pure $m = 0$, pure conduction! Alternatively, if the system is very noisy in that large disturbances are present, as M is increased from subcritical condition, the system could snap-through directly from conduction (at $M < M_c$) to the axi-symmetric state and completely by-pass the mixed-mode state for increasing M, yet return to it when M is decreased.

The above analysis should give a faithful representation of the nonlinear processes in fairly small containers in which Marangoni instability takes place. If the replacing of the ideal sidewalls with more realistic rigid walls does not change the sequence of the modal interlacings, then the theory could be applied to experiment in a straight-forward way. <u>If</u> the sequence of modal interlacings <u>does</u> change, then the theory should be applied by first locating the double eigenvalue by experimental observation. Thus location $a = a_B$, say, would be different from that of the "slippery" wall linearized analysis. However, once it is located, the raising of M for aspect ratios a

on either side of a_B should be well represented by the above theory. It is thus a relatively "simple" observation of flow pattern that would initially need verification.

There has been no previous nonlinear analysis of Marangoni convection in a bounded container. The present work represents a first exploration of the phenomena albeit with an idealized model. The idealization on the upper free surface $C \to 0$, will be relieved in our future work so that effects of free-surface deflection can be assessed. The dropping of idealization of slippery sidewalls entails a major computing program that will not be undertaken. Clearly, certain small imperfections on either the sidewalls or the free surface can lead to an imperfect bifurcation in which the predicted sharp instabilities become gradual changes. Our work here provides the framework for studying these effects as well.

REFERENCES

Bénard, H. 1900 Rev. Gen. Sci. Pure Appl. 11, 1261.

Davis, S. H. 1969 J. Fluid Mech. 39, 347.

Davis, S. H. and Homsy, G. M. 1980 J. Fluid Mech. 98, 527.

Eckhaus, W. 1965 Studies in Non-linear Stability Theory, Springer Tracts in National Philosophy, Berlin, Vol. 6.

Koschmieder, E. L. 1967 J. Fluid Mech. 30, 9.

Kraska, J. R. and Sani, R. L. 1979 Int. J. Ht. Mass Trans. 22, 535.

Liang, S. F., Vidal, A. and Acrivos, A. 1969 J. Fluid Mech. 36, 239.

Nield, D. A. 1964 J. Fluid Mech. 19, 341.

Palmer, H. and Berg, J. 1971 J. Fluid Mech. 47, 779.

Pearson, J. R. A. 1958 J. Fluid Mech. 4, 489.

Rosenblat, S. 1979 Studies Appl. Math. 60, 241.

Rosenblat, S., Homsy, G. M. and Davis, S. H. 1981 Pending publication.

Scanlon, J. W. and Segel, L. A. 1967 J. Fluid Mech. 30, 149.

Scriven, L. E. and Sternling, C. V. 1964 J. Fluid Mech. 19, 321.

Smith, K. A. 1966 J. Fluid Mech. 24, 401.

Sørensen, T. S. 1978 Dynamics and Instability of Fluid Interfaces, Proceedings, Lyngby, Springer.

Vidal, A. and Acrivos, A. 1966 Phys. Fluids 9, 615.

Zeren, R. and Reynolds, W. C. 1972 J. Fluid Mech. 53, 305.

CAPTIONS FOR FIGURES

FIGURE 1: A sketch of a possible static liquid-gas configuration in a wide container (a) on Earth at 1g, (b) in space at 10^{-6}g, (c) in space at 10^{-6}g, (d) in space at 10^{-6}g.

FIGURE 2: A sketch of a possible static liquid-gas configuration in a narrow container (a) when the interface is curved and (b) when the interface is flat.

FIGURE 3: Calculated stability curves, M versus a, for h = 0, R = 0 where m and i are the azimuthal and radial wave numbers, respectively. M_c is the envelope (minima) of the curves.

FIGURE 4: Calculated neutral stability curves. M_c versus a for h = 0 and various values of R. The m values take the same sequence as in Figure 3.

FIGURE 5: Calculated netural stability curves, M_c versus a for R = 0 and various values of h. The m values take the same sequence as in Figure 3.

FIGURE 6: The bifurcation diagrams for a = 1.80 corresponding to a pure axi-symmetric mode m = 0. Solid lines represent stable branches while dotted lines represent unstable branches. (a) The case of Pr = 0.1: the branch PQ represents downflow in the center. (b) The case of Pr $\geq$ 1; the branch PQ represents upflow in the center.

FIGURE 7: The bifurcation diagrams for a slightly less than $a_A \approx 1.20$ where $\Delta = M_2 - M_1$. Solid lines represent stable branches while dotted lines represent unstable branches.

FIGURE 8: The bifurcation diagrams for a slightly greater than $a_A \approx 1.20$ where $\Delta = M_1 - M_2$. Solid lines represent stable branches while dotted lines represent unstable branches. The curly lines represent time-periodic bifurcations.

FIGURE 9: The bifurcation diagrams for a slightly less than $a_B \approx 1.70$ where $\Delta = M_2 - M_0$. Solid lines represent stable branches while dotted lines represent unstable branches.

FIGURE 10: The bifurcation diagrams for a slightly greater than $a_B \approx 1.70$ where $\Delta = M_0 - M_2$. Solid lines represent stable branches while dotted lines represent unstable branches.

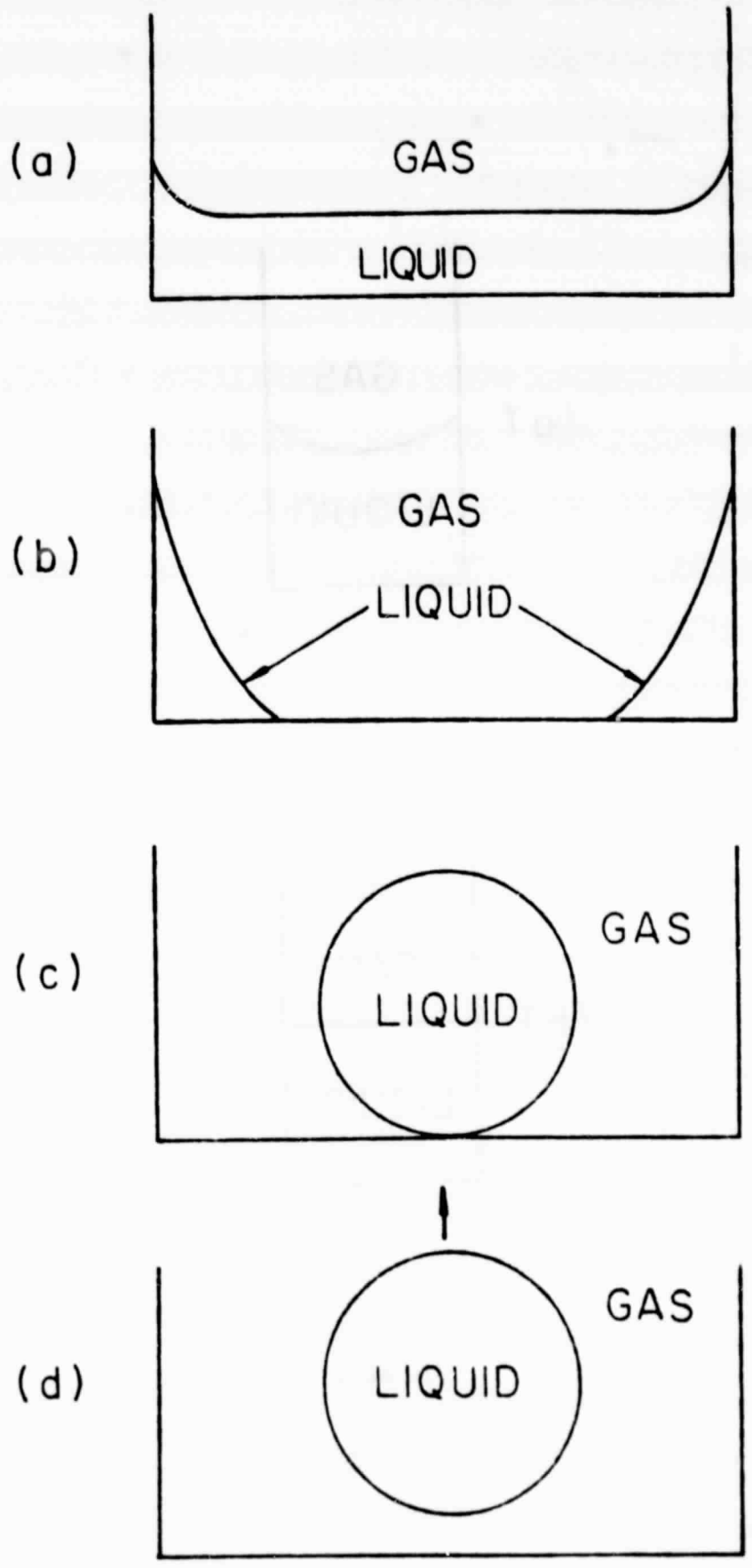

FIGURE 1

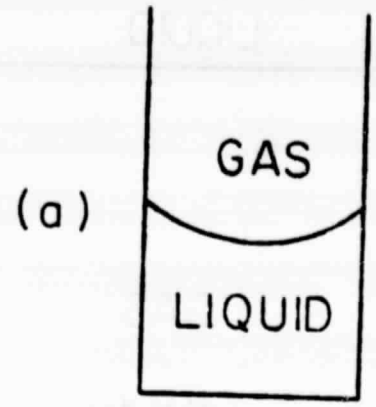

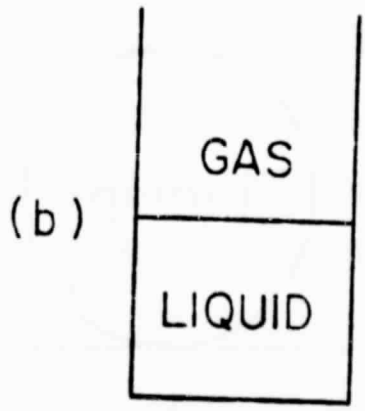

FIGURE 2

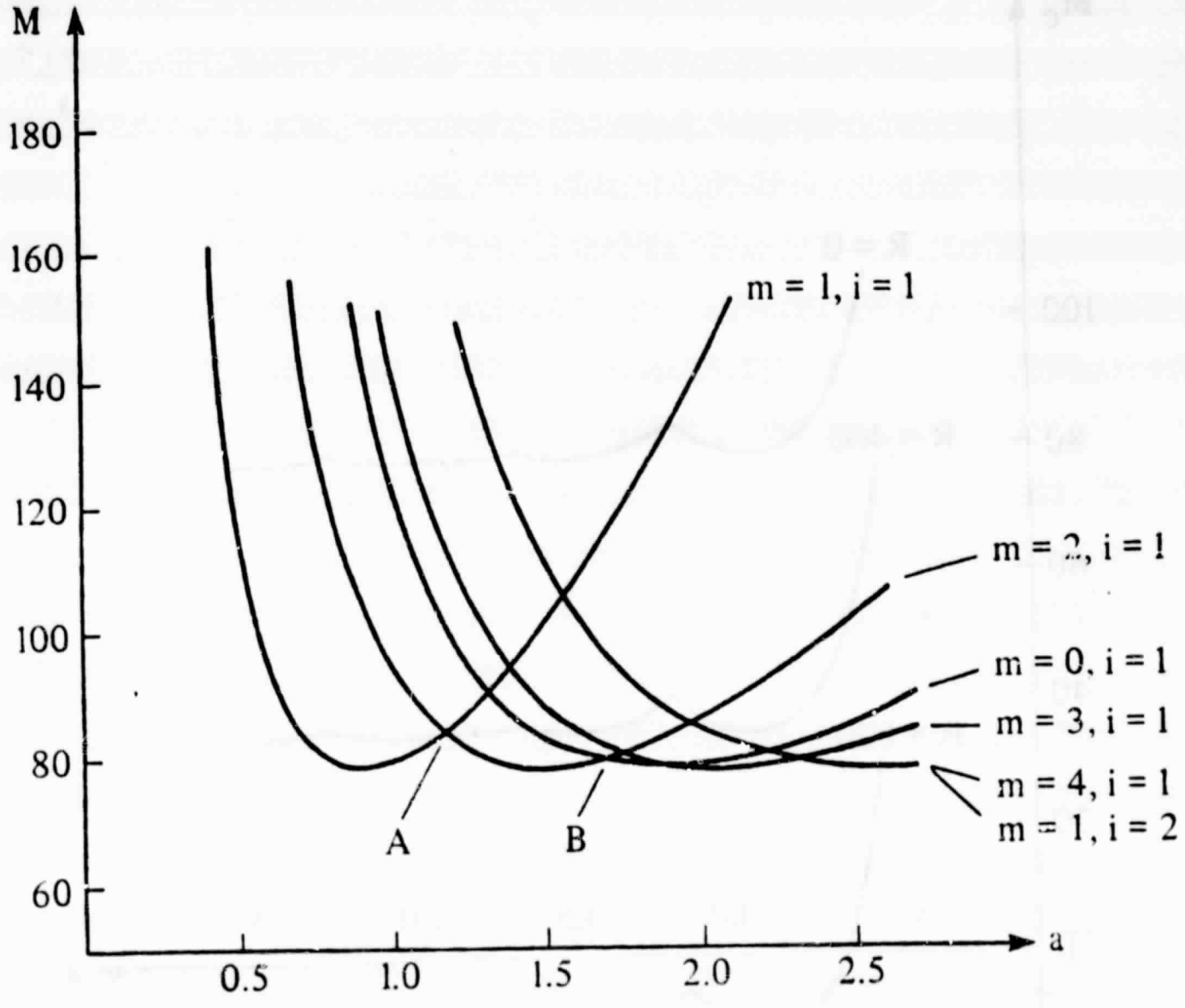
M
180
160
140
120
100
80
60
0.5
1.0
1.5
2.0
2.5
a
m = 1, i = 1
m = 2, i = 1
m = 0, i = 1
m = 3, i = 1
m = 4, i = 1
m = 1, i = 2
A
B

FIGURE 3

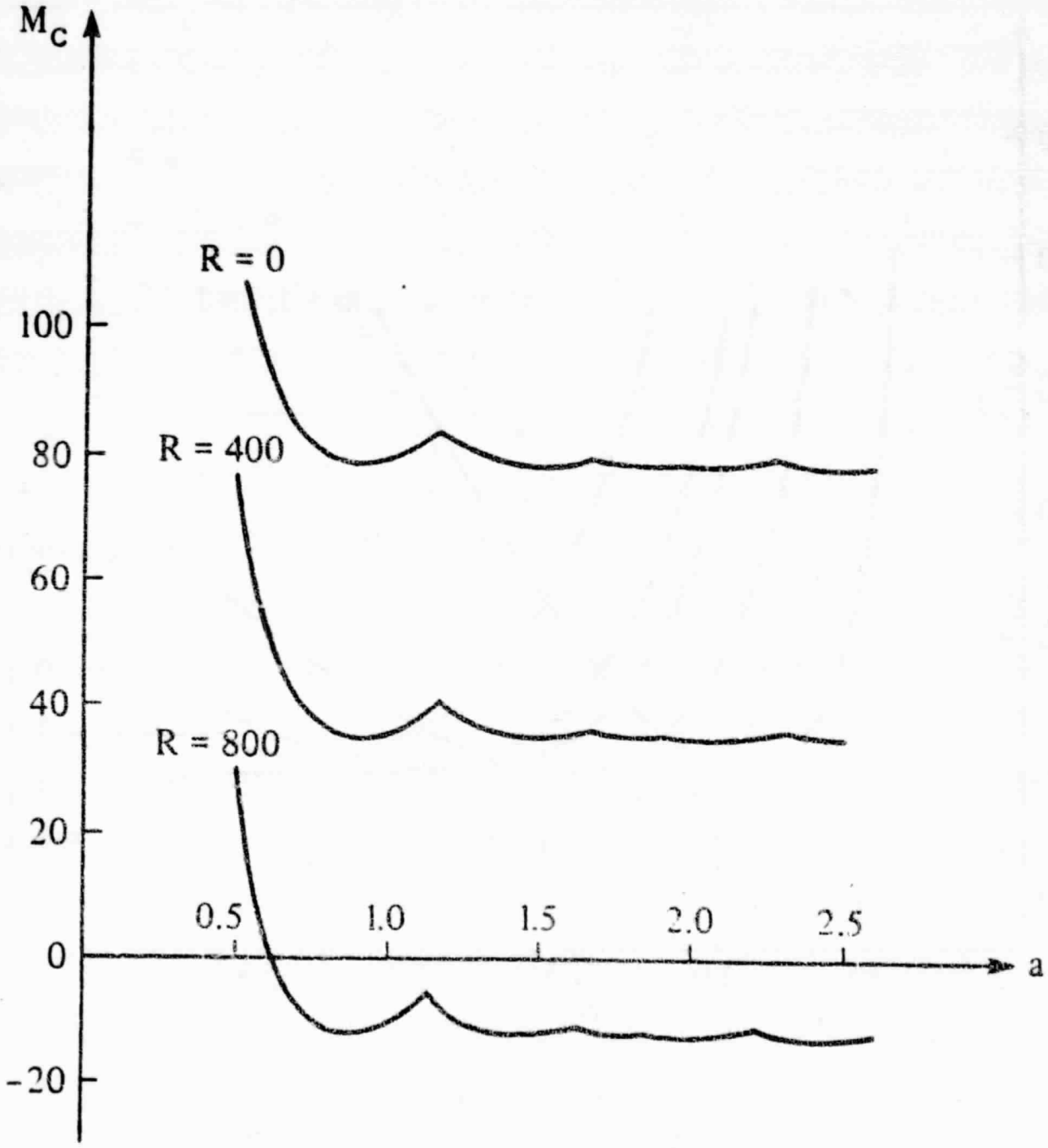

FIGURE 4

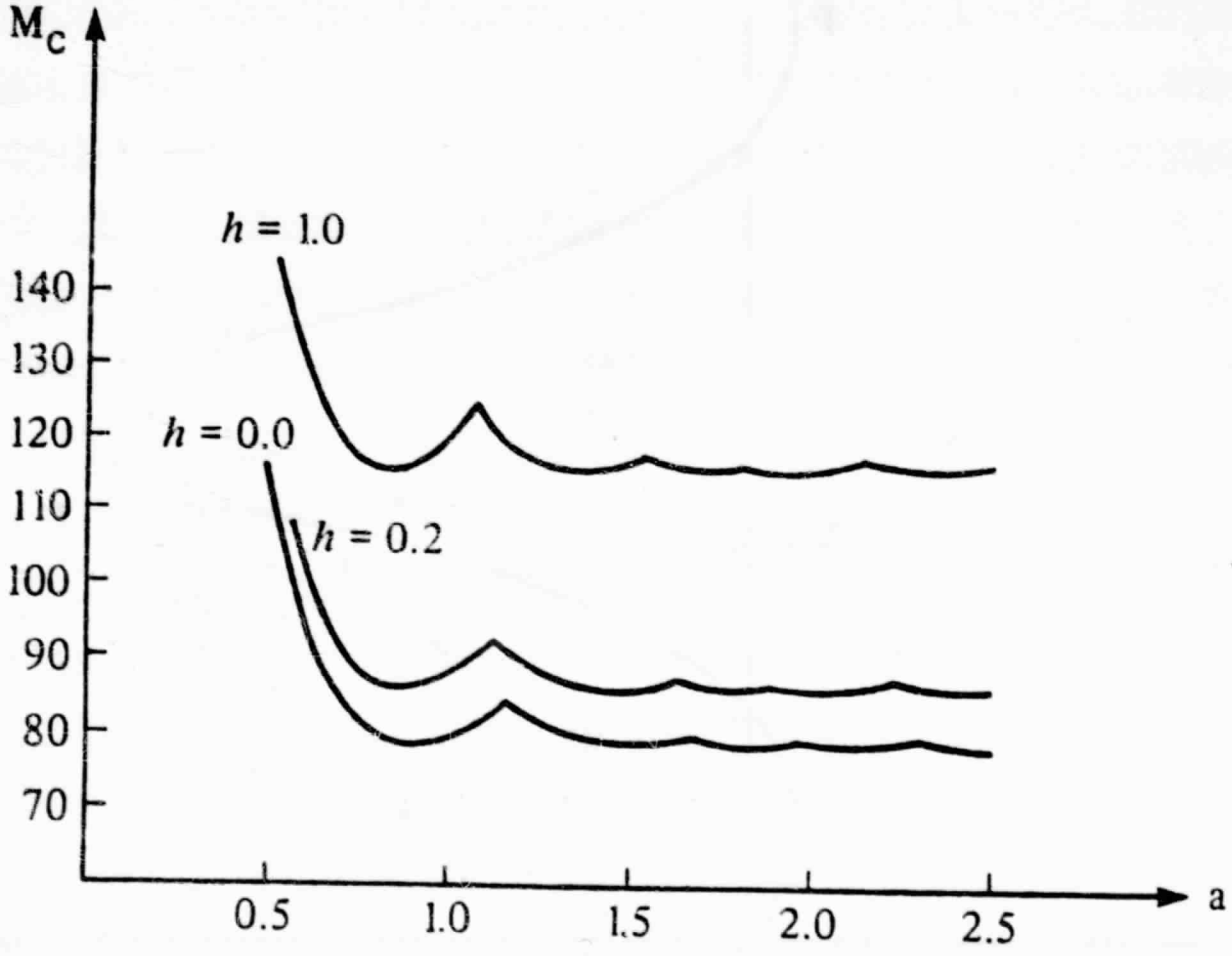

FIGURE 5

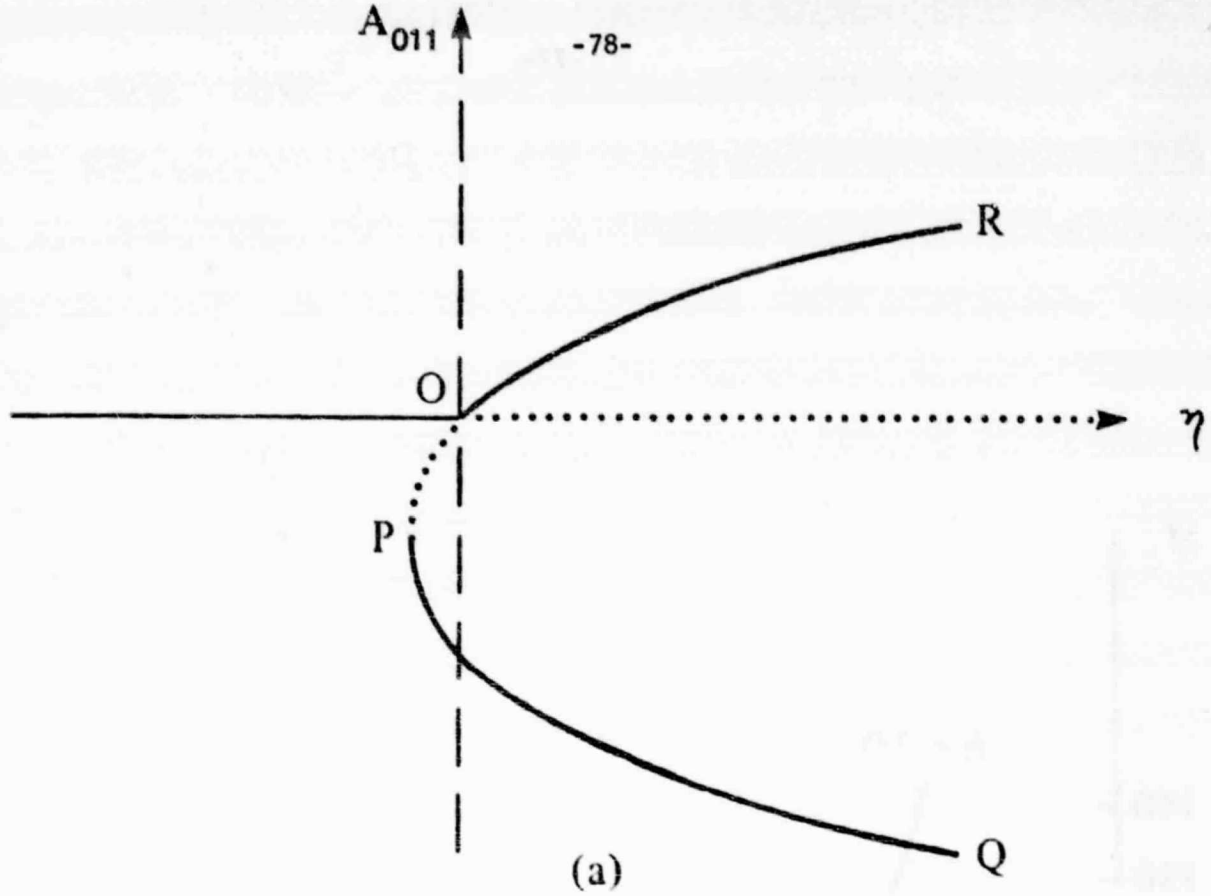

(a)

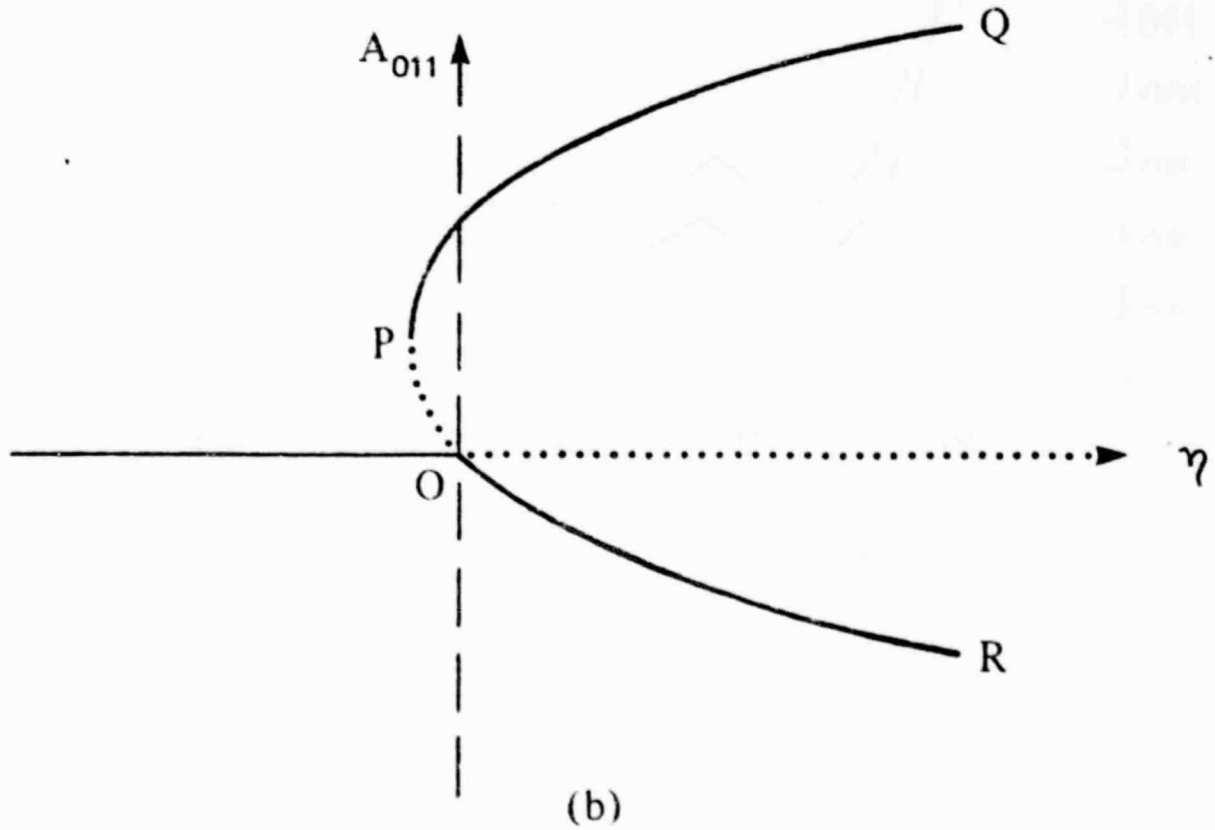

(b)

FIGURE 6

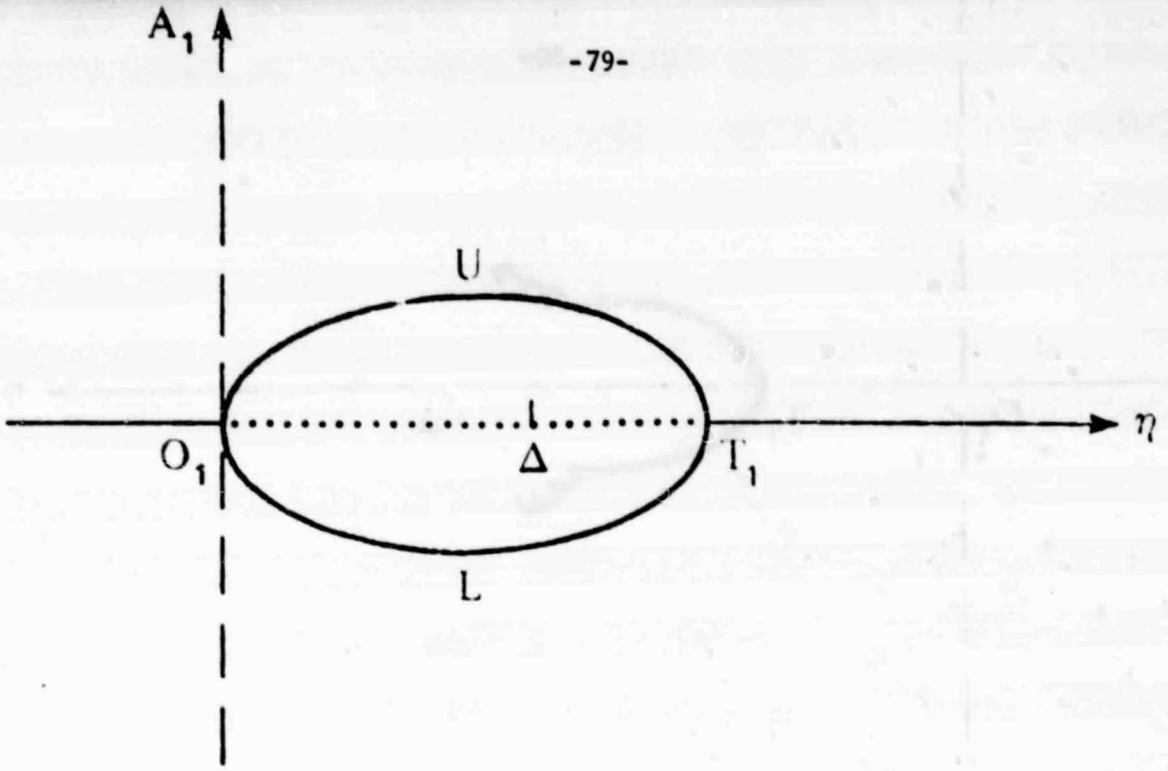

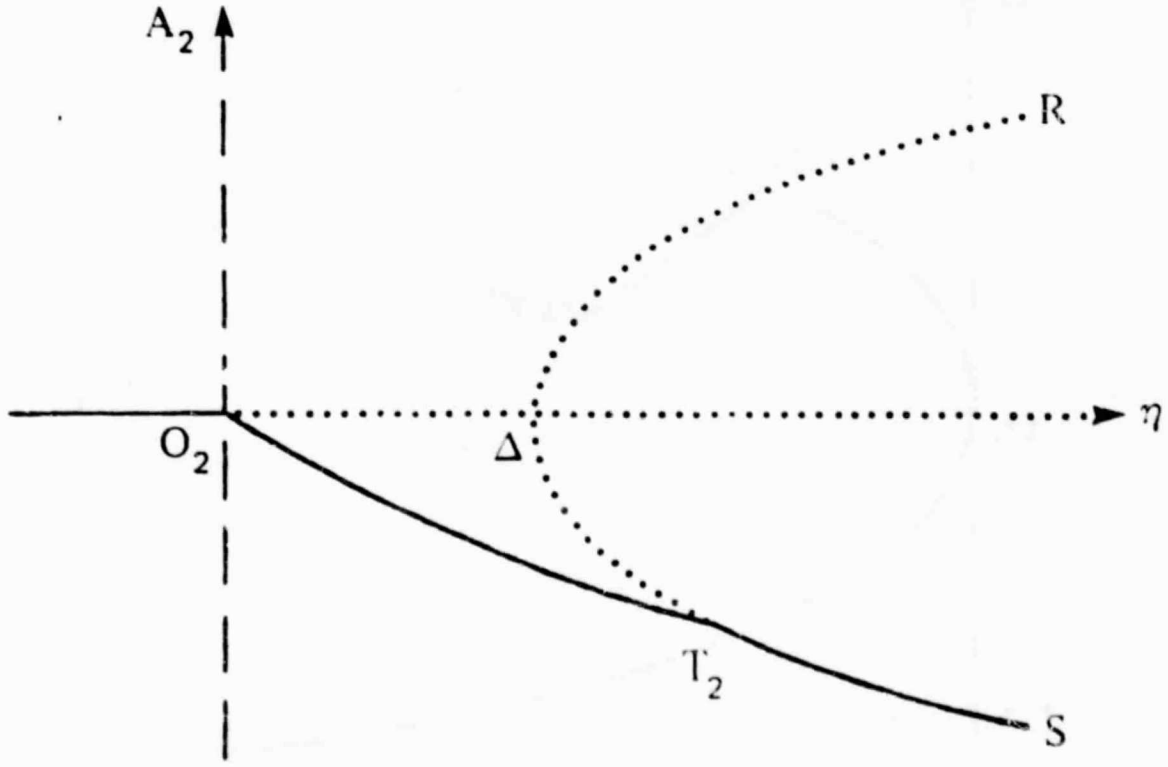

FIGURE 7

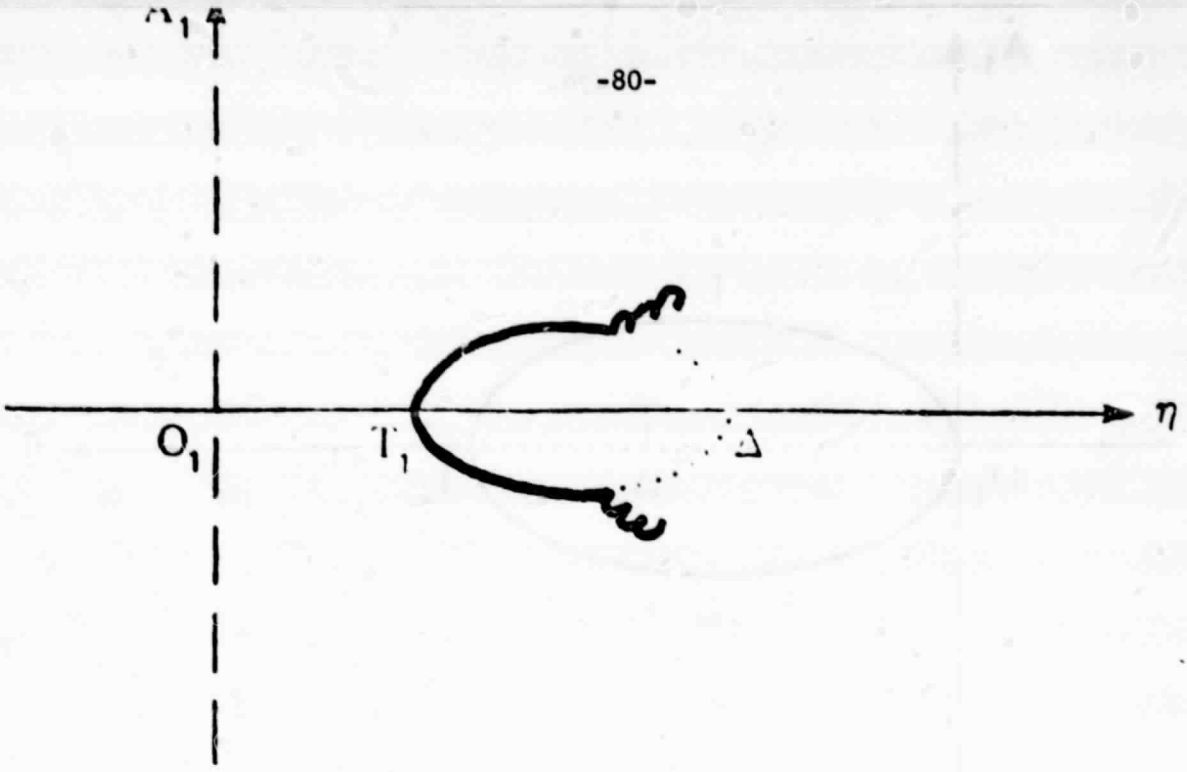

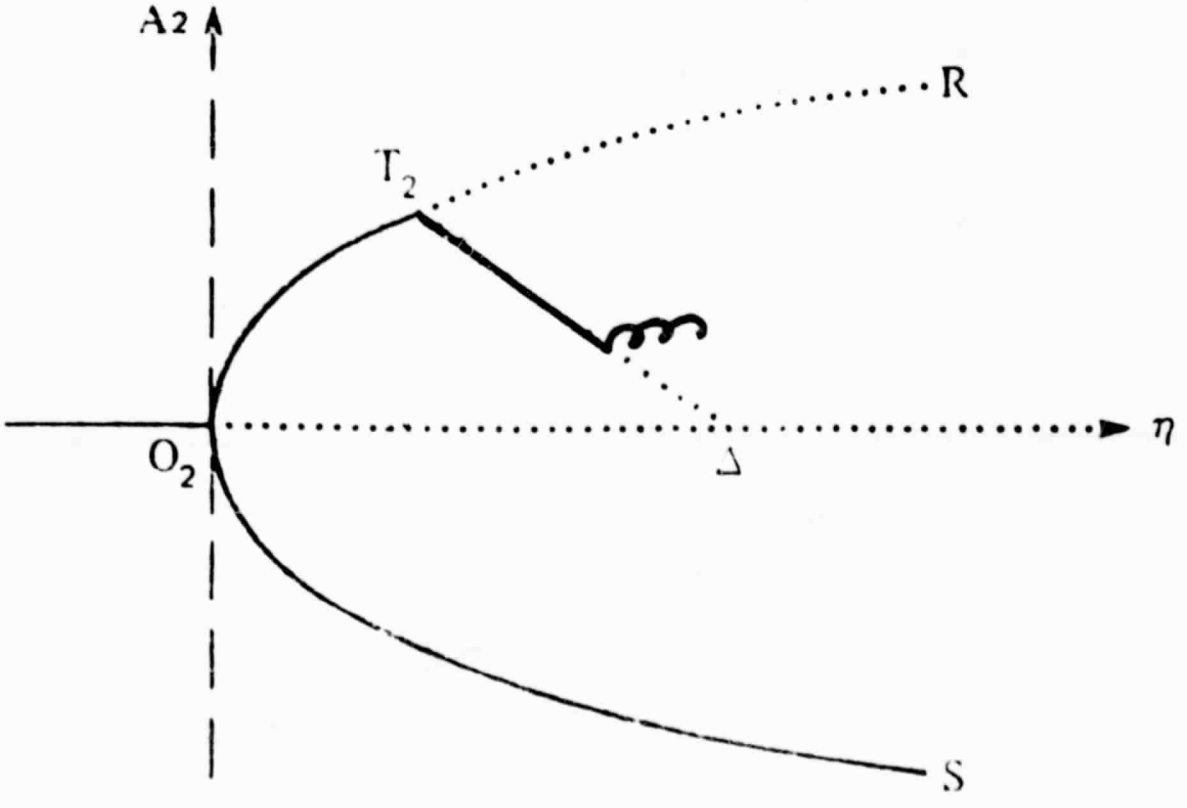

FIGURE 8

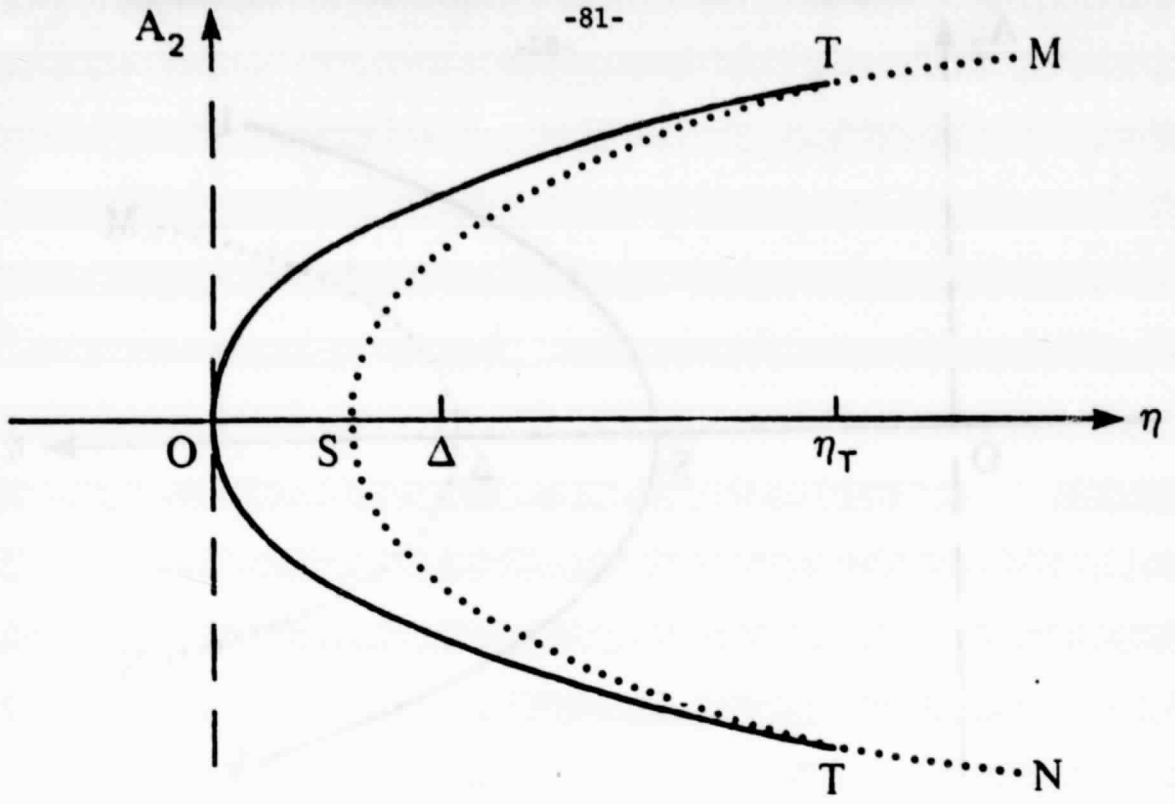

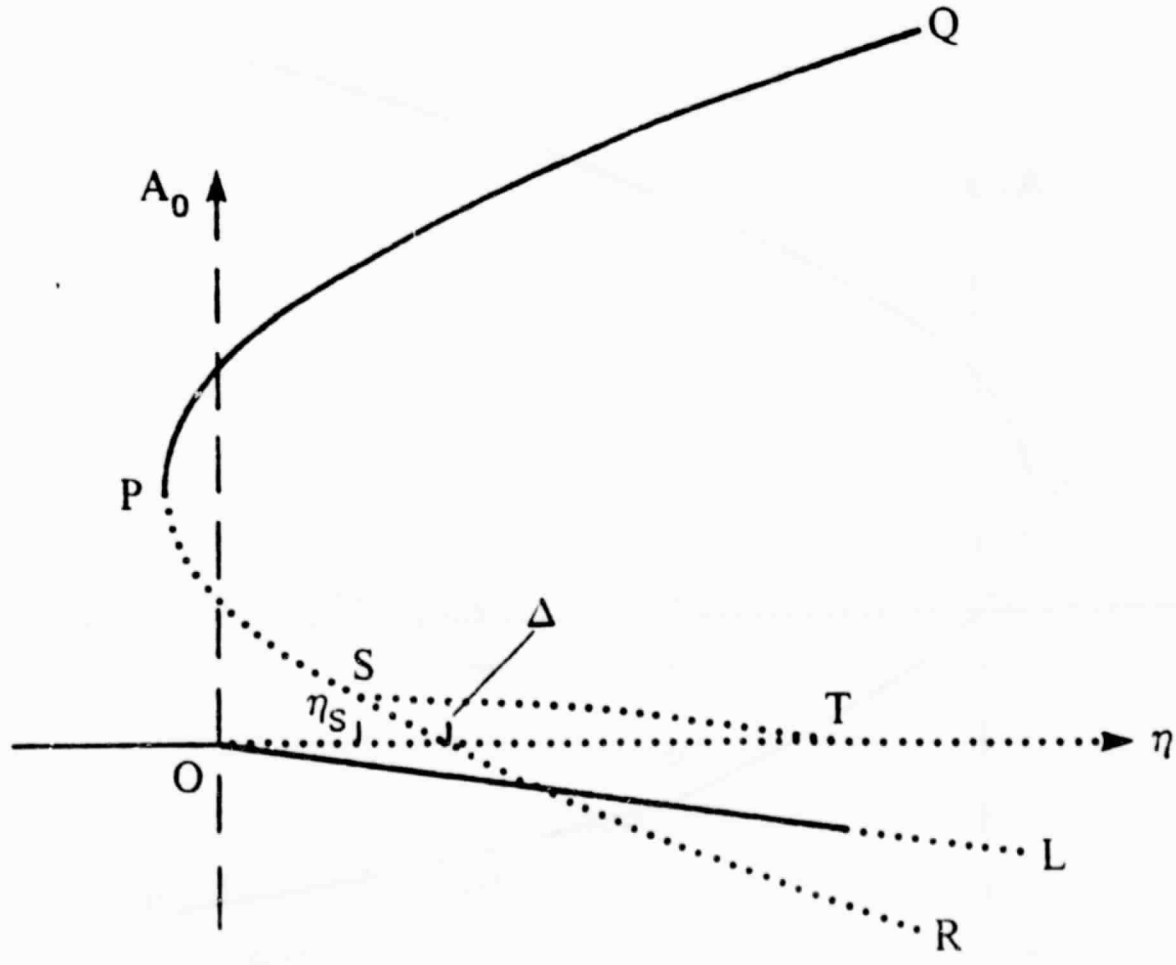

FIGURE 9

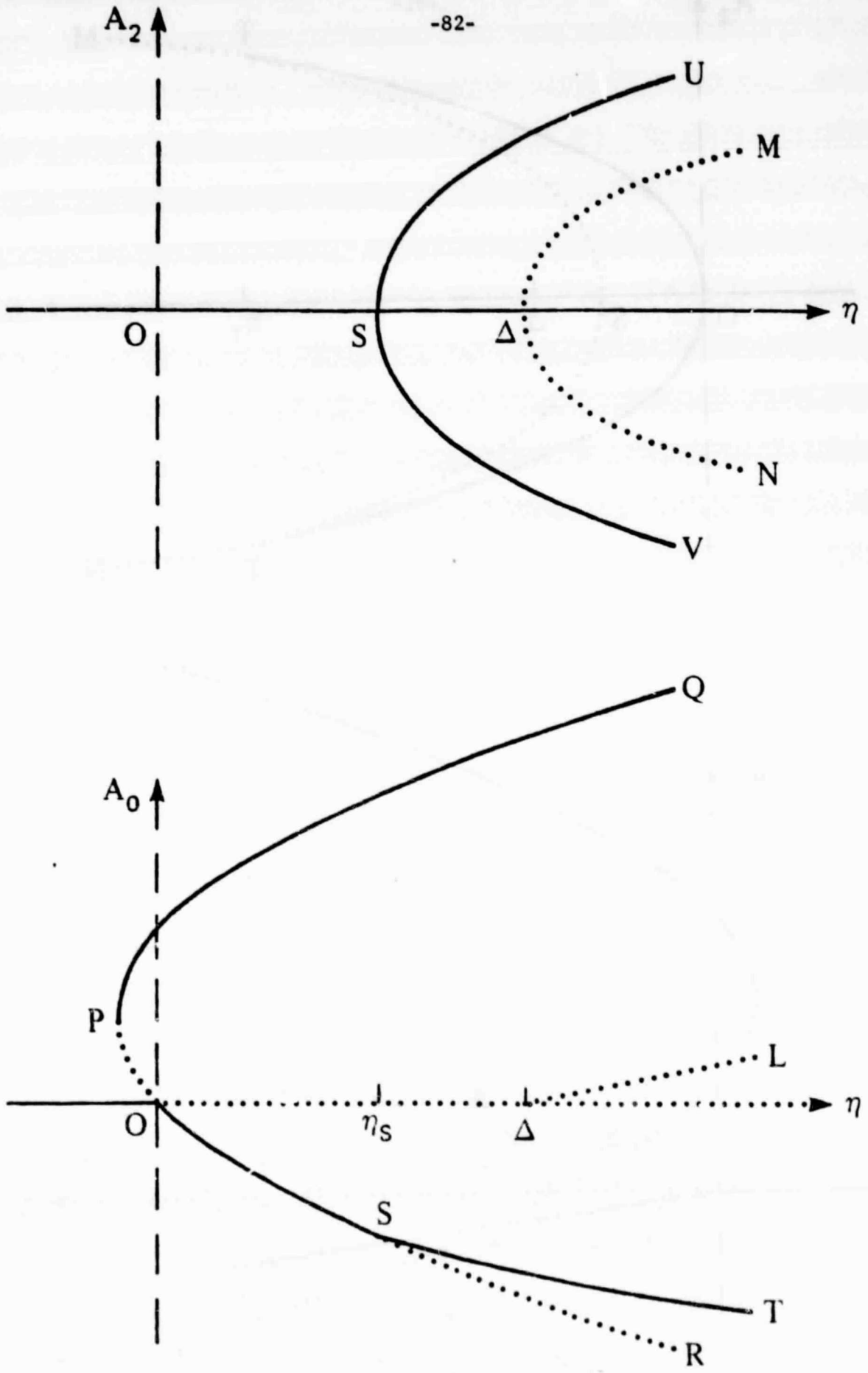

FIGURE 10

CHAPTER II. CONVECTION IN RECTANGULAR CYLINDERS

1. INTRODUCTION

In Chapter I, which we shall call I, we discussed Marangoni instabilities in a circular cylinder and distinguished between simple eigenvalues and double eigenvalues, where secondary bifurcations are possible.

In the present chapter, we examine Marangoni instability in rectangular containers. Again, we assume that the upper free surface is non-deformable, $C \to 0$, and the sidewalls are adiabatic and impermeable but "slippery", which in the rectangular geometry, corresponds to zero shear stress applied on the boundary. We use the asymptotic theory of Rosenblat (1979) to examine the steady convective states near M_c and how transitions from one state to another occur. We limit ourselves to interactions of modes in the form of two-dimensional roll-cells, which are predicted for rectangular containers having the shorter side comparable to the depth and the longer side larger than the depth. Since much of the full development is similar to that in I, we give only those details which distinguish convection in a rectangular container from convection in a circular cylinder.

2. FORMULATION

Consider a viscous liquid, which partially fills a container of rectangular cross-section. The mean depth of the liquid is d and a horizontal cross-section has lengths $a_1 d$ and $a_2 d$ in the x and y directions respectively. Hence, a_1 and a_2 are the aspect ratios. The axis of the cylinder is anti-parallel to the direction of gravity, and the upper surface of the liquid is open to an ambient gas.

The development of the non-dimensional nonlinear disturbance equations and boundary conditions parallels that in I. Again, in the limit of small capillary number and when the lateral boundaries are adiabatic and impenetrable but "slippery", we obtain the following nonlinear problem. From equations (2.19-2.21) of I,

$$Pr^{-1}M\left\{\frac{\partial \underline{v}}{\partial t} + (\underline{v}\cdot\underline{\nabla})\underline{v}\right\} = -\underline{\nabla}p + \nabla^2\underline{v} + M^{-1}R\theta\hat{\underline{z}} \tag{2.1}$$

$$\underline{\nabla}\cdot\underline{v} = 0 \tag{2.2}$$

$$M\left\{\frac{\partial \theta}{\partial t} - w + (v\cdot\underline{\nabla})\theta\right\} = \nabla^2\theta \tag{2.3}$$

where M, R and Pr are the Marangoni, Rayleigh and Prandtl numbers defined in equations (2.22) of I.

The bottom of the box is a rigid perfect conductor so that

$$\theta = 0 \quad \text{on} \quad z = 0 \quad , \quad 0 \le x \le a_1 \quad , \quad 0 \le y \le a_2 \quad , \tag{2.4a}$$

$$\underline{v} = \underline{0} \quad \text{on} \quad z = 0 \quad , \quad 0 \le x \le a_1 \quad , \quad 0 \le y \le a_2 \quad . \tag{2.4b}$$

Since the capillary number is zero, the upper surface is flat, so that from equations (3.5) of I, the heat transfer condition is

$$\frac{\partial\theta}{\partial z} + h\theta = 0 \quad \text{on} \quad z = 1 \ , \ 0 \le x \le a_1 \ , \ 0 \le y \le a_2 \tag{2.5a}$$

and the kinematic condition is

$$w = 0 \quad \text{on} \quad z = 1 \ , \ 0 \le x \le a_1 \ , \ 0 \le y \le a_2 \ . \tag{2.5b}$$

The conditions of thermocapillarity become

$$u_z + w_x + \theta_x = v_z + w_y + \theta_y = 0 \ , \ z = 1 \ , \ 0 \le x \le a_1 \ , \ 0 \le y \le a_2 \ . \tag{2.5c}$$

Finally, the "slippery" sidewalls reduce in Cartesian coordinates to adiabatic, impermeable stress-free planes. These conditions take the form

$$u = w_x = v_x = \theta_x = 0 \quad \text{on} \quad x = 0, a_1; \ 0 \le y \le a_2 \ , \ 0 \le z \le 1 \tag{2.6a}$$

$$v = w_y = u_y = \theta_y = 0 \quad \text{on} \quad y = 0, a_2; \ 0 \le x \le a_1 \ , \ 0 \le z \le 1 \tag{2.6b}$$

3. LINEAR STABILITY PROBLEM

The critical Marangoni number at which the conduction solution loses stability is determined from linearization of the system (2.1)-(2.3) together with the (linear) boundary conditions (2.4)-(2.6). As in I, we assume that M_c occurs at a state of neutral stability so that the governing linearized equations become

$$\nabla^4 w + M^{-1} R \nabla_1^2 \theta = 0 \tag{3.1a}$$

and

$$\nabla^2 \theta + Mw = 0 \quad . \tag{3.1b}$$

System (3.1) plus boundary conditions (2.4)-(2.6) may be solved by seeking separable solutions in the form

$$w(x,y,z) = \cos[\, m_1 \pi x/a_1] \cos[m_2 \pi y/a_2] Y(z) \tag{3.2a}$$

$$\theta(x,y,z) = \cos[\, m_1 \pi x/a_1] \cos[m_2 \pi y/a_2] X(z) \tag{3.2b}$$

with similar definitions for u and v. Here X and Y are the same functions as those in I since they are eigenfunctions of a set associated with the stability of the infinite conductive layer considered by Pearson (1958). Here m_1 and m_2 run over all non-negative integers.

When forms (3.2) are substituted into eqns. (3.1), an effective wave number λ appears where

$$\lambda^2 = [(m_1/a_1)^2 + (m_2/a_2)^2]\pi^2 \quad . \tag{3.3}$$

The effects of buoyancy through the Rayleigh number R and the effects of the free surface being a poor insulator through the surface Biot number can be explored as in I. The effects are the same in that increasing R decreases M_c and increasing h increases M_c. These results will not be

presented here. We shall confine ourselves to R = 0 and h = 0. In this case, we find that

$$M(\lambda) = \frac{8\lambda^2(\lambda - \sinh\lambda\cosh\lambda)\cosh\lambda}{\lambda^2\cosh\lambda - \sinh^3\lambda} . \tag{3.4}$$

We note that for an infinite layer, λ is the overall wave number which takes on all values on $[0,\infty)$. $M(\lambda)$ would then have the minimum $M_\infty \approx 79.6$ for $\lambda_\infty \approx 2$. This result is due to Pearson (1958). For the present enclosed layer, $M(\lambda)$ must be minimized over only those admissible λ given by eqn. (3.3).

The relationship between the box aspect ratios and the mode of convection, indicated by the integers (m_1,m_2), is given implicitly by equation (3.4). We have evaluated this relationship for a range of box sizes for all possible modes of convection. The results are given in Figures 1-6, in which M is given as a function of a_1 for fixed values of a_2. For clarity, modes having large critical Marangoni numbers are not shown. Consider first the case of $a_2 = 0.5$ shown in Figure 1. As the box size, a_1, increases, the preferred mode, i.e. the mode having the lowest critical Marangoni number, changes in a specific way. This sequence is among modes for which $m_2 = 0$. Thus, we have two-dimensional roll cells whose axes are aligned with the shorter dimension of the box. We shall call these x-rolls. It is seen that for box sizes $a_1 \cong \frac{m_1\pi}{2}$ with $m_1 = 1,2,3\cdots$ that $\lambda \cong 2$ and the critical Marangoni number is minimum at the value $Ma_\infty \approx 79.6$ appropriate to infinite layers. Away from these values, the sidewalls exert a stabilizing influence, even though they are "slippery". While the fact that several box sizes can have the same $M = M_\infty$ is presumably an artifact of the use of the slip-wall boundary conditions, the existence and progression of preferred modes due to the finite size of the container is not.

In the case of buoyancy-driven convection, the dependence of M on box size is monotonic but has kinks at the points of mode switching, Davis (1967), and the effect of sidewalls is to align the roll axes with the shorter side of the box. This is the same progression and alignment as predicted here for $a_2 = 0.5$, but we shall see below that the present treatment leads to some predictions of preferred mode orientation which are presumably artifacts of the slip-wall boundary conditions.

To summarize, the curves in Figure 1 predict preferred modes consisting of x-rolls, and the progression is to add more x-rolls as the box size increases. Of particular interest are the aspect ratios at which two modes have the same critical M, this is a double eigenvalue of the linear theory.

Figure 2 shows the results for $a_2 = 1.0$. Since the modes with $m_2 = 0$ are unaffected by the length a_2 the lower curves are identical to those of Figure 1. We anticipate however, that as a_2 approaches $m_2\pi/2$, there are two-dimensional rolls with axes aligned with the longer side of the box, (y-rolls), which might have lower critical Marangoni numbers than the x-rolls. This is not yet the case for the (0,1) mode for the conditions of Figure 2, but becomes so for the conditions of Figure 3. Finally, we note the occurrence of more complex three-dimensional modes of convection, e.g. the (1,1) and (2,1) modes, having Marangoni numbers close to, but above those for x-rolls.

Figure 3 gives results for $a_2 = 1.5$, and shows several complex features. First we note that the (0,1) y-roll has $Ma \approx Ma_\infty$ for this value of a_2, independent of a_1, and hence is often the preferred mode. However, since $a_2 \neq \pi/2$, there are small ranges of box sizes located near $a_1 = \pi m_1/2$, for which x-rolls are preferred. We also note that three-dimensional modes, e.g. the (1,1) and (2,1), become closer to being preferred. At $a_2 = 2.0$,

the results shown in Figure 4 indicate that the y-rolls (0,1), (0,2), are no longer preferred, and the three-dimensional (1,1) and (2,1) modes are preferred over x-rolls for some range of values of a_1 away from $a_1 = m_1\pi/2$. For $a_2 = 3.0$ (i.e. close to π) Figure 5 shows that a situation analogous to that in Figure 3 occurs; the y-roll (0,2) has $Ma \approx Ma_\infty$ and is preferred for all box sizes a_1 away from $m_1\pi/2$. Finally, as shown in Figure 6, as a_2 increases, the number of modes competing and having $Ma \tilde{=} Ma_\infty$ increases, and the envelope of these neutral curves becomes nearly the horizontal line $Ma = Ma_\infty$. This reflects the diminished effect of the sidewalls in determining the preferred mode.

The results may be summarized by a map in the a_1-a_2 plane of the preferred modes. We note that the pattern of preferred modes must be anti-symmetric about $a_1 = a_2$, corresponding to a rotation of the coordinate system. Thus, $M(a_1,a_2) = M(a_2,a_1)$ and the preferred modes, $(m_1(a_1,a_2), m_2(a_1,a_2)) = (m_2(a_2,a_1), m_1(a_2,a_1))$. It is clear from the previous discussion that this map will be complex, and that as a_1 and a_2 become large, many modes will have values of the critical Marangoni number close to that for the preferred modes. This map is shown in Figure 7. With one exception, it is difficult to speculate on the degree to which this complexity depends upon the use of slip-wall boundary conditions. Complexity of this degree does not occur for buoyancy-driven convection in a box, Davis (1967), but does occur for buoyancy-driven convection in a bounded porous media; Beck (1972). The persistence of y-rolls and x-rolls at $a_1 \approx m_1\pi/2$, $a_2 \approx m_2\pi/2$, $m_1,m_2 = 0,1,2,\ldots$ respectively, will not occur if more realistic no-slip boundary conditions are applied. Careful study of results similar to those in Figures 1-6 indicates that much of the complex mode-switching is due to neutral curve for y-rolls (x-rolls), being a horizontal line,

intersecting many times the neutral curve for other modes. No-slip sidewall conditions do not admit pure x-rolls or y-rolls, with the result that the neutral curves for modes which are close to y-rolls, (x-rolls), may not exhibit as many intersections. However, this does not imply that the bifurcation theory developed below will be simpler necessarily, as these modes may continue to be near-multiple eigenvalues of the linear theory.

C-2

4. EIGENFUNCTION EXPANSIONS

In the nonlinear theory we focus on certain special interactions appropriate to one horizontal box-dimension being comparable to the depth and the other much larger. In particular we shall take $a_2 = 1.0$ so that only x-rolls are predicted by linear theory. It is the interaction of rolls that we shall address. Although we must develop the theory for Rayleigh number $R \neq 0$ for completeness properties of the differential system, we shall, with no loss of generality, set $R = 0$ at the end. Hence, pure Marangoni instability will be analyzed.

Let us restate the linear stability problem for the case at hand:

$$\nabla^2 \underline{v} - \nabla p + M^{-1} R \theta \hat{\underline{z}} = \underline{0} \tag{4.1a}$$

$$\nabla \cdot \underline{v} = 0 \tag{4.1b}$$

$$\nabla^2 \theta + Mw = 0 \tag{4.1c}$$

with

$$\theta = u = w = 0 \qquad \text{on} \quad z = 0 \tag{4.1d}$$

$$\theta_z = w = u_z + \theta_x = 0 \qquad \text{on } z = 1 \tag{4.1e}$$

$$\theta_x = u = w_x = 0 \quad . \qquad \text{on } x = 0, a_1 \tag{4.1f}$$

The problem is now a two-dimensional problem since we are interacting only x-rolls; hence, $v, \frac{\partial}{\partial y} \equiv 0$.

For fixed $\hat{M}$ the eigenvalues are denoted by R_{mj} with $m,j = 1,2,\cdots$ and m is the horizontal wave number while j is the vertical wave number. Define

$$\lambda_m = m\pi/a_1 . \tag{4.2}$$

The eigenfunctions are

$$u_{mj} = -\lambda_m^{-1} \sin \lambda_m x \, DY_{mj}(z) \tag{4.3a}$$

$$w_{mj} = \cos \lambda_m x \, Y_{mj}(z) \tag{4.3b}$$

$$\theta_{mj} = \cos \lambda_m x \, X_{mj}(z) \tag{4.3c}$$

where the X_{mj} and Y_{mj} are the eigensolutions of the system (4.10)-(4.12) of I when $M = \hat{M}$, $R = R_{mj}$, $\lambda = \lambda_m$ and $h = 0$.

The adjoint problem is

$$\nabla^2 \underline{v}^* - \nabla p^* + \hat{M}\theta\hat{\underline{z}} = \underline{0} \tag{4.4a}$$

$$\nabla \cdot \underline{v}^* = 0$$

$$\nabla^2 \theta^* + \hat{M}^{-1} R w^* = 0 \tag{4.4c}$$

with

$$\theta^* = u^* = w^* = 0 \qquad \text{on } z = 0 \tag{4.4d}$$

$$\theta_z^* + w_z^* = w^* = u_z^* = 0 \qquad \text{on } z = 1 \tag{4.4e}$$

$$u^* = w_x^* = \theta_x^* = 0 \qquad \text{on } x = 0, a_1 . \tag{4.4f}$$

The adjoint eigenfunctions are

$$u_{mj}^* = -\lambda_m \sin \lambda_m x \, DY_{mj}^*(z) \tag{4.5a}$$

$$w_{mj}^* = \lambda_m^2 \cos \lambda_m x \, Y_{mj}^*(z) \tag{4.5b}$$

$$\theta_{mj}^* = \cos \lambda_m x \, X_{mj}^*(z) \tag{4.5c}$$

where X^*, Y^* satisfy system (5.14)-(5.16) of I with $h = 0$.

We now decompose all dependent variables into horizontal mean (i.e. x-mean) plus departures from the mean as follows

$$\underline{v} = \overline{\underline{v}} + \underline{v}' \quad , \quad \theta = \overline{\theta} + \theta' \quad , \quad p = \overline{p} + p' \tag{4.6a}$$

where for each quantity g,

$$\overline{g} = \frac{1}{a_1} \int_0^{a_1} g \, dx \, . \tag{4.6b}$$

For the case R = 0, the equations (2.1)-(2.3) are

$$\nabla^2 \underline{v} - \nabla p = MP_r^{-1}\{\underline{v}_t + (\underline{v}\cdot\nabla)\underline{v}\} \tag{4.7a}$$

$$\nabla\cdot\underline{v} = 0 \tag{4.7b}$$

$$\nabla^2\theta + Mw = M\{\theta_t + (\underline{v}\cdot\nabla)\theta\} \, . \tag{4.7c}$$

If forms (4.6) are introduced into system (4.7), then we get

$$\nabla^2\overline{\underline{v}} - \nabla\overline{p} = MP_r^{-1}\left\{\overline{\underline{v}}_t + (\overline{\underline{v}}\cdot\nabla)\overline{\underline{v}} + \overline{(\underline{v}'\cdot\nabla)\underline{v}'}\right\} \tag{4.8a}$$

$$\nabla\cdot\overline{\underline{v}} = 0 \tag{4.8b}$$

$$\nabla^2\overline{\theta} + M\overline{w} = M\left\{\overline{\theta}_t + (\underline{v}\cdot\nabla)\overline{\theta} + \overline{(\underline{v}'\cdot\nabla)\theta'}\right\} \tag{4.8c}$$

and

$$\nabla^2\underline{v}' - \nabla p' = MP_r^{-1}\left\{\underline{v}_t' + (\underline{v}'\cdot\nabla)\overline{\underline{v}} + (\overline{\underline{v}}\cdot\nabla)\underline{v}' + [(\underline{v}'\cdot\nabla)\underline{v}']_f\right\} \tag{4.9a}$$

$$\nabla\cdot\underline{v}' = 0 \tag{4.9b}$$

$$\nabla^2\theta' + Mw' = M\left\{\theta_t' + (\underline{v}'\cdot\nabla)\overline{\theta} + (\underline{v}\cdot\nabla)\theta' + [(\underline{v}'\cdot\nabla)\theta']_f\right\} \tag{4.9c}$$

where $[\ ]_f$ denotes the fluctuating part of $[\ ]$. The same boundary conditions hold for both systems (4.8) and (4.9).

As is well-known, there is no mean velocity field induced by the convection and thus

$$\overline{\underline{v}} = \underline{0} \ . \tag{4.10a}$$

Equation (4.8c) then simplifies considerably, and for steady or quasi-static convection,

$$\overline{\theta}_z = M\overline{(w'\theta')} \ . \tag{4.10b}$$

If these relations are used to simplify (4.7) we obtain,

$$\nabla^2\underline{v}' - \nabla p' = MP_r^{-1}\left\{\underline{v}'_t + [(\underline{v}'\cdot\nabla)\underline{v}']_f\right\} \tag{4.11a}$$

$$\nabla\cdot\underline{v}' = 0 \tag{4.11b}$$

$$\nabla^2\theta' + Mw' = M\left\{\theta'_t + Mw'\overline{(w'\theta')} + [(\underline{v}'\cdot\nabla)\theta']_f\right\} . \tag{4.11c}$$

We now take the scaler product of (4.11a,c) with the adjoint vectors $(\underline{v}^*_{mj}, \theta^*_{mj})$ at $M = M_c$, $R = R_{mj}$ and integrate over the fluid volume. This gives

$$\begin{aligned}(M - M_c)\langle\theta^*_{mj}w'\rangle - M_c^{-1}R_{mj}\langle w^*_{mj}\theta'\rangle = M\langle\theta^*_{mj}\theta'_t + P_r^{-1}\underline{v}^*_{mj}\cdot\underline{v}'_t\rangle \\ + M\langle\theta^*_{mj}\left\{[(\underline{v}'\cdot\nabla)\theta']_f + Mw'\overline{(w'\theta')}\right\} \\ + P_r^{-1}\underline{v}^*_{mj}\cdot[(\underline{v}'\cdot\nabla)\underline{v}']_f\rangle\end{aligned} \tag{4.12}$$

for each m and j. Equation (4.12) is the basis for the derivation of the amplitude equations.

5. SIMPLE AND DOUBLE INTERACTIONS

A. Simple eigenvalue for (1,0). Let us consider an aspect ratio $a_1 = 1.5$ which corresponds in Figure 2 to a simple eigenvalue M_c for convection with $(m_1,m_2) = (1,0)$.

We find that

$$M_c = 79.4 \tag{5.1}$$

and by hypothesis, $R_{11} = 0$. The quadratic interaction of mode 11 generates the 21 mode ($R_{21} \neq 0$) so the set $\mathcal{S}$ is

$$\mathcal{S} = \{11,21\}. \tag{5.2a}$$

We write

$$(\theta',\underline{v}') = A_1(\theta_{11},\underline{v}_{11}) + A_2(\theta_{21},\underline{v}_{21}) \tag{5.2b}$$

and substitute into equation (4.12). We obtain

$$\nu_1\dot{A}_1 = (M - M_c)A_1 - Z_1 \tag{5.3a}$$

$$\nu_2\dot{A}_2 = - M_c^{-1}R_2f_2A_2 - Z_2 \tag{5.3b}$$

when $M = M_c$, where

$$\nu_m = d_m^{-1}M_c\langle\theta_{m1}^*\theta_{m1} + Pr^{-1}\underline{v}_{m1}^*\cdot\underline{v}_{m1}\rangle \tag{5.3c}$$

$$f_m = d_m^{-1}\langle w_{m1}^*\theta_{m1}\rangle \tag{5.3d}$$

$$d_m = \langle\theta_{m1}^*w_{m1}\rangle \quad . \tag{5.3e}$$

We shall not give all the details of the evaluations since they are parallel to those of I. After a good deal of algebraic manipulation, we find that if α_1, α_2 and β_1 are constants that

$$Z_1 = \alpha_1A_1A_2 + \beta_1A_1^3 \tag{5.3f}$$

$$Z_2 = \alpha_2 A_1^2, \tag{5.3g}$$

and the governing amplitude equation takes the form

$$\nu_1 \dot{A}_1 = (M - M_c)A_1 - \omega_1 A_1^3. \tag{5.4}$$

The computations of the coefficients have been performed for various values of Prandtl numbers and some results are shown in Table 1.

Pr	$\nu_1 \times 10^{-4}$	$\omega_1 \times 10^{-4}$
0.1	0.37	5.2
1.0	0.13	0.64
10.0	0.10	0.43
∞	0.10	0.41

Table 1

Since $\omega_1 > 0$, the convective state results from supercritical bifurcation and is stable.

B. Simple eigenvalue for (2,0). Let us consider an aspect ratio $a_1 = 3.1$ which corresponds in Figure 2 to a simple eigenvalue M_c for convection with $(m_1,m_2) = (2,0)$. We find that

$$M_c = 79.2. \tag{5.5}$$

There is again a quadratic interaction and the set $\mathcal{S}$ is

$$\mathcal{S} = \{21,41\} \tag{5.6}$$

We omit all details and state the final amplitude equation,

$$\nu_2 \dot{A}_2 = (M - M_c)A_2 - \omega_2 A_2^3 \tag{5.7}$$

where the coefficients have the numerical values given in Table 2.

Pr	$\nu_2 \times 10^{-4}$	$\omega_2 \times 10^{-3}$
0.1	0.44	1.4
1.0	0.13	0.26
10.0	0.10	0.25
∞	0.098	0.25

Table 2

Again, $\omega_2 > 0$, the convective state results from supercritical bifurcation and is stable.

C. Double eigenvalues for (1,0) and (2,0). Let us consider an aspect ratio $a_1 = 2.21$ which corresponds in Figure 2 to a double eigenvalue for convection with $(m_1,m_2) = (1,0)$ and $(m_1,m_2) = (2,0)$. We find that

$$M_c = 90.2 \quad . \tag{5.8}$$

The quadratic interaction of modes 11 and 21 generate modes 31 and 41. The set $\mathcal{S}$ is

$$\mathcal{S} = \{11,21,31,41\}. \tag{5.9a}$$

We write

$$(\theta', \underline{v}') = \sum_{i=1}^{4} A_i(\theta_{i1}, \underline{v}_{i1}) \tag{5.9b}$$

and substitute into equation (4.12). We obtain

$$\nu_1 \dot{A}_1 = (M - M_c)A_1 - Z_1 \tag{5.10a}$$

$$\nu_2 \dot{A}_2 = (M - M_c)A_2 - Z_2 \tag{5.10b}$$

$$M_c^{-1} R_3 f_3 A_3 = - Z_3 \tag{5.10c}$$

$$M_c^{-1} R_4 f_4 A_4 = - Z_4 \tag{5.10d}$$

when $M = M_c$. Here the f_3, f_4, R_3, R_4 and functionals $Z_1 - Z_4$ are defined in analogous way as in I. Again, we omit details and state the final amplitude equations;

$$\nu_1 \dot{A}_1 = (M - M_c) A_1 - \alpha_1 A_1 A_2 - \beta_1 A_1^3 - \sigma_1 A_1 A_2^2 \tag{5.11a}$$

$$\nu_2 \dot{A}_2 = (M - M_c) A_2 - \alpha_2 A_1^2 - \sigma_2 A_1^2 A_2 - \omega_2 A_2^3 \ . \tag{5.11b}$$

Numerical values of the coefficients are given in Table 3.

Pr	$\nu_1 \times 10^{-4}$	$\nu_2 \times 10^{-3}$	$\alpha_1 \times 10^{-3}$	$\alpha_2 \times 10^{-2}$	$\beta_1 \times 10^{-3}$	$\sigma_1 \times 10^{-4}$	$\sigma_2 \times 10^{-4}$	$\omega_2 \times 10^{-3}$
0.1	0.58	3.9	- 0.88	1.5	0.18	2.3	1.3	5.0
1.0	0.23	1.2	- 0.34	0.43	0.18	0.33	0.17	0.95
10.0	0.20	0.90	- 0.29	0.32	0.18	0.24	0.12	0.77
∞	0.20	0.87	- 0.29	0.31	0.18	0.23	0.12	0.76

Table 3

We analyze the equations (5.11) in detail below.

D. Double eigenvalue for (2,0) and (3,0). Let us consider an aspect ratio $a_1 = 3.81$ which corresponds in Figure 2 to a double eigenvalue for convection with $(m_1,m_2) = (2,0)$ and $(m_1,m_2) = (3,0)$. We find that

$$M_c = 82.9 \ . \tag{5.12}$$

The quadratic interaction of modes 21 and 31 generates modes 11, 41, 51, 61 so the set $\mathcal{S}$ is

$$\mathcal{S} = \{11,21,31,41,51,61\}. \tag{5.13a}$$

We write

$$(\theta', \underline{v}') = \sum_{i=1}^{6} A_i(\theta_{i1}, \underline{v}_{i1}) \tag{5.13b}$$

and substitute into equation (4.2). We obtain

$$\nu_2 \dot{A}_2 = (M - M_c) - Z_2 \tag{5.14a}$$

$$\nu_3 \dot{A}_3 = (M - M_c) - Z_3 \tag{5.14b}$$

$$M_c^{-1} R_n f_n A_n = - Z_n \quad , \quad n = 1,4,5,6 \tag{5.14c}$$

when $M = M_c$. Here the f_n, R_n, Z_n are defined in analogous way as in I. Rather than give the details, we state the final amplitude equations.

$$\nu_2 \dot{A}_2 = (M - M_c)A_2 - \omega_2 A_2^3 - \tau_2 A_2 A_3^2 \tag{5.15a}$$

$$\nu_3 \dot{A}_3 = (M - M_c)A_3 - \tau_3 A_2^2 A_3 - \omega_3 A_3^3 \tag{5.15b}$$

and the coefficients are given in Table 4.

Pr	$\nu_2 \times 10^{-4}$	$\nu_3 \times 10^{-3}$	$\omega_2 \times 10^{-4}$	$\tau_2 \times 10^{-3}$	$\omega_3 \times 10^{-3}$	$\tau_3 \times 10^{-3}$
0.1	0.46	3.6	1.4	- 7.8	5.1	6.7
1.0	0.18	1.2	0.17	- 1.1	0.85	1.2
10.0	0.15	0.92	0.12	- 0.76	0.66	0.89
∞	0.14	0.89	0.11	- 0.72	0.64	0.86

Table 4

6. ANALYSIS AND DISCUSSION

In cases A and B of Section 5, the self-interaction of roll cells (1,0) and (2,0) is considered. In both cases, the interaction is governed by single amplitude equations containing cubic but no quadratic nonlinearities. These are equations (5.4) and (5.7) respectively. The values ν_1 and ν_2, depending on Prandtl number Pr, are values from the linear stability problem and for given λ of equation (3.3) are identical here to those of I. Careful comparison shows this. The values ω_1 and ω_2 of equations (5.4) and (5.7) are always positive so that these simple self-interactions always correspond to stable supercritical bifurcation. It is easy to show that for <u>any</u> values $(m_1,m_2) \neq (0,0)$ indicated in Figure 7 that self-interactions always have amplitude equations of the same form, i.e.

$$\nu\dot{A} = (M - M_c)A - \omega A^3 \tag{6.1}$$

where $\nu > 0$. Presumably, $\omega > 0$ for any of these so that stable, supercritical bifurcation is always predicted for self-interactions. This is likewise true in the case of the circular container of I for $m \neq 0$. It is only for the $(m = 0)$ axisymmetric mode that equation (6.1) is augmented by a quadratic term. Thus, the axisymmetric mode bifurcates subcritically and so has snap-through and hysteresis properties as discussed in I.

In case C of Section 5, the interaction of modes (1,0) and (2,0) is examined near the double eigenvalue at $a_1 = 3.1$ of Figure 2. The governing amplitude equations (5.11) are a pair of coupled equations identical in form to equations (7.10) and (7.11) of I which govern the interaction of modes $m = 1$ and $m = 2$ near their double eigenvalue. Again, the ν_i are linear theory values that depend on Pr and λ but not on the cylinder geometry.

Although the coefficients are not identical in the two cases, all of the qualitative predictions are. Figure 8 shows the results of our analysis of (7.10)-(7.11) for $a_1 < 3.1$. The mixed mode containing both modes (1,0) and (2,0) bifurcates supercritically at M_c and as M is further increased, A_1 follows either O_1UT_1 or O_2LT_1 while A_2 follows O_2T_2. At a value of $\eta \equiv M - M_1$ greater than $\Delta \equiv M_2 - M_1$, there is secondary bifurcation to a pure mode m = 2. This branch is labelled T_2S.

Figure 9 shows the situation for $a_1 > 3.1$. Here, as M crosses M_c, the pure mode m = 2 bifurcates supercritically and follows either curve O_2T_2 or O_2S. However, for $\eta \equiv M - M_2$ less than $\Delta \equiv M_1 - M_2$, the pure mode persists but only on the branch O_2S. Again, there is the possibility of branch O_2T_2 bifurcating first to the mixed mode and then to time periodic convection. The amplitude equations (5.11) are in form identical to those governing hexagonal cells as predicted by Scanlon and Segel (1967) for horizontally unbounded layers. However, since the contexts are quire different, the coefficients are quite different. Scanlon and Segel find subcritical hexagons. We find only supercritical convection of mixed mode or pure mode m = 2.

In case D of Section 5, the interaction of modes (2,0) and (3,0) is examined near the double eigenvalue at $a_1 = 3.81$ of Figure 2. The governing amplitude equations (5.14) are a pair of coupled equations. Again, ν_i are linear theory values that depend on Pr and λ but not on the cylinder geometry. Figure 10 shows the situation for $a_1 < 3.81$. The pure mode (2,0) bifurcates supercritically at M_c, $\eta \equiv M - M_2 = 0$, and steady convection follows either branch OS as M increases. At a value of $\eta > \Delta \equiv M_2 - M_1$ there is secondary bifurcation to the mixed mode containing both modes (2,0) and (3,0) and as M increases further, A_2 follows either branch SU and A_3 follows a branch ST.

Figure 11 shows the situation for $a_1 > 3.81$. Here, at M_c, the pure mode (3,0) bifurcates supercritically and follows either branch OS until $\eta \equiv M - M_3 = \eta_s < \Delta \equiv M_2 - M_3$. Here, there is secondary bifurcation to a mixed mode in which A_2 follows either SU and A_2 follows an ST. The sequence of events here, near a = 3.81, has no counterpart in I since there was no double eigenvalue there for modes m = 2 and m = 3. However, the amplitude equations (5.14) have the form typical of Rayleigh-Bénard convection in containers as discussed by Rosenblat (1981). The Figures 10 and 11 are typical of Rosenblat's results which apply to the buoyancy-driven convection.

In summary, we again find that interactions near double eigenvalues give qualitative features that strongly distinguish behavior for aspect ratios on one side from behavior on the other side. Parallels as well as differences in behavior exist between the circular and rectangular cases.

REFERENCES

Beck. J. L. 1972 Phys. Fluids 15, 1377.

Davis, S. H. 1967 J. Fluid Mech. 30, 465.

Pearson, J. R. A. 1958 J. Fluid Mech. 4, 489.

Rosenblat, S. 1979 Stud. Appl. Math. 60, 241.

Rosenblat, S. 1981 in preparation.

Scanlon, J. W. and Segel, L. A. 1967 J. Fluid Mech. 30, 149.

CAPTIONS FOR FIGURES

FIGURE 1: Stability curves M versus a_1 for L = 0 at a_2 = 0.5. The pairs (m_1,m_2) denote integral number of cycles in (a_1,a_2).

FIGURE 2: Stability curves M versus a_1 for L = 0 at a_2 = 1.0. The pairs (m_1,m_2) denote integral number of cycles in (a_1,a_2).

FIGURE 3: Stability curves M versus a_1 for L = 0 at a_2 = 1.5. The pairs (m_1,m_2) denote integral number of cycles in (a_1,a_2).

FIGURE 4: Stability curves M versus a_1 for L = 0 at a_2 = 2.0. The pairs (m_1,m_2) denote integral number of cycles in (a_1,a_2).

FIGURE 5: Stability curves M versus a_1 for L = 0 at a_2 = 3.0. The pairs (m_1,m_2) denote integral number of cycles in (a_1,a_2).

FIGURE 6: Stability curves M versus a_1 for L = 0 at a_2 = 3.5. The pairs (m_1,m_2) denote integral number of cycles in (a_1,a_2).

FIGURE 7: Stability map for preferred mode as a function of a_1 and a_2. L = 0. The figure is symmetric about $a_1 = a_2$. The pairs (m_1,m_2) denote integral number of cycles in (a_1,a_2).

FIGURE 8: The bifurcation diagram for a_2 = 1.5, and a_1 slightly less than 3.1 where $\Delta = M_2 - M_1$. Solid lines represent stable branches while dotted lines represent unstable branches.

FIGURE 9: The bifurcation diagrams for a_2 = 1.5, and a_1 slightly greater than 3.1 where $\Delta = M_1 - M_2$. Solid lines represent stable branches while dotted lines represent unstable branches. The curly lines represent time-periodic bifurcations.

FIGURE 10: The bifurcation diagrams for a_2 = 1.5, and a_1 slightly less than 3.81 where $\Delta = M_3 - M_2$. Solid lines represent stable branches while dotted lines represent unstable branches.

FIGURE 11: The bifurcation diagrams for a_2 = 1.5, and a_1 slightly greater than 3.81 where $\Delta = M_2 - M_3$. Solid lines represent stable branches while dotted lines represent unstable branches.

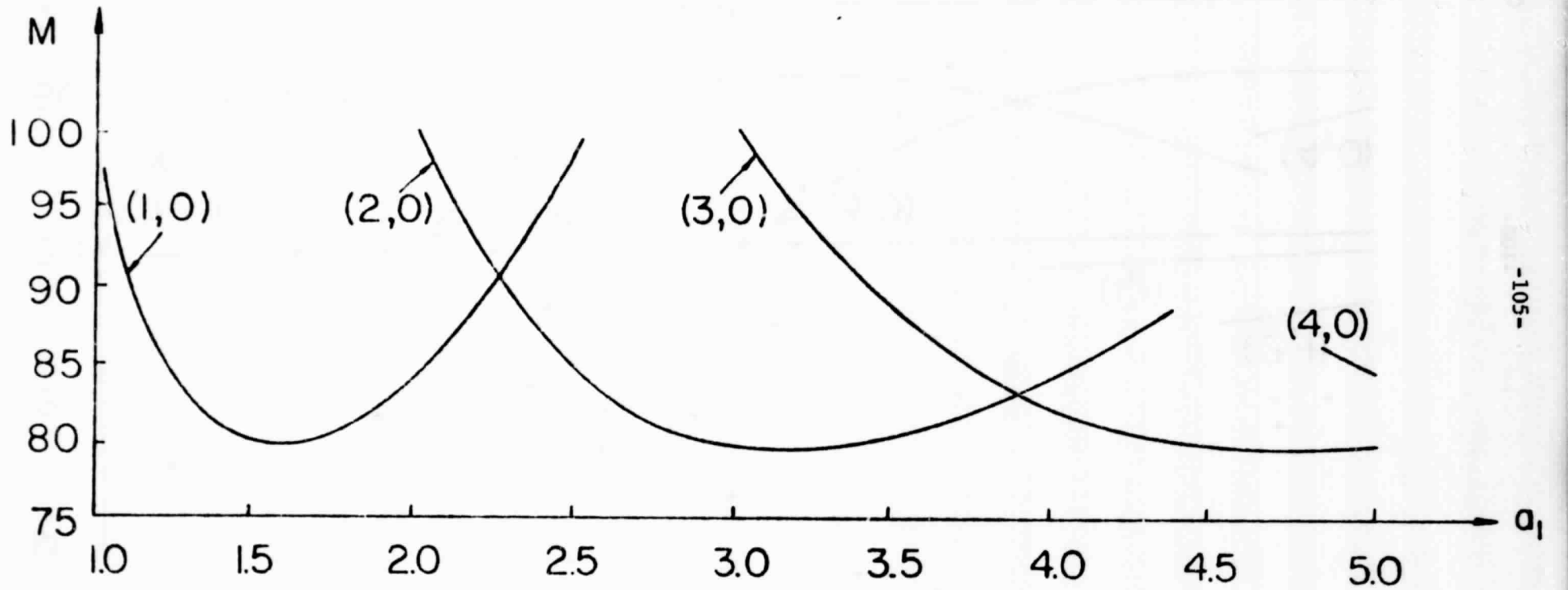

FIGURE 1

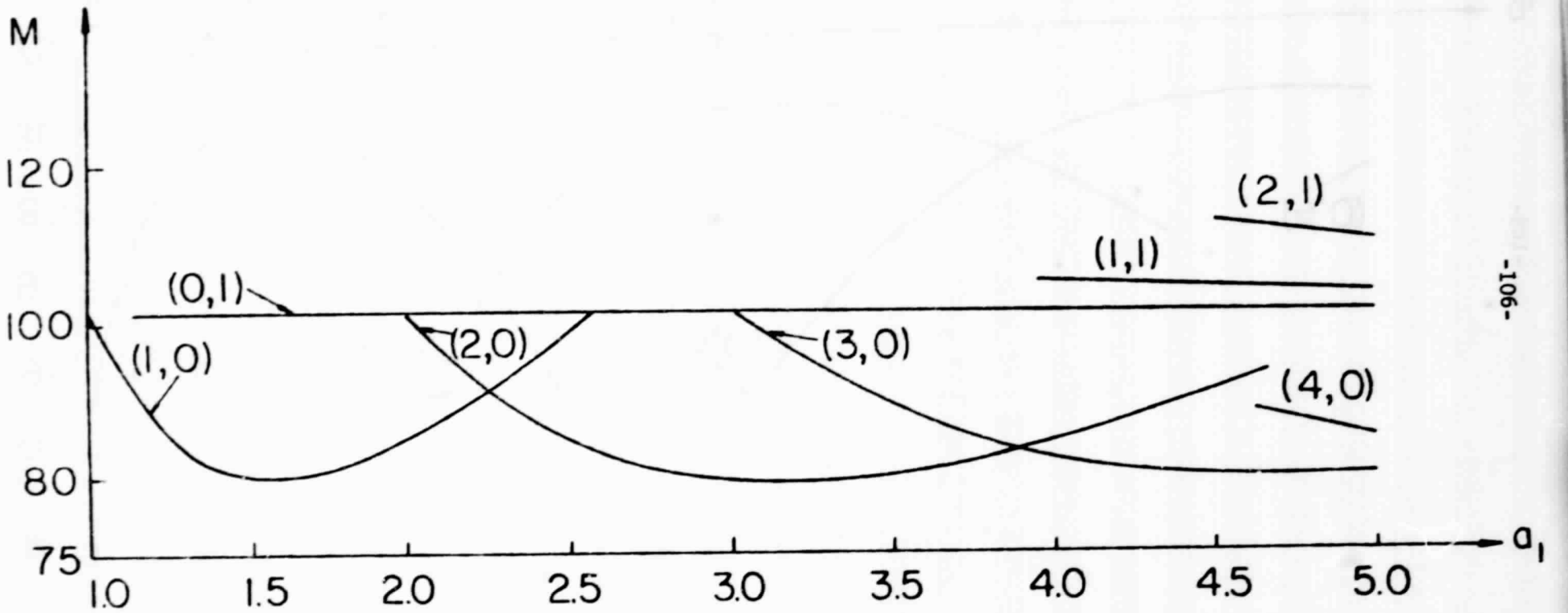

FIGURE 2

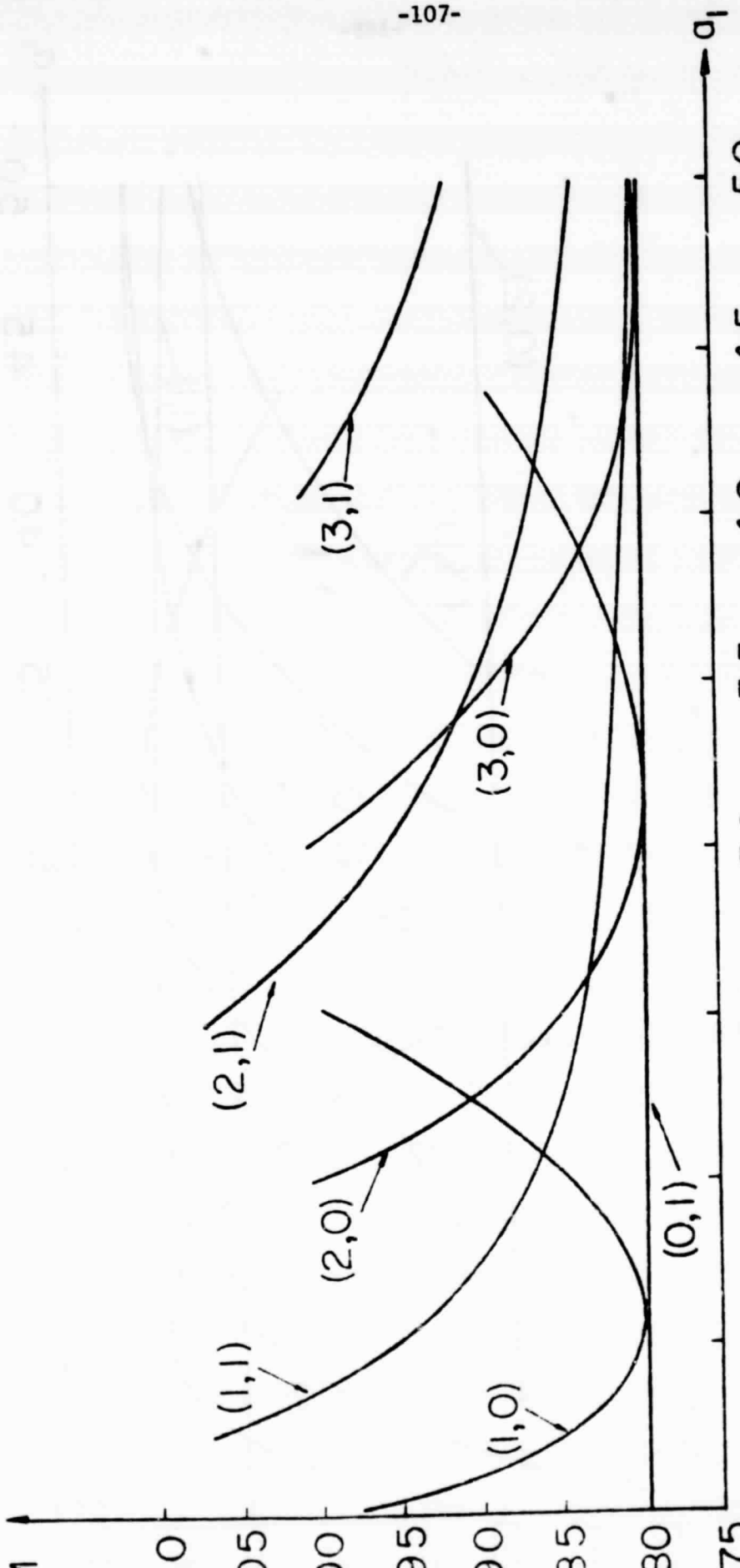
M
110
105
100
95
90
85
80
75
1.0
1.5
2.0
2.5
3.0
3.5
4.0
4.5
5.0
a_1
(1,1)
(2,0)
(2,1)
(3,0)
(3,1)
(1,0)
(0,1)

FIGURE 3

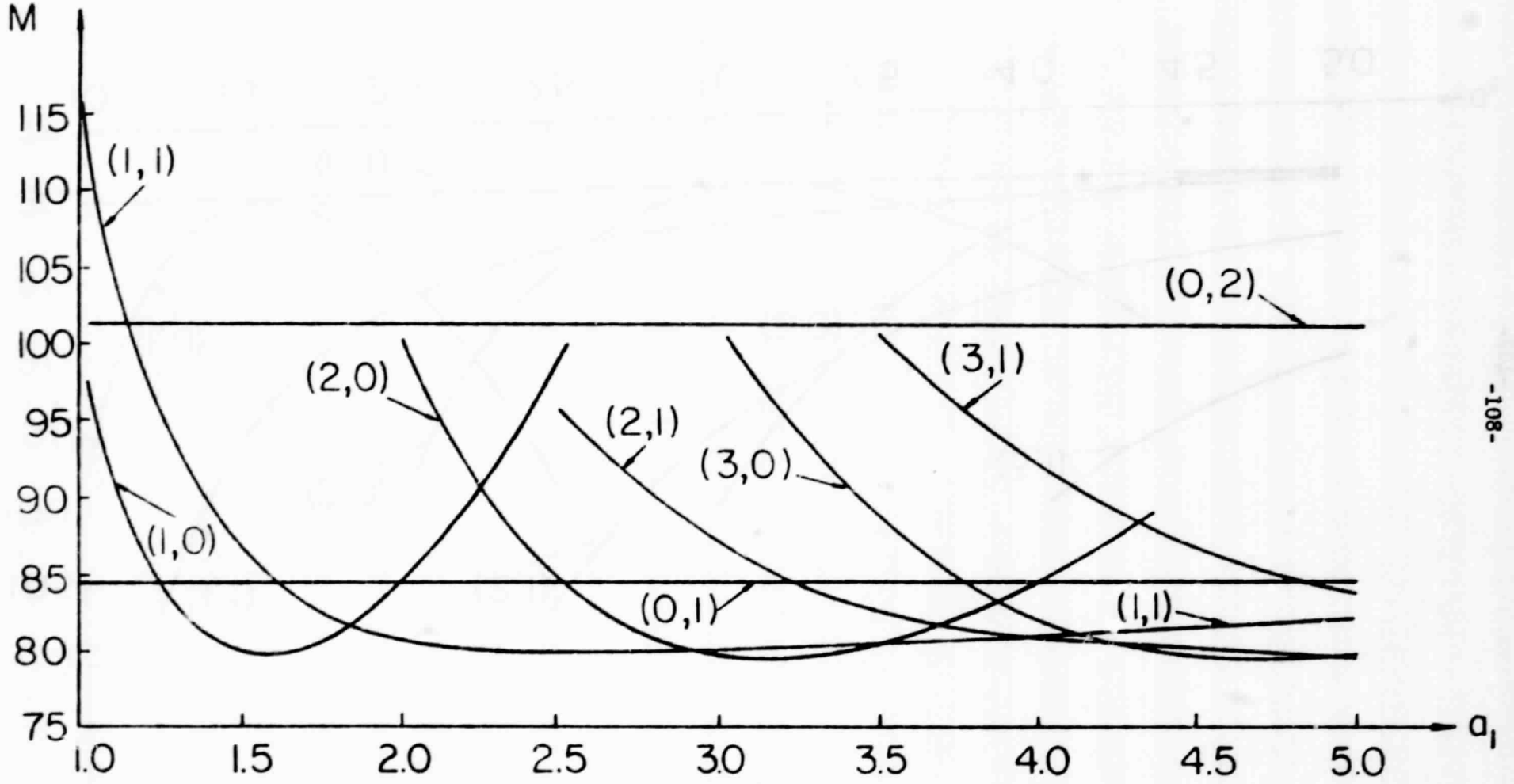
M
115
110
105
100
95
90
85
80
75
(1, 1)
(0,2)
(2,0)
(3,1)
(2,1)
(3,0)
(1,0)
(0,1)
(1,1)
1.0
1.5
2.0
2.5
3.0
3.5
4.0
4.5
5.0
a_1

FIGURE 4

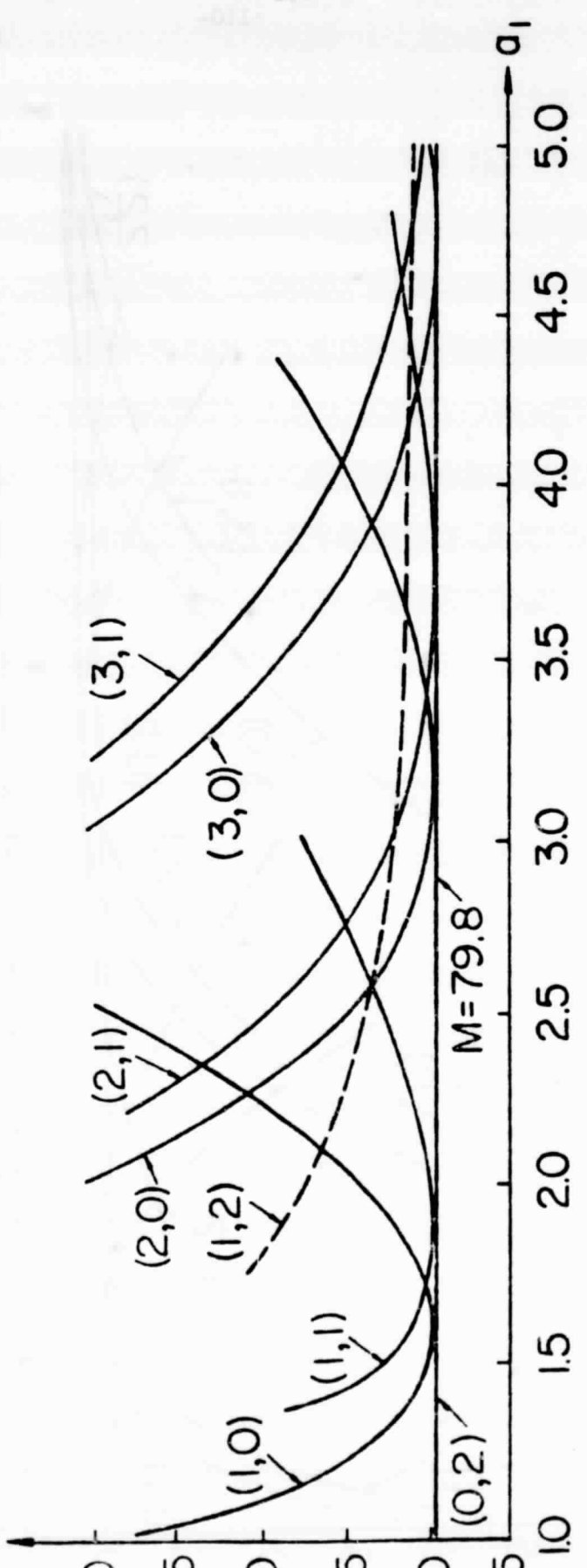
M
100
95
90
85
80
75
1.0
1.5
2.0
2.5
3.0
3.5
4.0
4.5
5.0
a_1
(3,1)
(3,0)
(2,1)
(2,0)
(1,2)
(1,1)
(1,0)
(0,2)
M=79.8

FIGURE 5

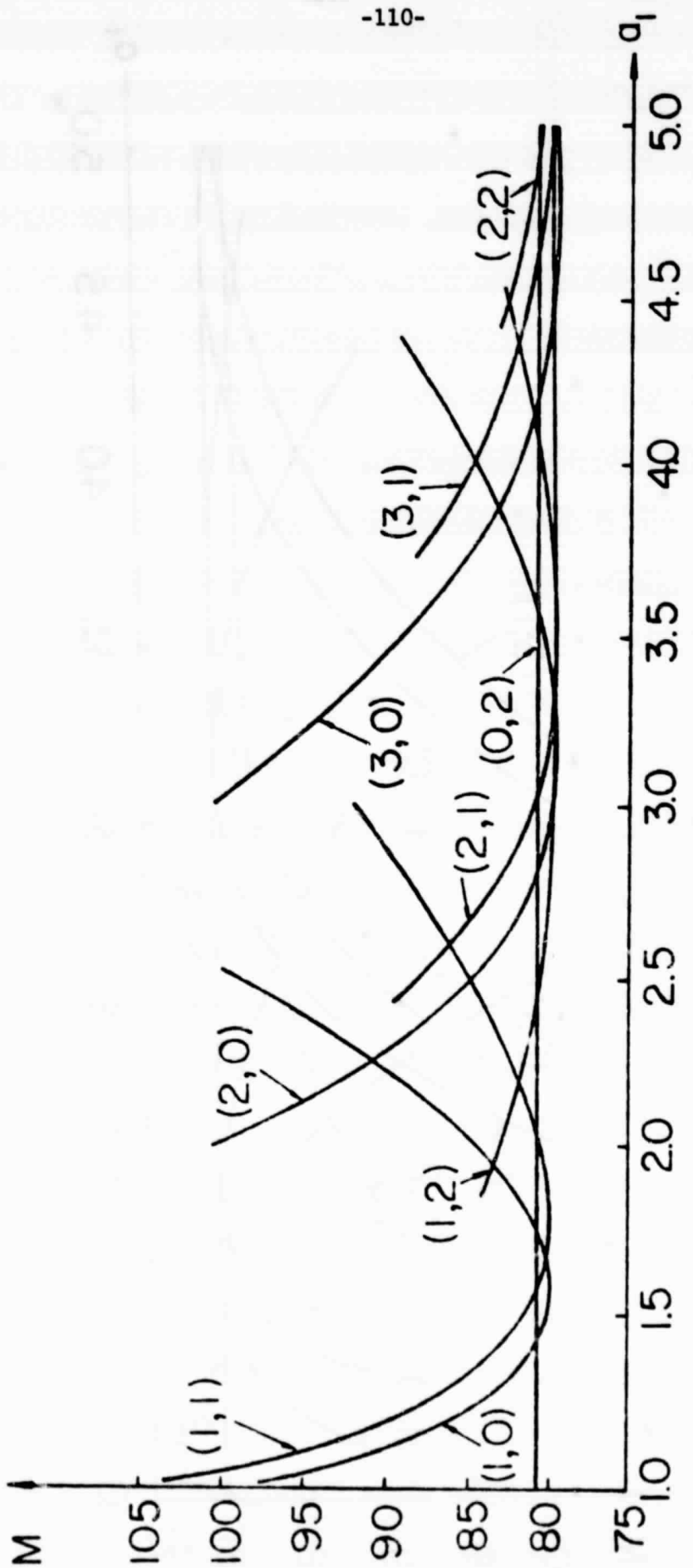
M
105
100
95
90
85
80
75
1.0
1.5
2.0
2.5
3.0
3.5
4.0
4.5
5.0
q_1
(1,1)
(1,0)
(2,0)
(1,2)
(3,0)
(2,1)
(0,2)
(3,1)
(2,2)

FIGURE 6

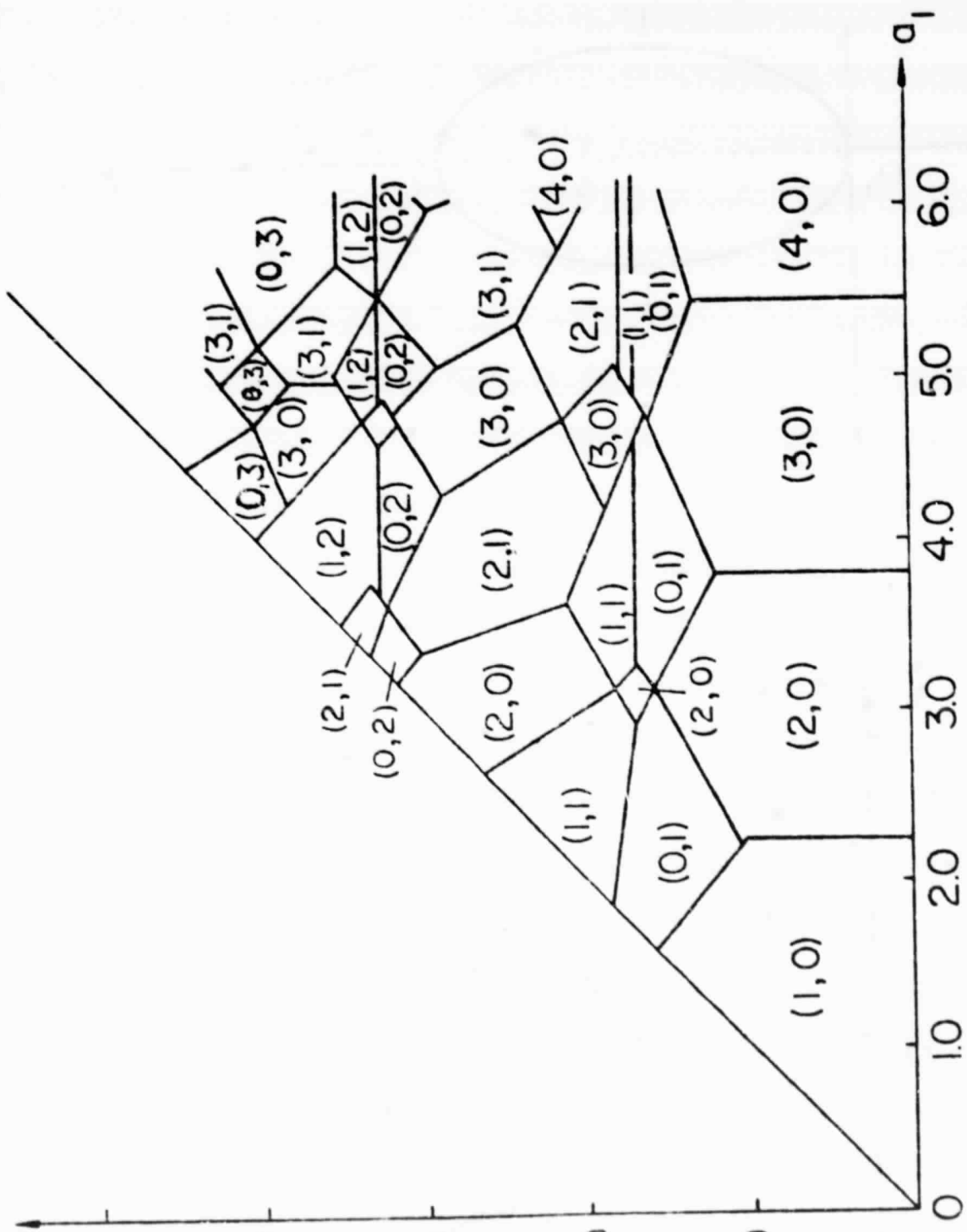
a_2
5.0
4.0
3.0
2.0
1.0
0
1.0
2.0
3.0
4.0
5.0
6.0
a_1
(1,0)
(2,0)
(3,0)
(4,0)
(0,1)
(1,1)
(2,1)
(3,1)
(0,2)
(1,2)
(0,3)
(3,1)
(3,0)
(2,0)
(2,1)
(0,2)
(1,2)
(0,3)
(3,1)
(0,3)
(3,1)
(4,0)
(0,2)
(1,2)
(0,2)
(3,0)
(2,1)
(1,1)
(0,1)
(3,0)
(2,0)
(1,1)
(0,1)
(2,0)
(1,1)
(0,1)

FIGURE 7

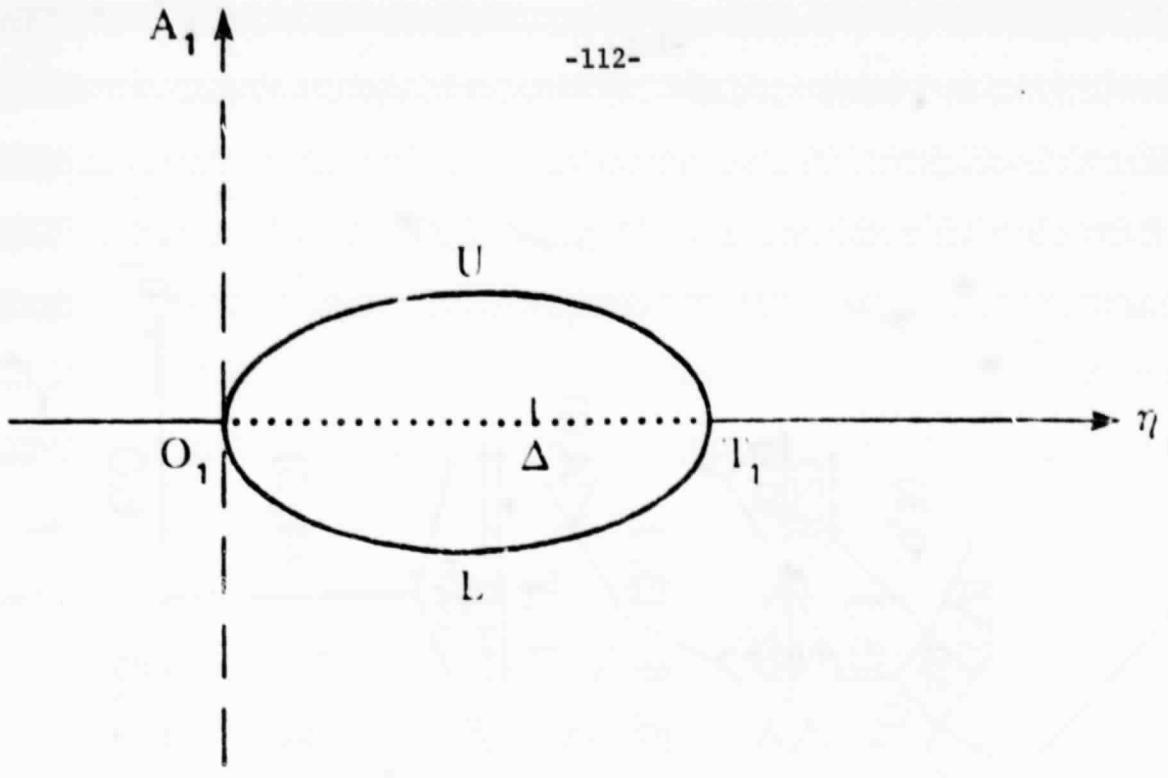

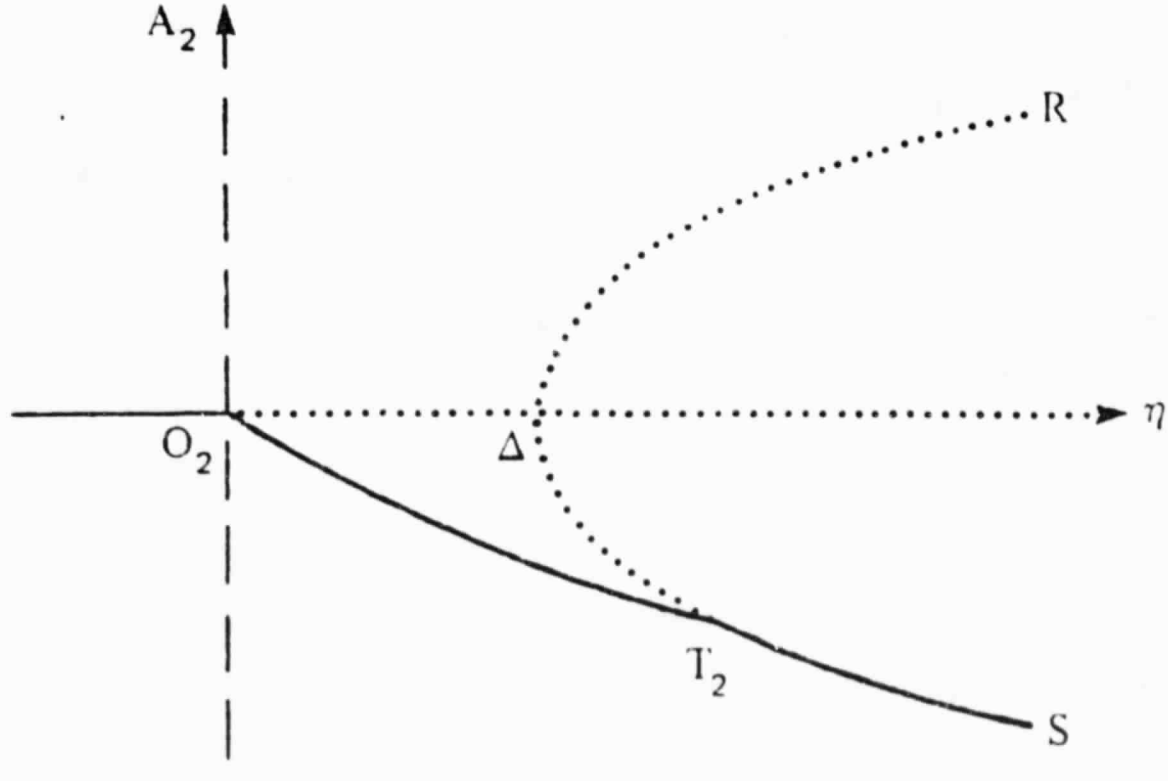

FIGURE 8

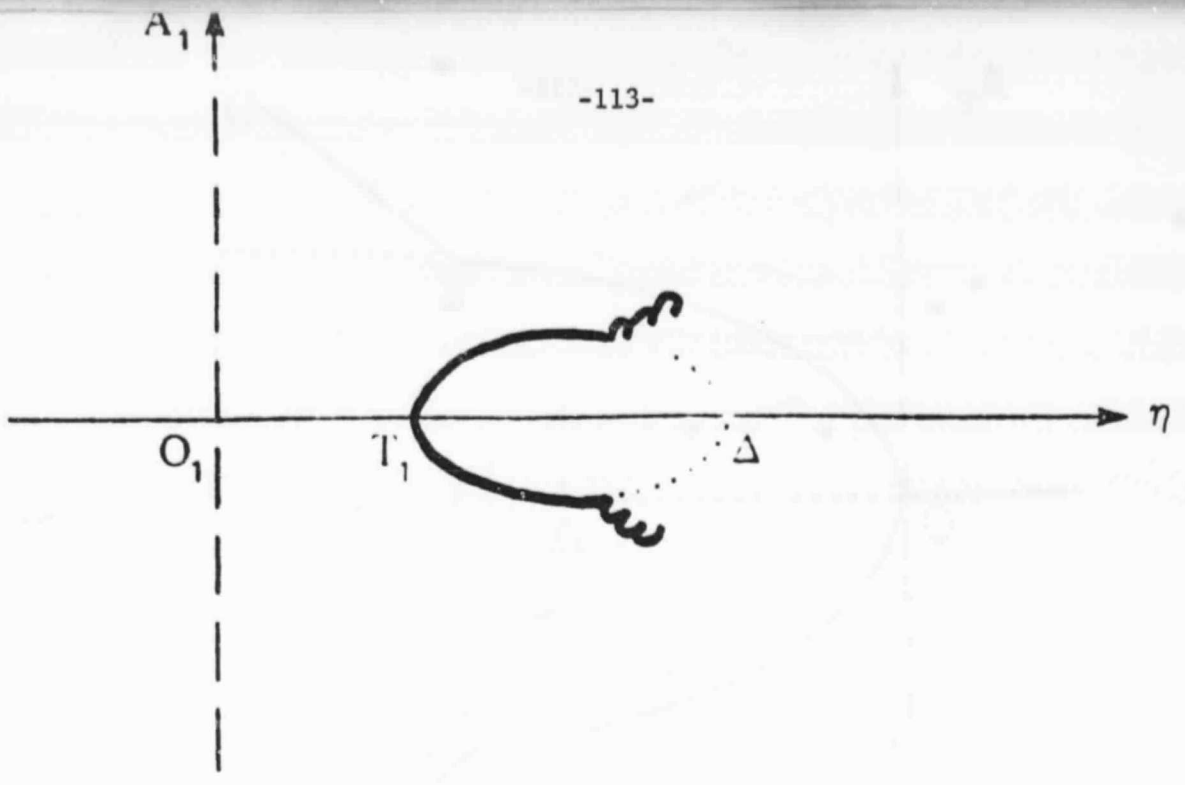

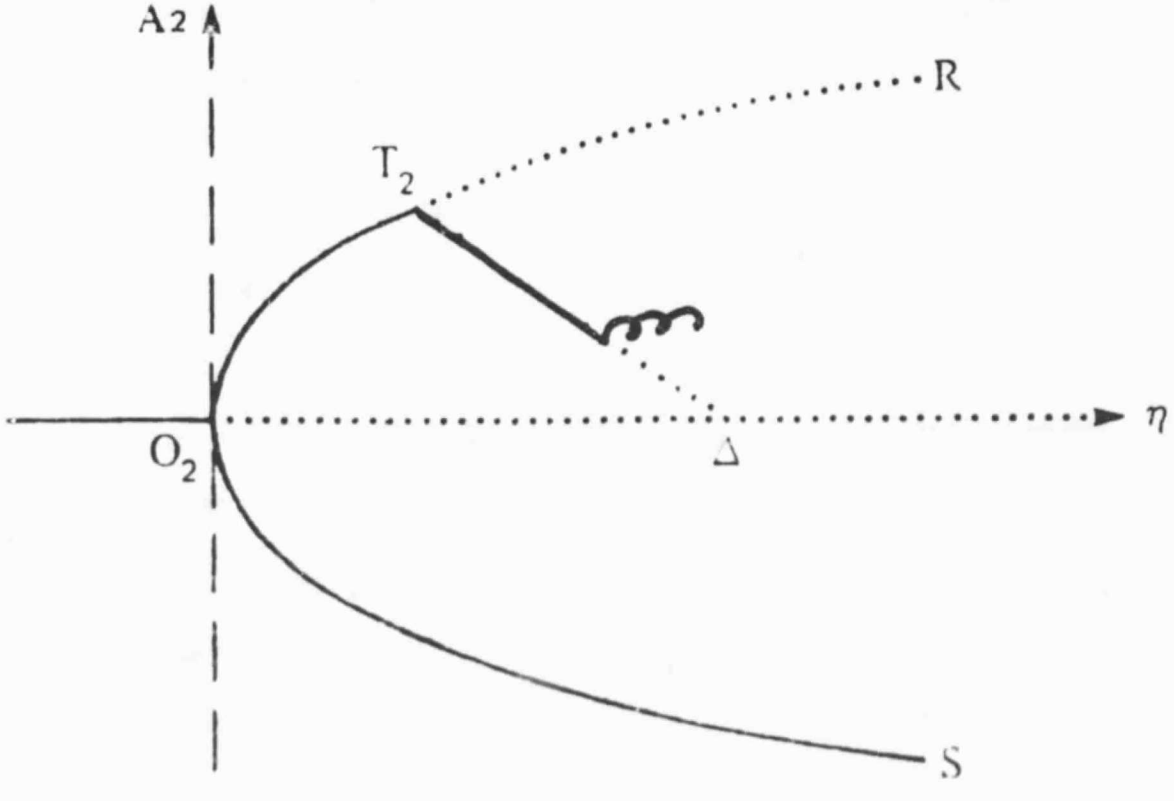

FIGURE 9

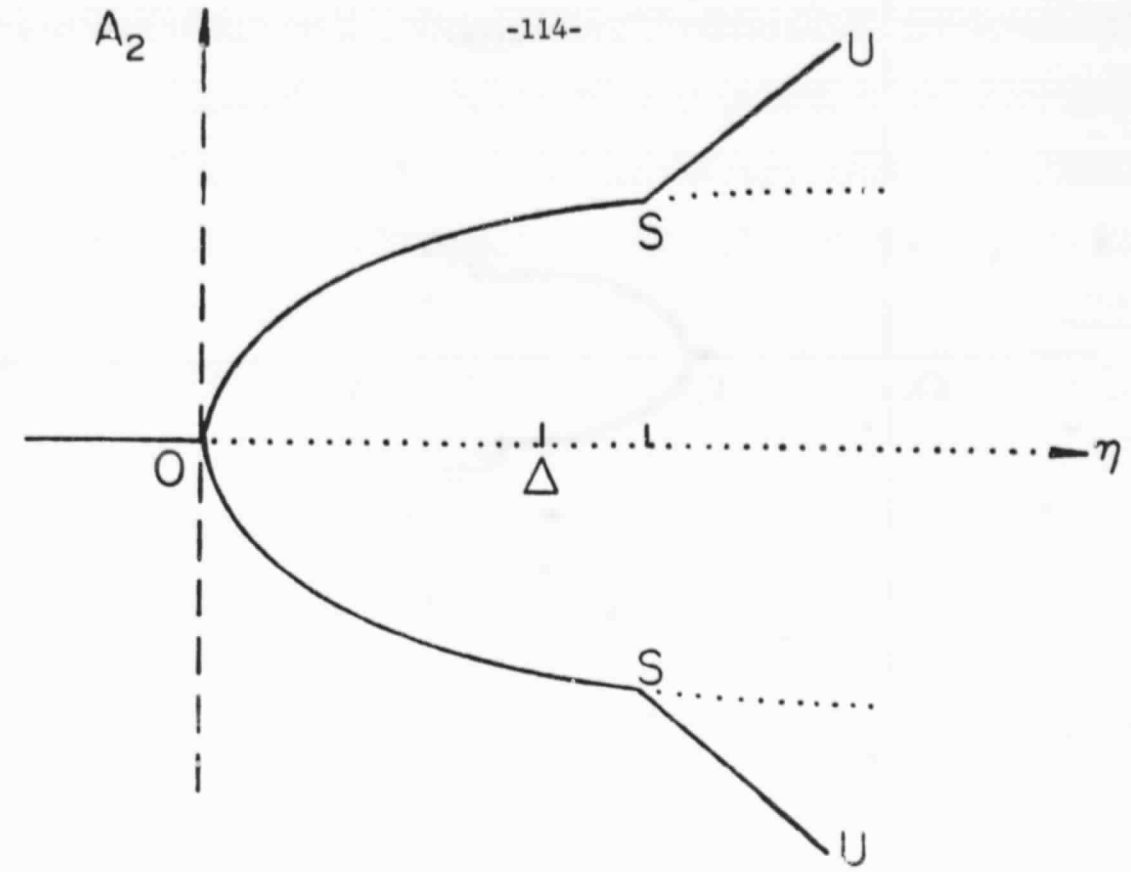

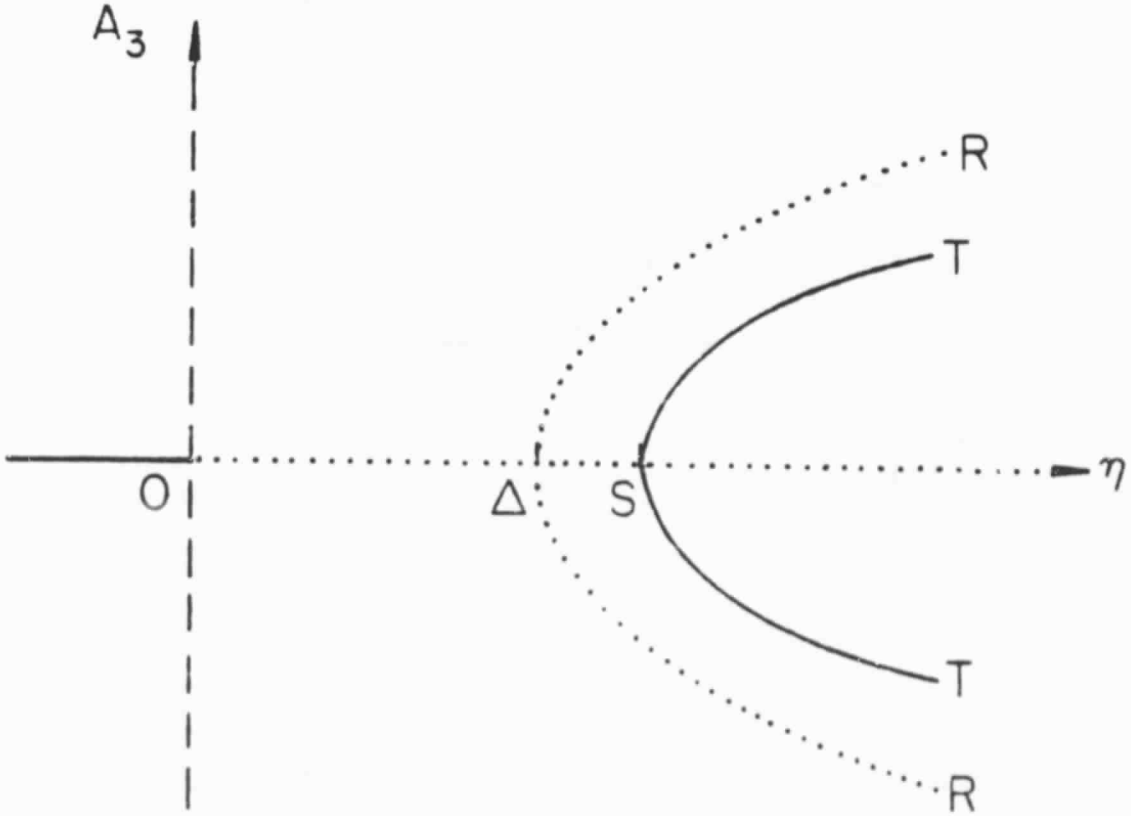

FIGURE 10

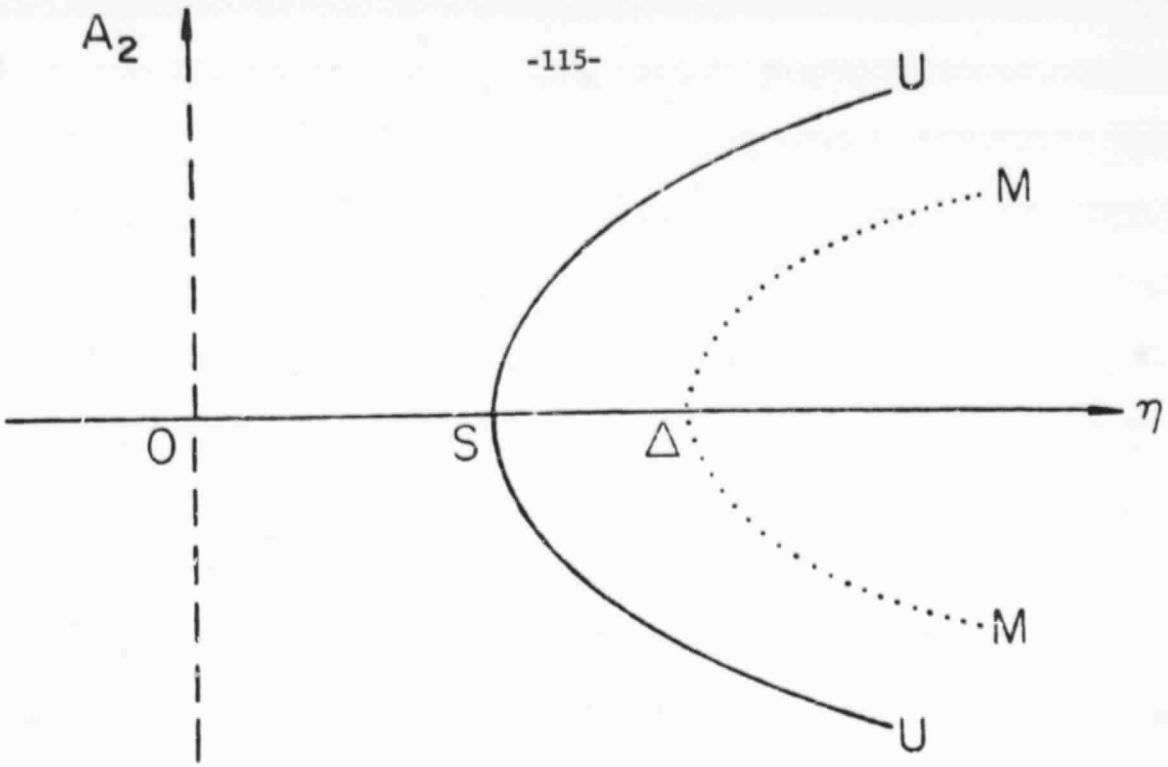

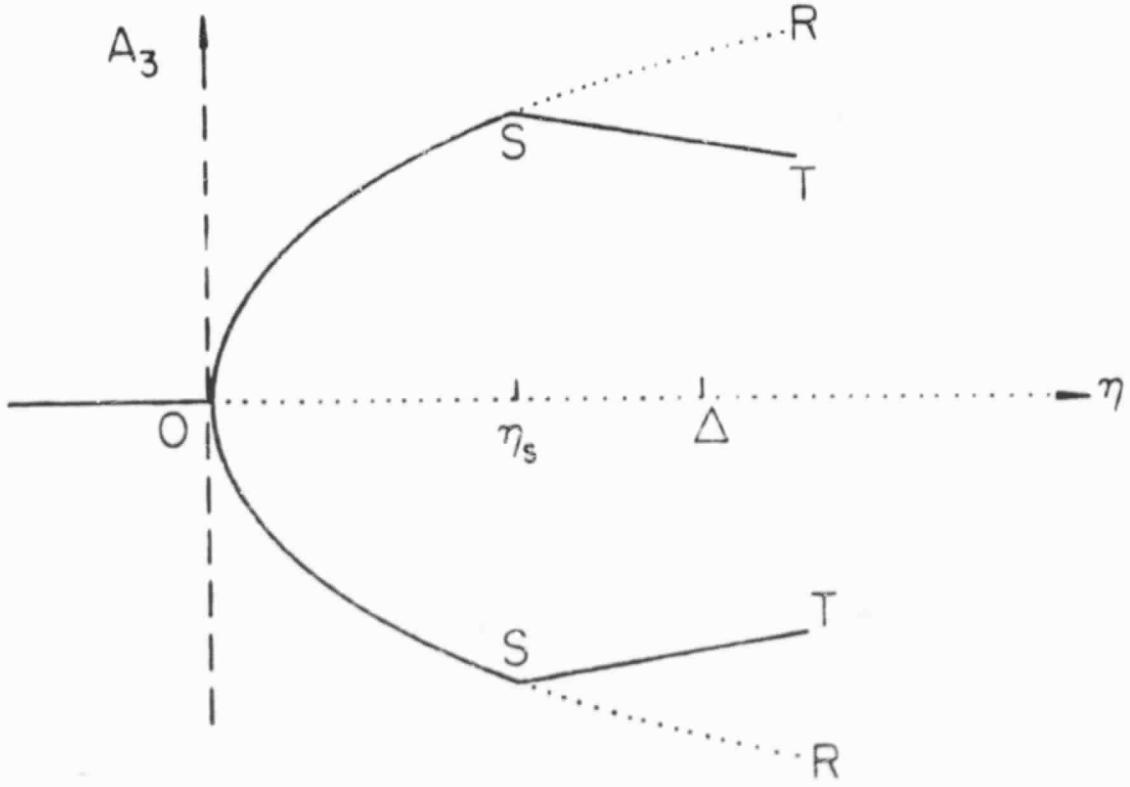

FIGURE 11

APPENDIX A

The classical Rayleigh-Benard problem for the stability of a horizontal layer of Boussinesq fluid heated from below can be reduced to the solution of the pair of ordinary differential equations[1]

$$(\frac{d^2}{dz^2} - a^2)\theta + w = 0, \quad (\frac{d^2}{dz^2} - a^2)^2 w - Ra^2\vartheta = 0, \tag{1}$$

where θ, w are respectively the temperature perturbation and the vertical velocity-component perturbation; a is the wave number of disturbances in the horizontal plane; z is the vertical coordinate; and R is the Rayleigh number, proportional to the vertical temperature gradient in the equilibrium state. Equations (1) hold on the interval $0 < z < 1$, and their solutions are required to satisfy prescribed boundary conditions of the form

$$P_k^0\theta + Q_k^0 w = 0 \quad \text{on} \quad z = 0, \quad P_k^1\theta + Q_k^1 w = 0 \quad \text{on} \quad z = 1, \quad k = 1, 2, 3. \tag{2}$$

Here P_k^0, Q_k^0, P_k^1, Q_k^1 are linear differential operators whose particular forms depend on the characteristics of the boundary surfaces.

For a layer of unbounded horizontal extent the boundary-value problem (1)-(2) has a nontrivial solution for infinitely many values of R. More precisely, there is a countably infinite number of simple eigenvalues for each wave-number a given by a characteristic equation of the form

$$R = R_n(a), \quad n = 1, 2, 3, \ldots \tag{3}$$

with

$$R_1(a) < R_2(a) < R_3(a) < \ldots \tag{4}$$

for each a. The critical Rayleigh number for the onset of instability is given by

$$R_c = R_1(a_c) = \min_a R_1(a). \tag{5}$$

Corresponding to each R_n there is an eigensolution

$$\theta_n(z; a),\ w_n(z; a),\quad n = 1, 2, 3, \ldots; \tag{6}$$

for various boundary conditions of the form (2) it can be shown that the eigenvectors (6) constitute a complete set, a fact which may be useful for computations of the corresponding nonlinear stability problem.

As an example, the simplest case is that when both boundaries are isothermal and stress-free. Conditions (2) then become

$$\theta = w = \frac{d^2w}{dz^2} = 0 \quad \text{on} \quad z = 0 \quad \text{and} \quad z = 1, \tag{7}$$

whereupon the characteristic equation (3) has the well-known form

$$R_n = \frac{[(n\pi)^2+a^2]^3}{a^2} \tag{8}$$

with eigenvectors

$$\theta_n = \sin n\pi z, \quad w_n = [(n\pi)^2 + a^2]\sin n\pi z. \tag{9}$$

Pearson[2] studied the Marangoni problem, in which the instability was driven by surface-tension gradients rather than by the buoyancy force. Subsequently, Nield[3] investigated the problem allowing the presence of both

buoyancy and surface tension. In these cases the governing equations again reduce to the system (1) (with R = 0 in Pearson's work). The boundary conditions have the general form (2) but of necessity contain a new parameter, the Marangoni number M. In the specific problem considered by both Pearson and Nield the boundary conditions were

$$\theta = w = \frac{\partial w}{\partial z} = 0 \quad \text{on} \quad z = 0 \tag{10}$$

and

$$\frac{d\theta}{dz} + h\theta = w = \frac{d^2 w}{dz^2} + Ma^2\theta = 0 \quad \text{on} \quad z = 1, \tag{11}$$

where h is a surface Nusselt number. These correspond to a rigid, isothermal lower boundary and a stress-free, conducting upper boundary.

Both Pearson and Nield were concerned to determine a critical Marangoni number for the onset of instability for fixed values of the other parameters of the problem. Detailed calculations by Nield[3] led to a single-valued characteristic equation of the form

$$M = M(a, R, h); \tag{12}$$

in other words, the boundary-value problem (1), (10)-(11) has a unique eigenvalue M for each value of a, R and L (and, correspondingly, a unique eigenvector). The critical Marangoni number was then found to be

$$M_c = M_c(R, h) = M(a_c, R, h) = \min_a M(a, R, h) \tag{13}$$

with $a_c = a_c(R, h)$. For example, Nield[3] found $M_c(0, 0) = 79.607$ with $a_c(0, 0) = 1.993$. The graph of the function (12) for the range $-500 < R < 1000$ with $a = 2$ and $h = 0$ is shown in Figure 1.

Figure 1

There appears to be a discrepancy between the Rayleigh-Benard problem and the Marangoni problem: the former has countably many eigenvalues R_n while the latter has only one eigenvalue M. This is somewhat surprising, since the boundary-value problem (1), (10)-(11) incorporates both buoyancy and surface-tension effects. A possibly disturbing consequence is that the Marangoni problem does not seem to have a complete set of eigenfunctions, which could be used for computations of nonlinear stability.

This discrepancy is reconciled by noting that the inverse of the function (12) has countably many values of R for each fixed value of M, a and h. In fact, the inverse of (12) is of the form

$$R = R_n(a, M, h), \quad n = 1, 2, 3, \ldots \tag{14}$$

Thus, for each M there are infinitely many eigenvalues R_n, but only one eigenvalue M for each R.

We have computed the functions (14) by inverting the explicit formula (12) given by Nield. In our notation

$$M = A/B \tag{15}$$

where

$$A = \left[1 + L + 2a^2 \sum_{m=1}^{\infty} \frac{d_m^2 - R}{\Delta_m}\right] \cdot \sum_{m=1}^{\infty} \frac{(m\pi)^2 d_m}{\Delta_m} + 2Ra^2 \left[\sum_{m=1}^{\infty} \frac{(m\pi)^2 \cos m\pi}{\Delta_m}\right]^2, \tag{16}$$

$$B = 2a^2 \sum_{m=1}^{\infty} \frac{(m\pi)^2}{\Delta_m} \cdot \sum_{m=1}^{\infty} \frac{(m\pi)^2 d_m}{\Delta_m} - 2a^2 \sum_{m=1}^{\infty} \frac{(m\pi)^2 \cos m\pi}{\Delta_m} \cdot \sum_{m=1}^{\infty} \frac{(m\pi)^2 d_m \cos m\pi}{\Delta_m} \tag{17}$$

with

$$d_m = (m\pi)^2 + a^2, \quad \Delta_m = d_m^3 - Ra^2. \tag{18}$$

Calculations were performed for the case h = 0 and a = 2, and are shown in Figure 2 as a graph of R against M, different scales being used because of the large range of parmeter values. The dotted segment of the lowest curve corresponds to the curve depicted in Figure 1.

Figure 2

We find from the calculations that the curves intersect the R-axis at values $R_1 = 676$, $R_2 = 2.11 \times 10^4$ and $R_3 = 2.05 \times 10^5$. These compare well with the values obtained from formula (8) at a = 2, namely, $R_1 = 668$, $R_2 = 2.06 \times 10^4$ and $R_3 = 2.00 \times 10^5$. Also, the lines $R = 6.7 \times 10^3$ and $R = 9.9 \times 10^4$ are asymptotes for the curves.

This analysis shows that although a critical value of M can be determined, the Marangoni number is not strictly speaking an eigenvalue of the boundary-value problem, whereas the Rayleigh number is.

This work was supported by a contract with the National Aeronautics and Space Administration, Lewis Research Center.

1. S. Chandrasekhar. Hydrodynamic and hydromagnetic stability. Oxford: Clarendon Press (1961).

2. J.R.A. Pearson. J. Fluid Mech., 4. 489. (1958).

3. D.A. Nield. J. Fluid Mech., 19, 341 (1964).

CAPTIONS FOR FIGURES

FIGURE 1: The first critical curve R versus M for h = 0.

FIGURE 2: The first three critical curve R versus M for h = 0.

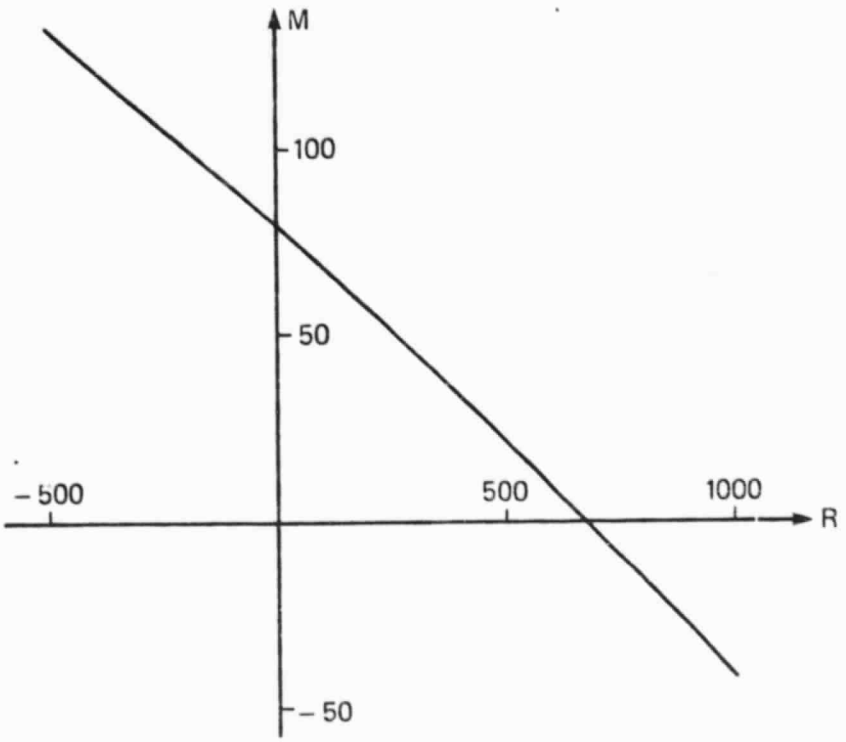

Figure 1

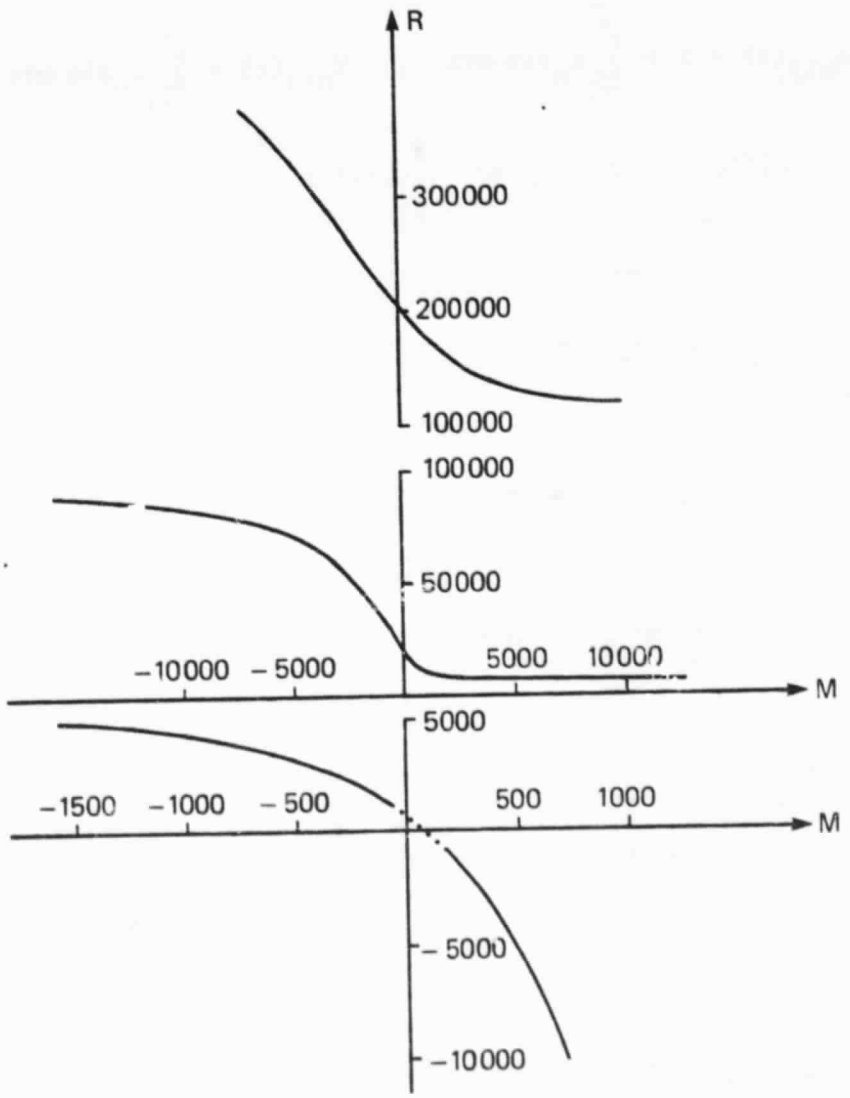
R
300000
200000
100000
100000
50000
-10000
-5000
5000
10000
M
5000
-1500
-1000
-500
500
1000
M
-5000
-10000

Figure 2

APPENDIX B

The eigenfunctions $X_{mij}(z)$, $Y_{mij}(z)$ used in the expansion procedure are the solutions of the boundary-value problem (4.10)-(4.12) for fixed $M = M_c$, for $R = R_{mij}$ and with $h = 0$. Using the Fourier series method of Nield (1964) we find that

$$X_{mij}(z) = z + \sum_{n=1}^{\infty} \alpha_n \sin n\pi z \quad , \quad Y_{mij}(z) = \sum_{n=1}^{\infty} \beta_n \sin n\pi z \tag{1}$$

where the coefficients α_n, β_n are defined in the following way. Let

$$d_n = (n\pi)^2 + \lambda_{mi}^2 \tag{2}$$

$$\Delta_n = d_n^3 - R_{mij}\lambda_{mi}^2 \tag{3}$$

and

$$J_n = d_n^2 - R_{mij} - (n\pi)^2 M_c \quad . \tag{4}$$

Then

$$\alpha_n = \frac{2\lambda_{mi}^2 \cos n\pi \; J_n - (n\pi)^2 Q}{n\pi \Delta_n} \tag{5}$$

and

$$\beta_n = \frac{n\pi \, \alpha_n \alpha_n - 2\lambda_{mi}^2 \cos n\pi}{n\pi \, M_c} \tag{6}$$

where

$$Q = \frac{1 + 2\lambda_{mi}^2 \sum_{k=1}^{\infty} (J_k/\Delta_k)}{\sum_{k=1}^{\infty} \left\{ (k\pi)^2 \cos k\pi / \Delta_k \right\}} \quad . \tag{7}$$

The formulas (A1) can also be used to calculate the first derivative of X_{mij} and the first and second derivatives of Y_{mij}, which are required in the nonlinear interactions of Sections 5-7.

The adjoint eigenfunctions X^*_{mij} and Y^*_{mij} are the solutions of the adjoint boundary-value problem (5.14)-(5.16) with $M = M_c$, $R = R_{mij}$ and $h = 0$, as before. We find that

$$X^*_{mij}(z) = z + \sum_{n=1}^{\infty} \gamma_n \sin n\pi z \quad , \quad Y^*_{mij}(z) = \sum_{n=1}^{\infty} \delta_n \sin n\pi z \tag{8}$$

where

$$\gamma_n = \frac{2\lambda_{mi}^2 \left\{ (d_n^2 - R_{mij}) \cos n\pi + (n\pi)^2 R_{mij} H \right\}}{n\pi \Delta_n} \tag{9}$$

and

$$\delta_n = \frac{2n\pi M_c (d_n H - \cos n\pi)}{\Delta_n} \tag{10}$$

with

$$H = \frac{\sum_{k=1}^{\infty} \left\{ (k\pi)^2 \cos k\pi / \Delta_k \right\}}{\sum_{k=1}^{\infty} \left\{ (k\pi)^2 d_k / \Delta_k \right\}}$$